8-2015

In Vivo Mechanics of Cam-Post Engagement in Fixed and Mobile Bearing TKA and Vibroarthrography of the Knee Joint

Sumesh M. Zingde
University of Tennessee - Knoxville, szingde@vols.utk.edu

To the Graduate Council:

I am submitting herewith a dissertation written by Sumesh M. Zingde entitled "In Vivo Mechanics of Cam-Post Engagement in Fixed and Mobile Bearing TKA and Vibroarthrography of the Knee Joint." I have examined the final electronic copy of this dissertation for form and content and recommend that it be accepted in partial fulfillment of the requirements for the degree of Doctor of Philosophy, with a major in Mechanical Engineering.

Richard D. Komistek, Major Professor

We have read this dissertation and recommend its acceptance:

William Hamel, Mohamed R. Mahfouz, Aly Fathy, Adrija Sharma

Accepted for the Council:
Dixie L. Thompson

Vice Provost and Dean of the Graduate School

(Original signatures are on file with official student records.)

In Vivo Mechanics of Cam-Post Engagement in Fixed and Mobile Bearing TKA and Vibroarthrography of the Knee Joint

A Dissertation Presented for the
Doctor of Philosophy
Degree
The University of Tennessee, Knoxville

Sumesh M. Zingde
August 2015

Dedication

This dissertation is dedicated to my parents, Drs. Mahesh and Surekha Zingde and my wife, Reshma Shah, who have always been a constant support in my life and have enabled me to achieve my goals. Above all, this dissertation is for “Nana” (Anand S. Nagarkatti), who made me what I am today.

Acknowledgements

Firstly, I would like to thank Dr. Richard D. Komistek for educating and guiding me through all the years at the Center for Musculoskeletal Research (CMR). My time at CMR provided me with the most thorough training, which is immensely helping me provide valuable contributions in the field of orthopedics. I would like to mention my special appreciation for Dr. Adrija Sharma, who has been my friend and mentor ever since I came to the University of Tennessee- Knoxville. I would also like to thank my committee members, Dr. Hamel, Dr. Mahfouz, and Dr. Fathy, for providing valuable insights for my work to be successful and for serving as my committee members.

Finally, I would like to all my lab members and friends, for being there for me when I most needed

Abstract

The objective of this dissertation was to determine the mechanics of the cam-post mechanism for subjects implanted with a Rotating Platform (RP) PS TKA, Fixed Bearing (FB) PS TKA or FB Bi-Cruciate Stabilized (BCS) TKA. Additionally, a secondary goal of this dissertation was to investigate the feasibility of vibroarthrography in correlating in-vivo vibrations with features exhibited in native, arthritic and implanted knees. In-vivo, 3D kinematics were determined for subjects implanted with nine knees with a RP-PS TKA, five knees with a FB-PS TKA, and 10 knees with a FB-BCS TKA, while performing a deep knee bend. Distance between the cam-post surfaces was monitored throughout flexion and the predicted contact map was calculated. A forward dynamic model was constructed for 3 test cases to determine the variation in the nature of contact forces at the cam-post interaction. Lastly, a different set of patients was monitored using vibroarthrography to determine differences in vibration between native, arthritic and implanted knees. Posterior cam-post engagement occurred at 34° for FB-BCS, 93° for FB-PS and at 97° for RP-PS TKA. In FB-BCS and FB-PS knees, the contact initially occurred on the medial aspect of the tibial post and then moved centrally and superiorly with increasing flexion. For RP-PS TKA, it was located centrally on the post at all times. Force analysis determined that the forces at the cam-post interaction were 1.6*body-weight, 2.0*body-weight, and 1.3*body-weight for the RP-PS, FB-BCS and FB-PS TKA. Sound analysis revealed that there were distinct differences between native and arthritic knees which could be differentiated using a pattern classifier with 97.5% accuracy. Additionally, vibrations from implanted knees were successfully correlated to occurrences such as lift-off and cam-post engagement. This study suggests that mobility of the

polyethylene plays a significant role in ensuring proper cam-post interaction in RP-PS TKA. The polyethylene insert rotates axially in accord with the rotating femur, maintaining central cam-post contact. This phenomenon was not observed in the FB-BCS and FB-PS TKAs.

Table of Contents

List of Tables

List of Figures

Chapter 1: Introduction

Knee joint injuries are one of the most commonly reported musculoskeletal problems. These injuries can occur due to various reasons. In young adults, sports are a major cause of injuries. In older subjects arthritic degeneration (such as rheumatoid or osteoarthritis) of knees is a well-known phenomenon, and is known to result from a variety of traumatic causes. According to the Arthritis Foundation, arthritis-related problems are second only to heart disease as the leading cause of work disability. Mechanical loading, especially dynamic loading, is believed to play a major role in the degenerative process, where the cushioning layers are damaged and creates bone to bone contact. Osteoarthritis can be extremely disabling, leading to discomfort and often excruciating pain. Therefore artificial orthopedic implants are designed so as to replace these damaged articulating surfaces and provide pain relief and allow a subject with severe osteoarthritis to return to a normal daily life. This leads many patients to undergo a Total Knee Arthroplasty (TKA) surgery to eliminate the pain and deficiencies.

At least 150 TKA designs exist in the market today, with advancements by physicians and engineers that simulate the geometry and behavior of a healthy knee joint (Carr 2009). The differences in these designs are based on factors such as condylar geometry, bearing mobility, ligament preservation vs. substitution, and fixation methods (Sharma 2007). In order to better understand the motivation of design engineers to introduce different designs in the market, it first becomes important to understand the working of the normal knee.

1.1 Kinematics of the Normal Knee in Flexion

In vivo fluoroscopic studies have determined that kinematics of the normal knee are, at least, partially defined by the integrity of the supporting soft tissue envelope (capsule, ligaments, myotendinous units, etc.) and the condylar geometry of the articular surfaces. In the normal knee, there is a complicated pattern of motion that occurs between the femoral and tibial articular surfaces during flexion and extension. Due to the stabilizing nature of the relatively immobile medial meniscus and various complicated interactions between surrounding ligamentous structures, flexion of the intact knee produces a relatively predictable controlled posterior rollback of the lateral femoral condyle on the lateral tibial plateau.

Previous studies on cadaveric knees have revealed that the lateral femoral condyle rolls back an average of 18mm from full extension to full flexion while the medial femoral condyle rolls back only 1.5mm (Freeman 2001) (Figure 1-1). In-vivo studies indicated a similar trend with the average lateral femoral condylar rollback for weight bearing flexion being 21mm and that for the medial femoral condyle being 1.9mm (Dennis 2005) (Figure 1-2).

A majority of normal knees demonstrate a medial pivot axial rotational pattern in which the lateral femoral condyle rotates around a relatively stationary medial femoral condyle. Under weight-bearing conditions, an average of 21^0 of axial femorotibial rotation occurs in the normal knee from full extension to flexion of 120^0 (Freeman 2001). Therefore, with flexion of the normal knee, the tibia typically internally rotates relative to the femur, and conversely, externally rotates with knee extension (i.e., screw home mechanism)

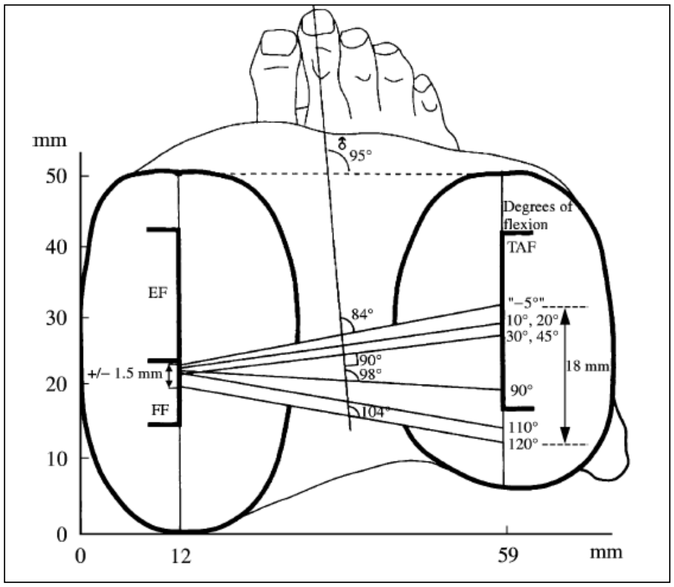

Figure 1-1: Posterior Femoral rollback in the normal knee (cadaver) from full extension to full flexion (Freeman 2001).

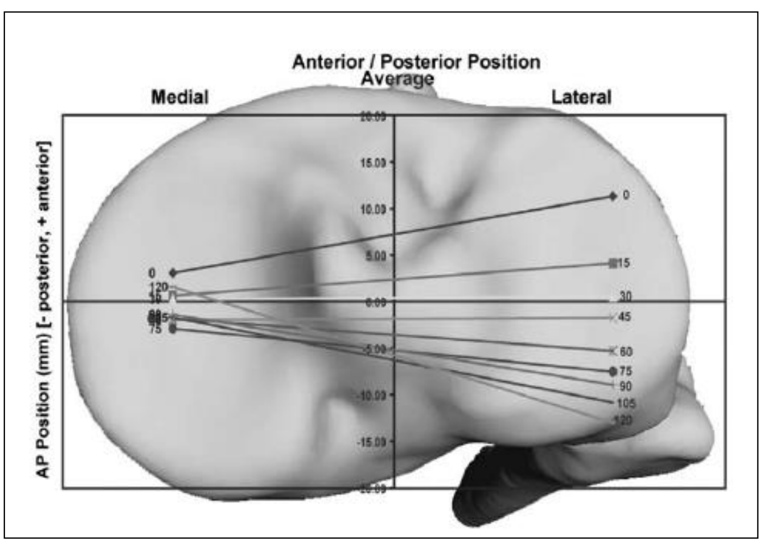

Figure 1-2: Posterior Femoral rollback in the normal knee from full extension to full flexion (Underweight bearing conditions) (Dennis 2005).

1.2 Total Knee Arthroplasty (TKA)

In a total knee arthroplasty (TKA), the diseased cartilage surfaces of the thighbone (femur), the shinbone (tibia) and the kneecap (patella) are replaced by prostheses made of metal alloys, high-grade plastics and polymeric materials. Most of the other structures of the knee, such as the connecting ligaments, remain intact.

In the modern knee replacement or total knee arthroplasty (TKA), the articulating surfaces of the knee are replaced by four components (Figure 1-3):

1. Femoral Component: To resurface the distal end of the femur.
2. Tibial Component: Attached to the proximal end of the tibia.
3. Polyethylene insert: Replicates the function of the meniscus and forms the articulation between the femoral and tibial components.
4. Patellar Button: Attached to the articulating surface of the patella-femoral joint.

The geometry of the femoral component varies between manufacturer's designs and has evolved with increasing knowledge of the in vivo mechanics of TKA. Earlier components had a close to circular sagittal profile but lately the trend has been to more closely mimic the natural knee by reducing the radius of sagittal curvature of the articulating surface towards the posterior femur. Manufacturers also use different profiles for the medial and lateral condyles. All new designs have a rounded profile in the coronal plane on each condyle, although the radius of curvature varies between designs.

The tibial component is typically a flat tray made of the same material as the femoral component and attaches to the boney architecture of the tibia. This tray holds a piece of plastic called the polyethylene insert, manufactured from wear resistant, cross-linked ultra-high molecular weight polyethylene (UHMWPE). The polyethylene insert acts as the bearing between the femur and tibia. The backside of the patella is resurfaced with a piece of plastic, sometimes referred to as a “patella button”. This button lies in a groove on the anterior surface of the femoral component and mimics the interaction between the normal patella and the trochlear groove on the non-implanted femur. This groove guides the motion of the patella which transfers force from the quadriceps to the tibia and acts as the extensor mechanism of the knee. The shape of the femur, the geometry of the insert and button, and the changes made to the soft tissue structures during the surgical procedure affect the mechanics (kinetics and kinematics) of the knee after replacement.

With the knowledge of the drawbacks of current designs and with the focus of attaining normal knee kinematics in TKAs, the design of knee implants have continuously evolved and there are various types of knee implants in the market. Modern TKA designs can be broadly classified into the following groups:

Based on the type of fixation to the bone TKAs can be broadly classified into two groups:

- Cemented Prosthesis
- Uncemented Prosthesis

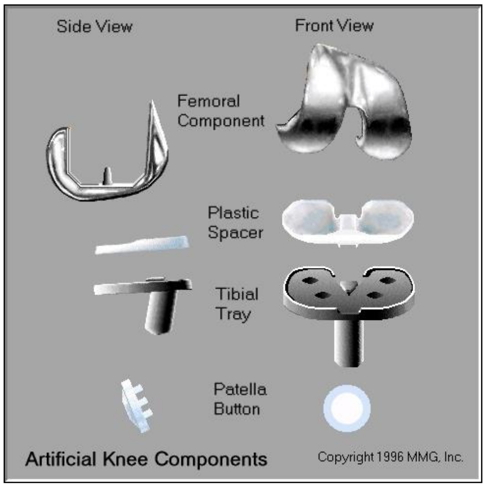

Figure 1-3: Basic components of a TKA.

Both types are widely used. In many cases, a combination of the two types is used. The choice to use a cemented or uncemented prosthesis is usually made by the surgeon based on the age of the patient, their lifestyle, and the surgeon's experience. A cemented prosthesis is held in place using epoxy type cement that attaches the metal to the bone. An uncemented prosthesis has a fine mesh of holes on the surface that allows the bone to grow into the mesh and attaches the prosthesis to the bone.

Based on the type of implant TKAs can be classified into two groups:

- Posterior Cruciate Retaining (PCR)
- Posterior Cruciate Sacrificing (PCS)
- Posterior Cruciate Stabilizing (PS)
- Bi-cruciate Stabilizing (BCS)

This distinction is basically based on the surgical procedure that is adopted during TKA for the cruciate ligaments (the main anterior-posterior stabilizers in the normal knee). Though some TKAs are designed to retain the anterior cruciate ligament (ACL), in most designs, the ACL is resected. With respect to the posterior cruciate ligament (PCL), TKAs can be PCL retaining (PCR), PCL sacrificing (PCS) or PCL substituting, also known as posterior stabilized (PS). PS designs differ from the PCR designs by having an additional post-cam mechanism between the femoral component and the polyethylene insert in order to initiate posterior femoral rollback, the primary role of the PCL. The post is located on the polyethylene insert and the cam is provided on the femoral component in between the two condyles. PCR designs do not have this mechanism as the PCL in these designs is not resected. The PCS designs resect the PCL and do not provide for any substitution. In some cases the cam-post interaction is modified in such a way that it can substitute the function of both the ACL as well as the PCL. In such a TKA the anterior aspects of the femoral cam and the tibial post geometries are designed to engage at full extension of the knee joint (hence preventing posterior slide which is the function of the ACL). Since these designs substitute both the ACL and PCL they are called Bi-cruciate stabilizing or BCS type TKAs.

Based on the type of tibial component TKAs can be classified as:

- Fixed Bearing (FP)
- Mobile Bearing/Rotating Platform (RP)

In the fixed bearing design the plastic component on the tibial component is fixed to the tibial tray. This means that there is no relative motion between the plastic and the tibial component. In the mobile bearing design the plastic component has been designed, such that, it can be fitted inside the hollow stem of the tibial component. It is not fixed to the tibial component and hence is free to move (to a certain degree) on the tibial tray (Figure 1-4). These designs can allow for free rotation, free translation or a combination of both free rotation and translation.

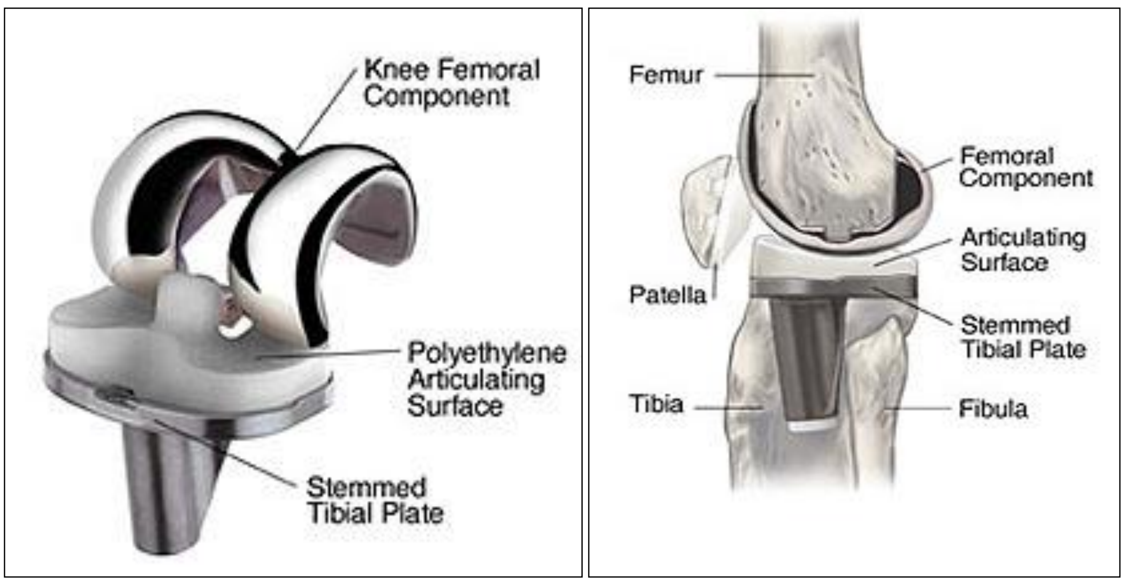

Figure 1-4: (left) PS fixed bearing TKA. (right) Implanted TKA.

1.3 Concerns rising from TKAs

Determination of knee kinematics (normal and implanted) has been investigated using multiple techniques, both in-vitro as well as in-vivo. These include the invasive cortical pins, Roentgen Stereophotogrammetric Analysis (RSA), skin marker analysis and fluoroscopy based model reconstruction techniques. Violation of the complex interactions between the natural stabilizing joint surface anatomy and surrounding ligamentous structures make it difficult to completely reproduce normal knee motions following TKA. Numerous kinematic variances from normal knee kinematic patterns have been demonstrated, including paradoxical anterior femoral translation during deep knee flexion (Dennis 2003), reverse axial rotational patterns (Dennis 2004), wear of the polytheylene contact surface, degeneration (and failure) of the tibial post in the PS type TKA, and femoral condylar lift-off (Scuderi 2003).

Anterior femoral translation during deep knee flexion (femoral component sliding anteriorly during deep flexion rather than posterior femoral rollback) has numerous potential negative consequences. First, anterior femoral translation results in a more anterior axis of flexion, lessening maximum knee flexion (Hass 2002). Second, the quadriceps moment arm is decreased, resulting in reduced quadriceps efficiency. Third, anterior sliding of the femoral component on the tibial polyethylene surface risks accelerated polyethylene wear (Bartel 1986).

Some TKAs induce a tendency to produce undesirable reverse axial rotation which risks patellofemoral instability due to lateralization of the tibial tubercle and an associated increase in the Q-angle during deep flexion, as well as lessening maximum knee flexion due to reduced posterior femoral rollback of the lateral femoral condyle (Dennis 2004).

Lift-off in TKA, whereas the a femoral condyle lifts off of the tibial insert, have been a focus of investigators since fluoroscopic analysis showed that it does occur (Steihl 1999). Femoral condylar lift-off creates excessive loads on the polyethylene bearing, risking premature polyethylene wear, and also causes increased load transmission to the underlying bone which increases the risk of prosthetic loosening (Scuderi 2003). These adverse effects are amplified in TKA designs which have flat-on-flat designs due to edge-loading of the prosthetic components.

1.4 Knee Vibration Data- The future of diagnosis?

Experimental studies in humans are difficult and often restrictive due to the exclusion of any measuring device that would require invasive techniques. Since cadaveric studies fail to simulate in-vivo conditions adequately (Komistek 2005), biomechanical researches have strived for new and unique methods for indirect measurements. These have been used to analyze the normal knee joint as well as to asses and justify design protocols of TKAs.

One of the major problems in discerning the progression of knee joint conditions is the inability to detect the cause of such conditions until it is too late. Use of X-rays, CT and MRI scans are limited to providing information on defects that are gross in nature. Arthroscopic procedures have become popular to overcome this deficiency; however, this procedure is semi-invasive. Hence, some research has dealt with early diagnosis of knee joint conditions by non-invasive means. Analysis of vibration signals from the knee joint has been found to be successful in determining these conditions at an early stage. Further development of such techniques may one day provide the care giver with options that are less-invasive compared to TKAs or at the very least prolong the time for the patient before they have to receive one. Hence, while discussing the mechanics of the knee joint a look at such innovative techniques becomes imperative.

Chapter 2: Research Aims and Contribution

2.1 Research Aims

While the TKA procedure is found to be very successful in treating severe osteoarthritis, failure, especially in the form of polyethylene wear limits its longevity (Howling, 2001; Currier, 2005).

Wear is ideally a function of kinematics, kinetics and the material properties (Wimmer, 1997). Interestingly enough, all the various types of TKA available today use similar kind of materials but have wide differences in the design and the dimension of the components. This suggests that the correlation of kinetics, kinematics and wear hasn't been developed (Sathasivam, 2001; Fregly, 2005). With the design goal of modern TKA designs being to acheive higher degree of flexion, which generates higher forces (Komistek, 2005), and also TKAs being implanted in younger and more active patients a perfecting understanding of the relation of kinematics, kinetics and wear has become increasingly important (Walker, 1999).

Methods to study wear behavior in UHMWPE have been limited to the use of simulators or retrieval studies. The greatest drawback with using simulators is the fact that it works on in-vitro conditions. Comparison between wear generated by simulators and that obtained from retrieval studies, for the same bearing designs and for similar cycles, have indicated greater amount of wear in the retrieved inserts (Harman, 2001). On the other hand retrieval studies involve a backward approach and can only give us an idea about what 'might have caused' such wear rather can pinpointing as to 'this is the cause'. Thus the correct approach would be to go in the forward direction and predict wear from the in-vivo kinematics and kinetics. At present there has been just one study attempting to do this (Fregly, 2005). However, this study is limited due to the fact that it assumes a linear material model, does not incorporate friction and assumes an axial force distribution.

Previously, fluoroscopy has been successfully used in our lab to determine the in-vivo kinematics of TKA of the tibio-femoral and patella femoral joint interactions, allowing for the determination of antero-posterior translation, axial rotation, femoral condylar lift-off and weight-bearing range-of-motion (Komistek, 2000, 2004; Dennis, 2003). The objective of this research is to devise a new computational methodology which would extend this capability to the calculation of kinematic properties of the cam-post interaction, in-vivo contact forces and torques, contact stresses at the cam-post interface and ultimately serve as reliable predictor for potential polyethylene wear.

This dissertation describes the initial process that has been derived for the comprehensive analysis of the cam-post mechanism in ten fixed bearing bi-cruciate stabilized TKA, five fixed bearing posterior stabilized TKA and nine mobile bearing rotating platform PS TKA. The study entailed the determination of the contact kinematics of the cam-post mechanism and the resulting contact forces occurring during a deep knee bend (DKB) activity. The effect of posterior femoral rollback (PFR) on the moments generated on the cam-post and the effect of contact location as well as contact height on cam-post fracture was analyzed.

Additionally, it is hypothesized that the magnitude of the vibration of the tibiofemoral joint increases with articular cartilage degeneration (i.e. increasing roughness of the articulating surfaces). Although this hypothesis is plausible from the mechanical point of view, it is not clear whether the vibration can be studied non-invasively. Therefore, this work also assessed the feasibility of using miniature accelerometers to study the vibration of the articulating surfaces (hence the name *vibroarthrography*) of the tibio-femoral joint (including the cam-post interaction).

To this end, additional 76 normal, degenerative and implanted knees, were recruited to investigate the possibility of the correlation between in-vivo kinematics and vibroarthrography signals. The goal was to assess if it is possible to distinguish, just based on vibration data, the occurrence of uni-compartmental degeneration and the difference between normal and degenerative knee joint signals. Patients with normal and well functioning TKA were also analyzed under in vivo, conditions using video fluoroscopy and vibration sensors while performing various normal day activities. This made it possible to record and compare the vibration signals recorded for patients that have intact cartilage with those whose cartilage has been considerably worn (for native knees) as well as to confirm the correlation of the signals to different condition occurring in the TKA joint for patients with well functioning as well as failing TKAs.

2.2 Fundamental Contributions

Most of the previous in-vivo kinematic studies pertaining to the knee joint have reported data only pertaining to the tibio-femoral or patella-femoral joint (Kellis 2005, Fellows 2005, Baker 2003, Sylvester 2009) However, the kinematic analysis of the cam-post interaction under in-vivo conditions has been largely omitted due to the complexity of analysis. Therefore, determining the cam-post contact kinematics will contribute to better understanding of the in-vivo interaction conditions in a PS type TKA. The effect of the nature of contact, location of contact, contact areas and the resulting effects on the tibial post wear, which to the best of the author's knowledge, has never been done under in-vivo, dynamic, weight-beating conditions. Utilizing a 3D-to-2D registration technique and an in-house developed analysis software based in MATLAB, it is possible to undertake this analysis, which is the first of its kind.

The present work also provides important contribution to better understand the forces in the cam-post interaction. The proposed methodology utilizes the use of a 3D forward dynamics mathematical model of the lower limb, based on Kane's dynamics. The mathematical model makes it possible to simultaneously solve for all the interaction forces in the PS TKA. Previous models have been utilized to determine the lateral and medial condyle contact force as well as the patello-femoral contact force in a variety of TKA designs. However, in the PS type TKA the interaction of the cam with the post and the resulting forces generated have been neglected. This is the first attempt in providing all the contact forces simultaneously

Finally, vibroarthrography data was evaluated for its potential use of detecting the articular cartilage condition in native knees and the occurrence of cam-post interaction and condylar lift-off in PS TKA. Although this methodology has been used by a few other researchers, the current work is the first to correlate the vibration signals with the 3D, in-vivo kinematics. This allows in the determination of not only the severity but also the location of the articular cartilage degeneration. This information will be very helpful for surgeons planning TKA procedure and may eliminate the need for imaging modalities involving harmful radiation.

Chapter 3: Literature Review and Motivation

With new designs being created and modern TKA designs aiming at higher degree of flexion, which generates higher forces (Komistek 2005), and TKAs being implanted in younger and more active patients, analyses of their kinematics and contact mechanics quickly and efficiently become increasingly important (Walker 1999). The objective of this study was to provide an initial computational methodology to determine the mechanics of the cam-post interaction in PS type TKA. This involves three main areas of consideration:

1. Kinematics
    a. Contact angle and location
    b. Nature of contact
2. Kinetics
3. Vibrtoarthrography

There are numerous studies that deal with the determination of kinematics, kinetics and wear of the knee joint (native as well as TKA). However, data pertaining to similar studies that specifically deal with the cam-post interaction are limited at best, in some areas, such as wear, and nearly nonexistent in others, such as contact kinematics and forces. Therefore, when trying to establish a protocol for a computational methodology for the cam-post interaction, the first steps involve the understanding of the various different techniques used to assess the kinematics, kinetics and wear in the knee joint as a whole and then determine the most suitable combination of techniques which can be successfully applied to the cam-post interaction analysis. The most crucial aspect of developing this methodology is to understand the scope of these technologies in bridging the knowledge gap between current data available on the mechanics of the cam-post interaction to that of the more in depth understanding already available for the knee joint as a whole.

3.1 Techniques used to determine knee joint kinematics

Many different methods have been used to determine TKA and native knee kinematics. Researchers have used in vitro cadaveric studies, non invasive skin markers (Kostuik 1975, Steihl 1998, Antonsson, 1989) and external fixation devices (Scuderi 2003, Insall 2004, Wasielewski 2005, Cappozzo 1993), invasive bone pins (LaFortune, 1992), in vivo roentgen stereophotogrammetric analyses (RSA) (Karrholm 1989; Nilsson, 1995), externally worn goniometric devices (Chao, 1980), single plane and biplanar fluoroscopic techniques (Banks, 1996; Hoff, 1998).

Use of tools such as use of cadavers is often ineffective since they fail to simulate in vivo conditions adequately. Skin markers are non-invasive and involve no radiation exposure, but have been shown to induce measurement errors of up to 18 degrees for internal/external rotation (Murphy, 1990; Sati, 1996; Holden 1997). Another study found that skin markers produced errors of 21% for flexion/extension, 63% for internal/external rotation, and 70% for abduction/adduction during gait. Modifications have been made to reduce the errors associated with it. Some of these methods include artifact assessment (Lucchetti, 1998), Point Cluster Technique (Andriacchi, 1998; Alexander, 2001) and optimization using minimization techniques (Spoor, 1988; Lu 1999).

Intra-cortical bone pins have been found to yield highly accurate measurements (with errors less than 0.4 mm), but the insertion process is invasive and stressful, limiting the application of this process to small sample sizes. External linkages attached to the limbs offer a non-invasive approach to bone pins, but assume that there is negligible mobility between the external apparatus and the underlying bone. RSA yields highly accurate results, but it is often non-weight bearing, and can only be performed when specially designed replacements were implanted at the time of TKA. Video fluoroscopy has proved to be a highly accurate and non-invasive procedure that exposes patients to minimal radiation. Mahfouz et al (Mahfouz 2003) employs a novel, semi-automated algorithm to register three-dimensional (3-D) computer automated design (CAD) models to two dimensional (2-D) fluoroscopy images. This procedure yields in vivo 3-D kinematics, susceptible to errors of less than 0.5 mm for in-plane translations and less than 0.5º for in-plane rotations. It is believed that this technology offers the most practical and reliable method for determining knee kinematics.

3.2 Knee Kinematics-Mobile or Fixed, PCR or PS?

Numerous other kinematic evaluations have found a larger magnitude of femoral rollback in native knees when compared to TKAs, during deep flexion activities (Dennis 2005, D'Lima 2006). The magnitudes of posterior femoral rollback during deep flexion in TKA designs are less than in the normal knee. This contributes to the decreased knee flexion following TKA compared to the normal knee as well as abnormal kinematic patterns leading to joint pain and, in some cases, failure of the TKA. In spite of these limitations, TKAs in general have provided good mid to long term survivability. However, the question pertaining to which type of implant configuration provides the best post-surgery outcomes is still a cause for debate. One area of contention is bearing mobility. The mobile bearing implant was designed to reduce contact stress, thereby reducing wear, and recreate more "normal like" knee kinematics. In vitro studies have shown reduced wear with the use of a mobile bearing implant (Fisher 2004, 2006). However, kinematics, clinical outcomes and survivability between fixed and mobile bearing implants have produced similar results. A review study conducted by Post et al (Post 2009), could not find any basis to justify one design over the other. Clinical success and long-term survivorship were found to be mainly dependent on the accuracy with which the components are implanted. They concluded that the best design is the one with which the surgeon is most comfortable and most able to reproducibly implant (Post 2009). Studies that have compared the performance of the mobile and fixed configurations in the same patient have also concluded that the patient does not demonstrate any difference in terms of range of motion, knee scores and survivorship (Ranawat 2004, Kim 2007, Sharma 2007). Pagnano et al (Pagnano 2004) conducted a study on 240 rotating platform TKAs and found that it did not improve patellar tracking. A multicenter study conducted by Wasielewski et al (Wasielewski 2008) on 527 mobile bearing TKAs found that only 12% of the knees exhibited greater than 10 degrees of axial rotation during a Deep Knee Bend (DKB) activity. Also, nearly half the knees analyzed experienced less than 3 degrees of axial rotation. They also found that the rotational parameters were comparable with results reported for fixed bearing TKA by Dennis et al (Dennis 2004).

Another area of contention is whether the posterior cruciate ligament should be retained or substituted. During gait, fixed and mobile-bearing posterior stabilized TKA designs have experienced similar kinematic patterns as those designs that lacked a cam and post mechanism. This has been attributed to the fact that the cam and post mechanism of most posterior stabilized TKA designs do not engage during lesser flexion activities such as gait. During a deep knee bend, however, posterior stabilized TKA designs typically experience greater posterior femoral rollback than designs without a cam and post mechanism.

Numerous studies have shown that certain cruciate retaining (CR) total knee designs exhibited paradoxical femoral sliding, decreasing clinical weight-bearing flexion (Cates 2008). This paradoxical femoral rollback (PFR) has not been seen in posterior stabilized (PS) TKAs. However, a study comparing PS TKAs to CR TKAs with asymmetrical condyles found that, while the CR design did exhibit lesser medial PFR, both designs achieved similar amounts of lateral PFR. Proponents of the CR design have suggested that the PFR seen in PS TKAs is due to the "guided motion" provided by the cam-post engaging, which leads to higher rates of implant failure due to cam-post wear. In their chapter on failure of the cam-post mechanism, Bourne et al (Bourne 2005) found that all post-cam mechanisms are not the same and that substantial differences exist from one implant type to another. They also suggest that the cam-post mechanism does not always engage as designed. Though they did find evidence that cam-post mechanism may result in increased wear, this was limited to implants with varus/valgus constraints.

Few studies have been conducted that accurately report the function of the cam-post engagement mechanism in PS TKAs. Two-dimensional computerized models have been used to investigate the effect of position and height of the tibial post on the tibiofemoral translation of the knee (Piazza 1998, Delp 1995). However, these studies have not incorporated the three-dimensional effect that includes knee axial rotation, which can significantly alter the data. Also, these studies were not conducted on live TKA subjects, but rather, used non physiological kinematics inputs to run their models. Banks et al, reported the minimum distance between the cam and post as a function of flexion in five knees with a primary posterior stabilized knee (Banks 1997). That study estimated cam–post engagement to occur at 40^o of flexion during a step-up maneuver assuming the cam and post engaged when the minimum distance between them was less than 1 mm. Suggs et. al in their paper, investigated the flexion range at which cam-post engagement occurred, during a lunge activity for 24 TKA subjects in-vivo. They analyzed fluoroscopy images using an image registration technique at 15^o degree intervals from full extension to maximum knee flexion. The exact contact angle was estimated between the flexion intervals where cam-post contact first occurred (Figure 3-1). They reported average contact angle of 91.1^o with a range from 69^o to 114^o. Though this is the first study to investigate the cam-post interaction in-vivo, it does not incorporate the necessary level of accuracy that would be desirable for a thorough understanding of the interaction mechanism.

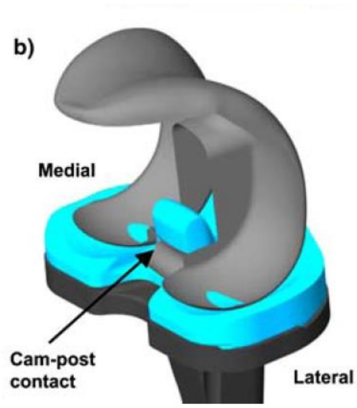

Figure 3-1. In-vivo cam-post contact as assessed by Suggs et al.

In vivo cam-post contact area is another area in which data is not available. The only notable paper to effectively quantify cam-post contact area, utilized the use of knee simulators to investigate three different TKA designs at three static flexion angles (90, 120 and 150 degrees) Nakayama (Nakayama 2005). A relatively small force of 500N was assumed to be applied by the femoral cam on the tibial post. This paper reported that at the assessed angles the cam-post contact area varied for the three different designs investigated, varying from $40mm^2$ to $65mm^2$. The study also reported that contact area reduced with increasing flexion. One of the major drawbacks of this study was that they assumed the knee to be in neutral position during flexion, with no effect of femoral rollback of either the medial or lateral condyle and no axial rotation (Figure 3-2). Also, the forces applied on the cam-post interaction were merely assumed and were not derived using any computational or experimental modality. The paper itself mentions this as their major limitation and attributed it to the lack of research data on this topic.

Figure 3-2: Axial view (left) and Sagital view (right) for the implant set-up by Nakayama et al.

3.3 Techniques used to determine joint forces

The value of determining in vivo forces and torques could lead to three important factors: (1) prediction of how new designs will perform, (2) simulation of orthopedic surgery procedures and prediction/optimization of clinical outcome based on surgical parameters under consideration, and (3) investigation of loading mechanisms that contribute to degenerative joint disease, as well as movement modifications or clinical interventions to reduce these effects (Komistek 2005). The in-vivo force studies related to the knee joint can be divided into two broad categories – telemetry and mathematical modeling.

The use of telemetry has gained wide scale approval in the research community since it has the capability of reporting very accurate, real-time data. D'Lima et al. (D'Lima 2005) have reported the first in vivo measurement of tibiofemoral forces via an instrumented implant in a TKA patient in 2006. This technique is capable of measuring resultant knee forces in six degrees of freedom (D'Lima 2007, Varadarajana 2008). This study consisted of three patients, each implanted with a custom made telemetric implant (Zimmer Warsaw, IN). Forces at the tibiofemoral interface were assessed for the lunge and chair rise activities. All three patients experienced higher forces during the lunge activity. Forces during the lunge activity ranged between 1.7 and 2.77 times body weight (BW), with the peak force occurring between 27% and 82% of the cycle. For chair rising–sitting, all patients showed two peaks in net force. One peak (average 1.83*BW) was found at early part of chair rising (between 11-20% of cycle), while another peak (average 1.61*BW) was found at late part of the cycle (78-83%). Patient specific force distribution on the two condyles was nearly equal for the lunge activity, with both condyles experiencing nearly equal forces. For the chair rising activity, it was seen, that the lateral condyle experienced higher force ratios (between 61.7-74.2% of total force) when compared to the medial condyle. Another study conducted by the same authors (D'Lima 2008) assessed tibiofemoral forces for the same patient group while performing daily activities like walking, bicycling and exercising on an elliptical trainer. They found that during level walking the knee experienced forces between 1.8-2.5 times BW. These forces were similar to those experienced by subjects comfortably walking on a treadmill. During the bicycling activity the forces peaked at 1.03 times BW. Patients experienced higher forces while exercising on the elliptical trainer with the mean peak tibial force being 2.24 times BW.

One restriction with telemetry is the fact that implantation of such devices is not feasible across different TKA designs that are available today. Also, data reported so far is restricted to a few patients and expanding that to a large patient population will take a long time. Another disadvantage of telemetry is the fact that it can only be used to observe forces in implanted knee joints. Hence, mathematical modeling techniques have been utilized as an alternative theoretical methodology to calculate knee joint forces. Mathematical modeling approaches can be categorized two ways; those that use optimization techniques to solve an indeterminate muscle force system (Taylor 2004) and those that utilize a reduction method that minimizes the number of muscle force unknowns, keeping the system solvable as the number of equations of motion are equal to the number of unknown quantities (Komistek 2005, Sharma 2007, 2007).

A study conducted by Lundberg et al (Lundberg 2009), developed a parametric model to determine tibiofemoral contact forces for TKA patients during level walking. The peak force reported was 3.3 times BW with a range of 0.5 times BW for normal forces and a range of 0.82 times BW for resultant forces. These results compared well with previously published literature pertaining to optimization techniques to determine knee joint forces. The medio-lateral force distribution was also found to correlate with other studies (Andriacchi 1997, Hsu 1990, Johnson 1980, Shelburne 2006). However, these forces were higher when compared to those reported for a similar activity using telemetry.

Another computational route to solve biomechanical problems has been the use of optimization techniques, where the number of unknowns is greater than the number of equations that can be generated for the solution (Komistek, 2005). Therefore, the process deals with the solution generated by the minimization of a suitably chosen objective function (Seireg 1973, Brand 1982, Anderson 2001, Piazza 2001). However, there still lacks a consensus as to which objective function is physiologically most suitable (Komistek 2005).

Komistek et al., used the reduction technique and utilized a fluoroscopy driven inverse model based on Kane's method of dynamics. They reported that the maximum force acting between the femur and the tibia for a healthy female subject having a normal knee was 1.7–2.3 BW, depending mainly on walking speed. Using a similar approach Sharma et al (Sharma 2007) assessed tibiofemoral forces for subject with either a PS or a CR high flexion TKA while performing DKB. They found that forces for each type of implant increased with increasing flexion. Also, medial condyle force was always higher than the lateral condyle force. To check for the amount of error the model was also compared to data obtained from a fixed bearing telemetric implant. The results showed that, for the telemetric implant the maximum force on the medial side was 1.9BW experienced at 90 degrees of flexion and 2.2BW at 105 degrees for the lateral side. The model predicted 1.89BW (at 89 degrees) and 2.05 (at 101 degrees) for the medial and lateral condyles respectively. Another study (Sharma 2007) by the same group analyzed 5 patients with a fixed bearing TKA and 5 patients with a mobile bearing TKA during the DKB activity. They reported that tibiofemoral force for both the types of implants was similar in nature and magnitude. Also, as in the previous study, they found that the force distribution was unevenly distributed between the medial and lateral condyles, with the medial condyle always having higher forces than the lateral condyle. The average medial tibiofemoral force varied from 0.5BW at full extension to

2.72BW at full flexion for the mobile bearing subjects, while for the fixed bearing subject the medial force varied between 1.04BW at full extension to 2.73BW at full flexion. On the lateral condyle the medial force varied between 0.34BW to 0.91BW for mobile bearing subjects, and between 0.43BW to 0.92BW for the fixed bearing subjects. These results are in accordance to reported data from telemetric devices under similar conditions.

Despite these comprehensive analysis conducted by various research groups there still exist variances in the force data generated by the studies (Table 3-1). This is because data collected by telemetry and the data input to the mathematical models for the same type of activity are collected at different speeds. The interactive forces increase as the speed of the activity is increased. However, it is now a well-accepted fact that the contact forces increase with the increase in the angle of flexion (Komistek, 2005).

Table 3-1: Knee Contact Forces from Previous Studies (Modified from Komistek, 2005).

Authors	*Technique*	*Activity*	*Knee Force*
Taylor et. al.	Telemetry	Normal gait	2.2 – 2.8 BW
		Treadmill gait	2.75 BW
		Stair descent	3.1 BW
		Stair ascent	3.8 BW
		Jogging	3.6 BW
Colwell et. al.	Telemetry	Walking	2.4 BW
		Stair ascent	3.3 BW
Seireg et. al.	Optimization	Walking	7.1 BW
Paul	Reduction	Walking	2.7 – 4.3 BW
		Stair descent	4.9 BW
		Stair ascent	4.4 BW
		Up ramp	3.7 BW
		Down ramp	4.4 BW
Wimmer et. al.	Reduction	Walking	3.3 BW
Komistek et. al.	Reduction	Walking	2.1 – 3.4 BW
		Deep knee bend	1.8 – 3.0 BW

3.4 Contact pressure analysis

To estimate contact pressures, in-vitro experimental methods are extensively used mainly due to their ability to generate data fast. Some experimental techniques used previously include stereophotogrammetric methods (Ateshian 1994), dye injection methods (Greenwald 1971, Black 1981), silicone rubber methods (Kurosawa 1980), 3S technique (Yao 1991), Fuji pressure sensitive film (Stewart 1995), resistive ink sensors (K-Scan™) (Ochoa 1993), ultrasound (Zdero 2001), piezoelectric transducers (Mikosz 1988, Buechel 1991) and micro-indentation transducers (Ahmed 1983). All of these experimental methods, however, are in vitro techniques that either assumes the contact forces and/or the orientation of the implanted components. Also, the differences between these various techniques and loading conditions make direct data comparisons difficult.

Rigid body contact analyses using multibody simulation methods have been successfully used to predict knee motion and contact forces (Godest 2000, Piazza 2001, Komistek, 2005, Sharma 2007, 2008) build on subject-specific models. Other studies have used a deformable polyethylene model based on the use of Hertzian contact analysis to calculate the stresses in polyethylene insert (Bartel, 1985; Walker, 1988). However, the accuracy of this method is limited due to the simplifying assumptions on which the theory is based (Lewis, 1998). The most resorted to and an accurate method used today is finite element analysis (FEA) (Lewis 1998). FEA has been used to study knee joint contact mechanics under static loading conditions (Bartel 1986, 1995, D'Lima 2001, Machan 2004, Périé 1998, Otto 2001, Rawlinson 2002, Sathasivam 1998, 1999). Dynamic FEA has recently been applied to simulations of knee implant components under well-defined loading conditions (Giddings 2001, Godest 2002, Halloran 2005). Apart from a significant amount of preprocessing required, one major drawback of these analyses is their intensive use of CPU time. This makes them impractical for incorporation into larger multi-dynamic musculoskeletal models. Furthermore, detailed stress analyses carried out by FEA are unimportant in gross movement simulations. Though FEA provides the best capability to model the polyethylene accurately and calculate stresses in it, however, the greatest disadvantage of this method lies in the high amount of effort, time and computational infrastructure required for the analysis. Thus most studies, using FEA have used simplifying assumptions to reduce the complexity of the method.

One key point to note is that apart from the FEA analysis, all other analysis schemes have been utilized to calculate the tibio-femoral contact pressures/stresses. Also, as with most types of studies in this field, the stress and contact area data generated by the various methods have a lot of variability in them (Table 3-2).

Table 3-2: Summary of some Previous Contact Area and Contact Stress Studies (Thompson, 2001).

Method	Reference	Load	Average Contact Area	Maximum Contact Stress
Elasticity	Bartel et. al.	1.5 KN	N/A	18.0 MPa
FEA	Bartel et. al.	1.5 KN	N/A	20.0 MPa
Fuji film	Collier et. al.	2.8 KN	N/A	23.5 MPa
Fuji film	Collier et. al.	0.7 KN	0.3 cm^2	N/A
K-scan sensor	Harris et. al.	3.6 KN	3.5 cm^2	N/A
Fuji film	Harris et. al.	3.6 KN	2.3 cm^2	N/A

In-vitro testing has been employed to determine cam-post forces. In vitro robotic tests using cadaveric knees measured cam–post contact forces during knee flexion under simulated muscle loads (Suggs 2008)). The in vitro data showed that a sharp increase in cam–post contact force was measured at around 90^o, accompanied with an increase in posterior femoral translation. Knee simulators have also formed a useful tool in determining contact stresses at the cam-post interaction. In their paper on contact area and contact stress at the cam-post interaction, Nakayama, et al., utilized the use of knee simulators to investigate three different TKA designs at three static flexion angles (90, 120 and 150 degrees). They found that the peak contact stress varied between 22.1 to 34.1 MPa. However, as mentioned above (see section 3.2), this study did not reproduce any of the physiological conditions that would be routinely encountered by a patient having a TKA.

Hence, an in depth study of mechanics (kinematics, kinetics and stresses) of the cam-post interaction in fixed and mobile bearing TKA devices is necessary to provide a better understanding of such a long standing dispute.

3.5 Vibroarthrography of the Knee

3.5.1 Historical background

Knee joint pain is one of the most frequently reported musculoskeletal complaints in all age groups. Most often the patient's complains are nonspecific and the correct diagnosis may be difficult. The diagnosis is often limited to detailed interview with the patient, careful physical examination (palpitation) and x-ray imaging. X-ray screening may reveal bone degeneration, but does not carry sufficient information of the soft tissues' conditions. More advanced imaging tools such as MRI or CT are available, but expensive, time consuming and are suitable only for detection of advanced arthritis. The arthroscopy is often the only reliable option, however due to its semi-invasive nature, it cannot be considered as a practical diagnostic tool.

Early physicians examining knees noticed that the joints often make certain noises while evaluated under functional tests, or even during everyday use. These noises may exist because, when the bones are in motion the interaction between articulating surfaces induces vibrations of the bones, that may reach audible level. In a healthy joint the articulating surfaces are smooth and the vibration is minimal, but as the cartilage degenerates, the articular surfaces become rougher and vibrations increase, and may become audible. Therefore the auscultation of the knee joint has been considered an interesting and promising alternative to the abovementioned techniques.

The first attempts to use auscultatory tools to the diagnosis of the pathological changes were used in the 19th century. Heuter (Heuter 1885), in 1885 was the first to use myo-dermato-ostetoscope to localize the joint bodies. In 1902, Blodgett (Blodgett 1902) used a stethoscope to auscultate the knee joints and noted that the sound increased with the age of the subjects. He reported creaking, grating and cracking sounds present in chronic arthritic joints. In order to determine if the auscultation offers any practical value in distinguishing between different forms of joint affections, in 1929, Walters examined nearly 1600 knee joints (Walters 1929). He categorized the joints into 5 groups: *smooth*, *rough*, *grating I*, *grating II* and *grating III*, and found, similar to Blodgett, that joints became more rough with age. The joints appeared smooth in the first decade of life but the rough and grating noise increased with increasing age and 81.5% of subjects in their 80s were audible (Figure 3-3).

Later, joint sounds were studied to investigate the patella chondromalacia, different types of arthritis and meniscus lesions (Steindler, 1937, Peylan 1953, Erb 1933). Fisher and Johnson (Fisher 1961) found that the rheumatoid arthritis could be recognized in the early stage, before the changes could be observed in x-ray images. However, these evaluations of the knee joint sounds were subjective and lacked a more precise, repetitive methodology.

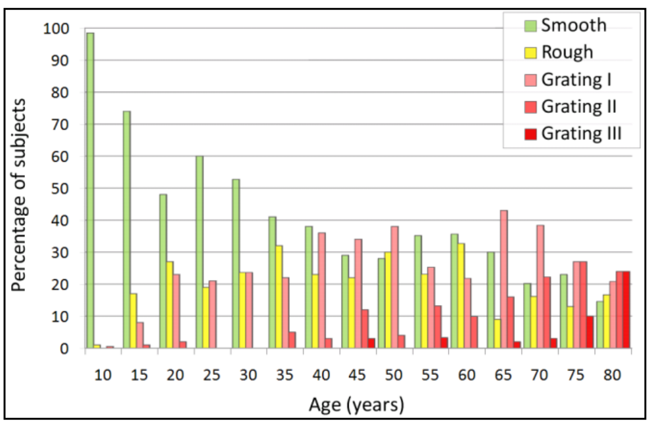

Figure 3-3: Walters 1929 experimentation on 1600 knees. ***Source: Walters et al*****.**

Therefore the auscultation of the knee joint has been considered an interesting and promising alternative to the abovementioned techniques.

The first graphical presentation of the joint sounds was presented by Erb in 1933. The author investigated chondromalacia of the patella, arthritis and meniscus lesions, and reported low frequency of meniscus sounds. Later, Steindler practiced ausultation of joints, particularly knee and used cardiophone (Figure 3-4) because its soft-rubber attachment helped to eliminate the friction noises of the skin.

[A cardiophone used to study of the auscultation of the knee joint.]

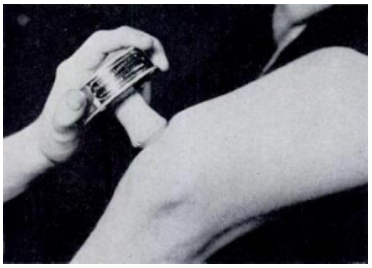

[Experimantal set-up used by Steinler in 1933.]

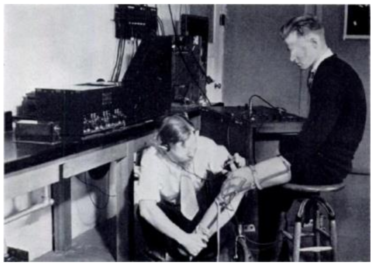

Figure 3-4: Steinler experiment using cardiophone (top**) to minimize the friction noises of the skin.** ***Source: Steindler.***

Peylan, in 1953, investigated 214 patients with different types of arthritis by the means of a regular and an electronic stethoscope (Peylan 1957). Fisher and Johnson (Fisher 1961) found that rheumatoid arthritis could be recognized in the early stage, before the changes could be observed in x-ray images. However, these evaluations of the knee joint sounds were subjective and lacked the more precise, repetitive methodology. The first objective methods, based on statistical parameters of the signals were proposed by Chu et al. in late 1970s (Chus 1976, 1978). The authors used a double-microphone differential-amplifier sound-retrieval setup to record the knee joint sounds. They found that the normal knees had very low acoustic power output (ranging from 0-0.02 W/cycle), while the pathological knees revealed significantly higher power outputs (Figure 3-5). They noted that on average the acoustic power varied logarithmically with the surface roughness.

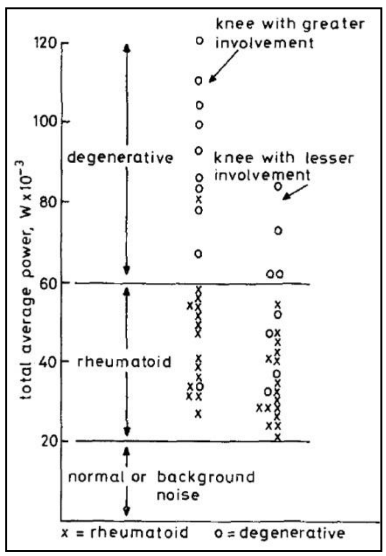

Figure 3-5: Chu's experiments to classify the knee joint conditions based on the relative acoustic power. ***Source:Chu 1976.***

Further improvements were done by Mollan et al. who compared the joint vibration detected using microphones and accelerometers and concluded that the microphone was a poor transducer in terms of frequency and dynamic sensitivities for use with human joint emission. Particularly limiting the use of microphones, were the skin friction noise and the ambient room noise. Therefore, they replaced the microphone with three tiny accelerometers taped around the knee (Molan 1982, 1983, Kernohan 1982, 1986, McCoy 1987). The authors also used a goniometer to simultaneously record joint angle so that any episode of emission might be referred to a flexion angle. They extensive works gave good understanding of the nature of the knee joint signals, they diagnostic potentials and possible practical problems with vibration arthrography.

The decision made by Molland et al. to replace microphones with accelerometers was later proven to be right, by scientists studying sounds emitted by temporomandibular joint (TMJ) (Gay 1988, 1987, Christensen 1992 (i), 1992 (ii), 1992 (iii), Ishigaki 1993). Christiansen et al. (Christensen 1992 (i)) reported that the condenser microphone is highly sensitive to 'irrelevant' sound fields leading to artifact information of any airborne wave. They recommended that in general microphones should not be used for recording TMJ sounds - only accelerometers could be advocated for recording of solid borne TMJ vibrations. In the next study, Christiansen further noted that errors were found in sound frequency measurements recorded with microphones, while comparable measurements made with skin-contact vibration transducers were accurate (Christensen 1992 (i)). Similar conclusions were described by Kernohan et al. in an article reviewing the development of various techniques to evaluate sounds from human joints (Kernohan 1982).

Parallel to the technological developments of the recording devices, new mathematical methods were also proposed. Since the vibroarthrogaphic signals are inherently nonstationary, the Fast Fourier Transform (FFT) could not be accurately used to localize the frequency content in time and therefore to correlate the abnormal signals with the joint kinematics. The Windowed Fourier Transform (WFT, also called Short-Time Fourier Transform, STFT) offered some help in localizing the frequency content in the time domain, but the breakthrough came with the introduction of the wavelet transform. Using the continuous wavelet transform, signals can be locally characterized in both the time and frequency domains simultaneously and self-adaptively. The pattern recognition techniques have also undergone significant development and nowadays advanced signal classifiers are built as neural networks. The wavelet theory and pattern classification techniques have found countless applications and are among the fastest developing methods at present. The use of the new sensors and analytical tools accelerated the development of the vibroarthrography and resulted in a number of clinical trials, publications and patents (Gay 1989, Radke 1995, 1996, Rangayan 2003, Russell 1989) and has a great potential of becoming a reliable diagnostic tool for early diagnosis of patellofemoral disorders.

3.5.2 Current research

Currently, in our laboratory, the vibration signals are derived, most frequently, by means of highly sensitive, miniature accelerometers attached externally to the skin by an adhesive or elastic wrapping tape. The vibrations are recorded while the subject is asked to perform various activities, such as flexion-extension of the knee, gait, squat etc. During these activities, the entire knee joint is moving. Thus, the sensors record the changes in acceleration resulting from both, the motion and the vibration. Generally, the bones move less rapidly than they vibrate, therefore it is possible to decompose a raw vibroarthrogram into the motion and vibration components by using a low-pass filter. Next, the signal-to-noise ratio of the vibration signals is often increased by using adaptive TF decomposition methods (Krishnan 2000)

Then statistical parameters of these signals are extracted and processed by pattern recognition algorithms. Usually a database containing a larger number of training datasets is build so that the pattern of a new signal can be compared to datasets of known conditions and classified as indicating a pathology or a lack of it, similarly to the existing techniques employed in ECG or EEG.

Krishnan et al. (Krishnan 2000 (ii)) used an adaptive time-frequency distribution to calculate entropy, energy spread, frequency and frequency spread of the VAG signals and was able to discrimante the normal vs. abnormal conditions with up to 77.5% accuracy. Umapathy and Krishnan (Umapathy 2006) used wavelet packet decompositions and modified local discriminant bases algorithm and obtained accuracy as high as 80% on a set consisting of 51 normal and 38 abnormal samples. More, recently Rangayyan and Wu (Wu 2008) used simpler statistical parameters, such as form factors, skewness, kurtosis and entropy and were able to obtain comparable accuracies to the aforementioned, more sophisticated methods. Application of simpler statistical features, however, required application of a more sophisticated algorithm based on radial basis functions network.

Jiang et al. (Jiang 2000) applied vibration arthropometry to study patients with total knee replacement. They found that VAG signals in rapid knee motion can be used to detect early stage of polyethylene wear of the patellar component. They were also able to detect prosthetic metal wear in the late stage, when the knee was being swing slowly, at 2^{o}/s speed.

Analysis of vibration signals from the knee joint has been found to be successful in determining knee joint conditions at an early stage. Also, data can be captured at much higher frequencies, ensuring that important findings can be derived, whereas other data capturing modalities that utilize lower capture frequencies may miss these findings. Further development of such techniques may one day provide the care giver with options that are less-invasive compared to TKAs or at the very least prolong the time for the patient before they have to receive one. Extending the capability of vibration analysis to be able to directly correlate with in vivo kinematics is the next step in the evolution of vibroarthrography. It will provide for comparison of specific vibration patterns with knee joint motion as well as knee joint condition, and will make it possible to determine a more direct cause-and-effect relationship between the two. Hence, while discussing the mechanics of the knee joint a look at such innovative techniques becomes imperative.

Chapter 5: Materials and Methods

4.1 Patient Selection

The patients selected for this study were part of two different kinematic studies conducted at the center for Musculoskeletal Research. Eight subjects (9 TKA) implanted with a PFC Sigma RP-PS TKA (DePuy Inc), five subjects (5 TKA) implanted with a NexGen FB-PS TKA (Zimmer Inc) and nine subjects (10 TKA) implanted with the Journey BCS TKA were selected (Smith & Nephew Inc). Each set of TKAs was implanted by the same surgeon. The implanted knee (left or right), age of the patients and post-op time was kept as close to equal as possible (Table 4-1). This was done in order to create a more controlled data set during analysis. Each subject was asked to perform a series of successive weight-bearing deep knee bends cycles on the implanted knee. Patients were examined while performing these activities using a C-Arm type fluoroscopic unit. The fluoroscopic images were stored on videotape for subsequent re-digitization and analysis using a frame grabber.

Table 4-1: Demographic information for all patients.

GROUP	# OF SUBJECTS	# OF TKA	AGE (YEARS)	SIDE	POST-OP TIME (YEARS)
RP-PS TKA	8	9	68 (50-77, SD=6.9)	4 Left, 5 Right	4.9 (4.7-5.1)
FB-PS TKA	5	5	66 (55-78, SD=6.1)	5 Right	3.7 (3.2-4.1)
FB-BCS TKA	9	10	67.1 (40 to 82, SD=8.9)	5 Left, 5 Right	4.1 (3.9-5.5)

For the vibroarthrography part of the study, a different set of 76 native knee (both arthritic and normal) patients and 8 failed TKA patients were enrolled for the study. This cohort included five category of patients:

1. Normal well functioning knees
2. Older well functioning knees
3. Arthritic knees
4. Well functioning TKAs
5. Failed TKAs

During examinations, each patient was asked to perform a number of different activities. These included: Deep knee bend, gait, leg swing (2 second cycle and 4 second cycle), chair rise and stair assent and descent. The vibration data was correlated with either fluoroscopy driven 3D kinematics or detailed cartilage condition information provided by the surgeon (for arthritic knees).

4.2 Fluoroscopy

To collect the fluoroscopy data, each patient was asked to stand within the scope of a C-arm fluoroscopy unit. The fluoroscopic machine was operated by a certified radiation technician. The use of fluoroscopy allows for the formation of a basic projection image, captured by passing pulsated radiation through the subject's joint and onto an image intensifier (usually a ten to twelve inch diameter circle). A high frequency pulsed fluoroscopy unit (OEC 9800, General Electronic Medical Systems, Salt Lake City, Utah, USA), consisting of a C-arm with high resolution intensifier and a high power rotating anode X-ray tube was used in this study.

The patient was asked to place their implanted knee close to the image intensifier and the non-affected knee placed outside the intensifier range. The subject then performed a deep knee bend from full extension to maximum knee flexion, moving at a slow pace. The patient was asked to keep the foot of the affected knee firmly planted on the ground at all times (Figure 4-1). The fluoroscopic video was captured at 30 frames per-second with a resolution of 720x680 pixels.

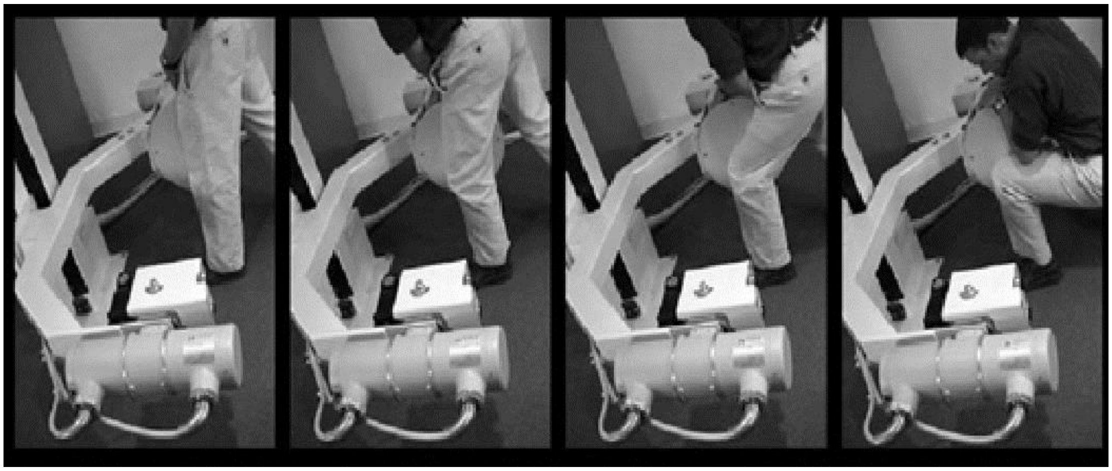

Figure 4-1: Fluoroscoping the Deep Knee Bend Activity (Mahfouz, 2003).

The captured videos (720*480) were broken down into still images of size 640 x 480 and were saved in tiff format in order to gain the best quality. For each patient, images from zero to maximum flexion at increments of 10° of flexion were used for the analysis.

4.2.1 Image distortion removal

The individual fluoroscopic images are distorted due to the effects of pincushion and spiral distortion. Pincushion distortion is caused due to mapping of electrons from the input screen of the image intensifier, which is curved, to the flat output screen. This phenomenon is dependent on the distance between the X-ray source and the image intensifier and causes larger magnification at the periphery of the final image than at the center of the image.

Spiral distortion, also known as S-distortion, is due to the effect of the magnetic field encompassing the image intensifier. The component of the magnetic field parallel to the image intensifier affects the radial electron velocity thereby causing a rotation of the image. The transverse component of the magnetic field affects the longitudinal electron velocity causing a translation of the final image. This generates the resultant image with a characteristic S-shape.

The distortion, within each fluoroscopic image, was corrected using the image of a board containing beads, at known positions, which acted as control points (Figure 4-2). By comparing the known positions of the control points with it corresponding location in the distorted image, transformation coefficients for each pixel of the image is determined (Mahfouz, 2003). By applying the obtained transformation coefficients on the distorted image, the true image is recovered.

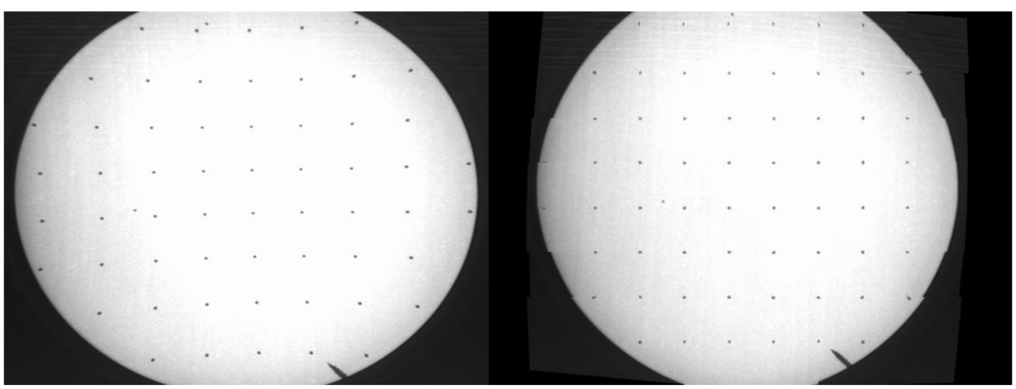

Figure 4-2: Image of distorted bead board (left) and correct image (right).

4.2.2 3D-to-2D registration algorithm

This is a semi-automated process that uses direct image to image similarity measure and works on the principle of recreation of the 3D scene in which the patient was fluoroscoped. This requires the calibration of the camera for the fluoroscopic unit. The CAD models are loaded in the software with their geometrical center coinciding with the global origin of the system. The geometrical center of the CAD models are found by drawing a 3D bounding box and then joining the diagonals. The common intersection of the diagonals is the geometrical center. For the automated process to start, the user must orient the models (translate and rotate) to the pose they feel is the best estimate. Starting from this initial pose, the models are automatically oriented to their final position by the use of an automated optimization algorithm known as Simulated Annealing (SA). In its search for the global minimum, the SA algorithm searches the 6-dimensional space (3 rotational and 3 translational) and needs a metric for scoring how the pose of the model compares with that of the fluoroscopic image. This is done using the fluoroscopic image (input image) and a 2D projection image of the model (predicted image) which is generated in white against a black background. Using morphological operations, edge images are created for both the input and the predicted images. Also the input image is inverted to be similar in color with the predicted image (Figure 4-3).

The match between the input image and the predicted image is calculated by two metrics. The first metric compares the pixels of the predicted image and the inverted input image. The second metric evaluates the overlap of the contours in the edge images generated for both the input and the predicted image. The final matching score is obtained by multiplying the two images together, summing the result and then normalizing it with the sum of the predicted image. This method has been found to be robust and converges to the global minimum and is insensitive to image noise and occlusions.

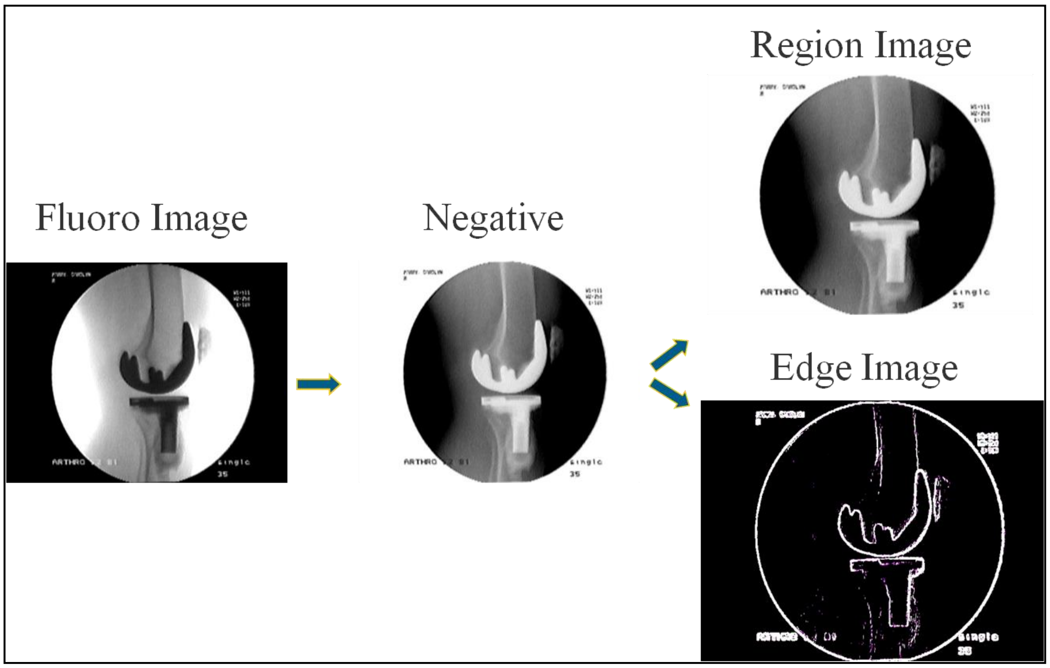

Figure 4-3: Original Image (left); Inverted Image (center); Region Image (Right top) and Edge Image (right bottom) (Mahfouz, 2003).

4.2.3 Error Analysis

An error analysis has been conducted using a fresh cadaver, to verify the accuracy of the 3D-to-2D registration process. The tested included placing discrete points on the femoral and tibial components. Using an Optotrack system (Northern Digital Inc., Waterloo, Canada), these points were digitized and the femur was defined relative to the tibia, in the tibial reference frame. Each orientation of the femur, relative to the tibia was fluoroscoped. Using the 3D model-fitting software package, the relative orientation of the femur with respect to the tibia was predicted and compared to the known orientation determined using the Optotrack system. The results from this error analysis and accuracy tests revealed average errors in X, Y, and Z translations that were -0.023, -0.086, and 1.054 mm respectively (standard deviations were 0.473, 0.449, and 3.031 mm, respectively). Likewise, the average errors in x, y, and z rotations were -0.068, 0.001, 0.253 degrees (standard deviations were 0.942, 0.771, and 0.841 degrees, respectively). These numbers represent the errors in the model-fitting process plus the errors associated with the independent measurement system as well (i.e. the upper bound). Since the knee joint is imaged in the sagittal (XY) plane, then the relative translational motion of the implants in the Z direction is minimal and is not of interest for this study.

4.2.4 Determining 3D orientations

Utilizing the above mentioned three-dimensional (3D) model fitting approach, the relative poses of the femoral and tibial knee implant components is determined in 3D using a single-perspective fluoroscopy image in the sagittal plane and manipulating CAD models in three-dimensional space.

In the case of the Sigma RP-PS TKA, the 3D orientation of the radiolucent polyethylene (PE) bearing is by embedding four metallic beads in the PE insert during the manufacturing process. Subsequent CAD models of the PE component having the strategically positioned beads are also created. Since three non-collinear points are needed to define a rigid body’s spatial orientation, the four beads are inserted out-of-plane and as far away from one another as possible without compromising the integrity of the insert. This increases the probability that at least three of the beads are visualized during fluoroscopy and enabled for determination of the PE CAD model's position using the same 3D model fitting technique previously mentioned.

A three-dimensional scene of the fluoroscopic unit is created using a client based server application on the Windows (Redmond, WA) platform using the Open Inventor Toolkit (Mountainview, CA) library. The scene consists of a light source (x-ray), an image plane on which to project the fluoroscopic image (image intensifier), an area to manipulate a 3D model (subject area), and a camera to view the entire scene.

Individual fluoroscopic frames at specified degrees of flexion for the deep knee bend activity. The images are projected onto the image plane with the corresponding implant models added to the scene. Initially, the 3D orientations of the femoral and tibial components are positioned by the operator manipulating the 3D CAD models into a position closely corresponding with their respective silhouettes in the digitized fluoroscopic image (Figure 4-4). Then the automated computer algorithm uses intensity-based matching to determine the best orientation of the models. In order to determine the 3D orientation of the polyethylene component, the PE insert is made transparent, which results in only the embedded beads within the CAD model being visible. The bead portion of the PE insert is then matched to the fluoroscopic silhouettes of the imbedded beads (Figure 4-5). Once complete, the full orientation of the PE insert can be seen.

In the case of the fixed bearing Journey BCS TKA the polyethylene insert is rigidly fixed to the metallic tibial tray and there is no relative motion between the tibial component and the polyethylene insert. In order to achieve the correct 3D orientation, the polyethylene CAD model is fixed to the tibial CAD model before the overlay process.

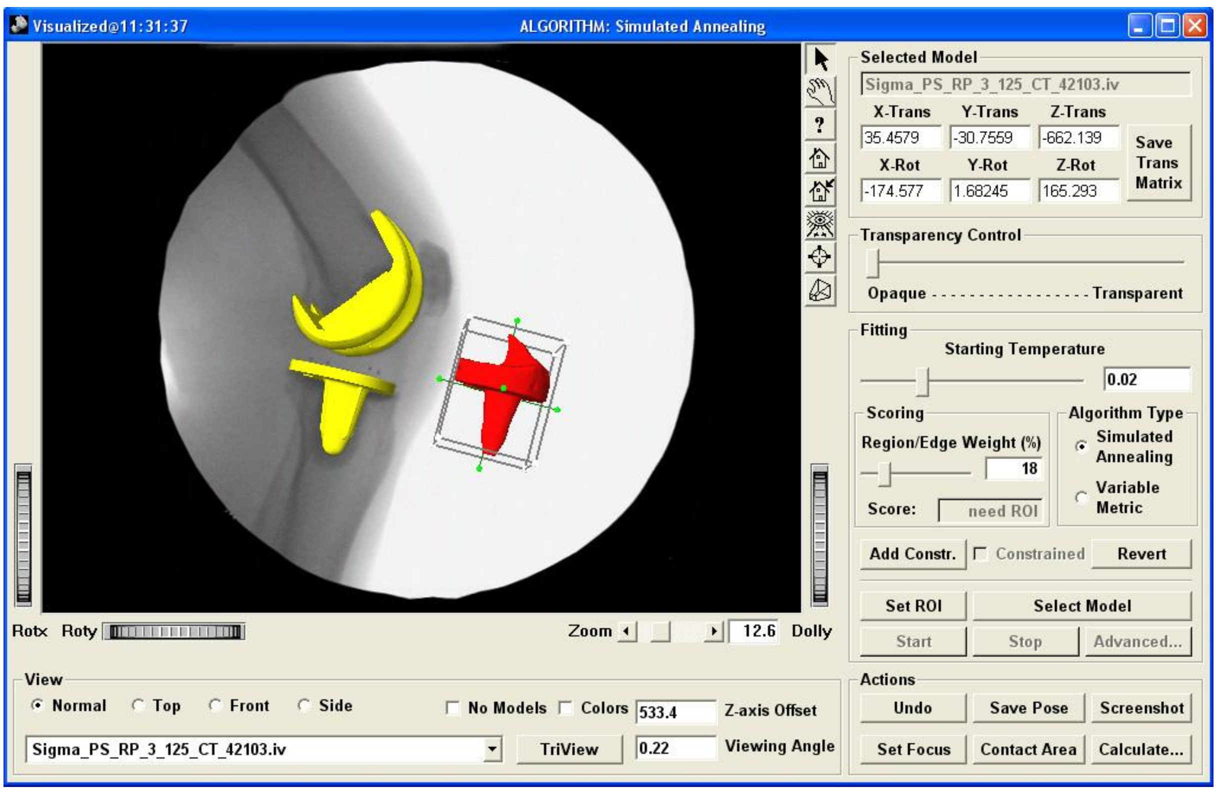

Figure 4-4: User interface of model fitting software.

The correct fit for each of the models is achieved when the silhouettes of the femoral and tibial components and the beads embedded (only for Sigma RP-PS) in the polyethylene bearing best matched their corresponding components in the fluoroscopic image (Figure 4-6 and 4-7).

Figure 4-5: Fluoroscopy image with femoral and tibia CAD model of Sigma PS RP TKA and four visible bead silhouettes that allow for proper positioning of PE bearing when silhouettes match.

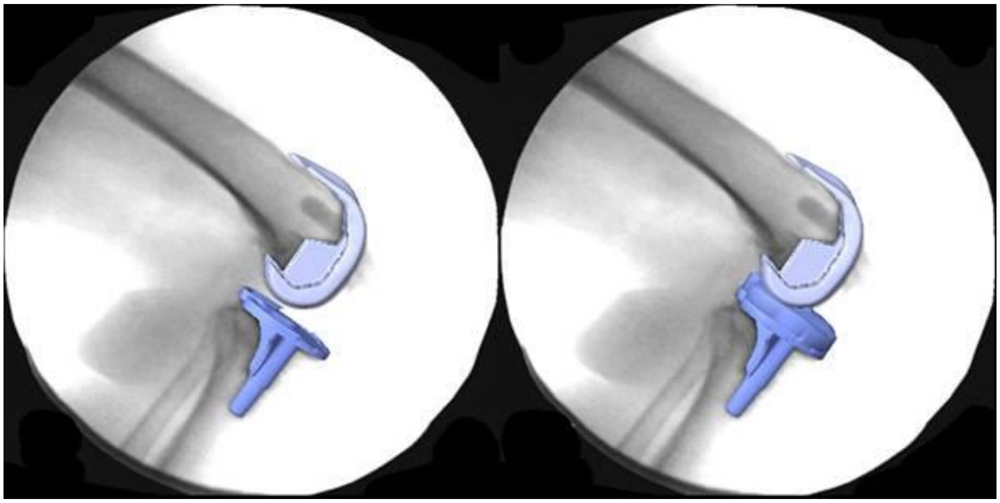

Figure 4-6: Fluoroscopy image from Journey BCS patient at 90° with registered 3D CAD models of femoral and tibial components (left) and the same fluoroscopy image with tibial and polyethylene insert model combination in same orientation as the registered tibial component (right).

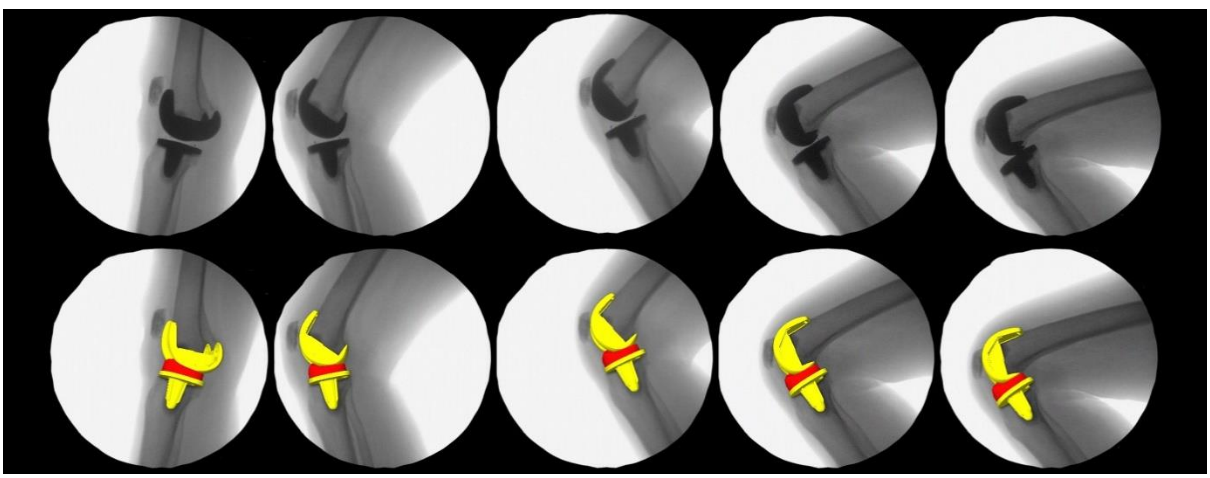

Figure 4-7: Series of digitized fluoroscopy images (top row) and corresponding fluoroscopy with CAD model overlay (bottom row) from a random subject with a Sigma RP-PS TKA.

4.2.5 Generating required kinematics

4.2.5.1 Tibio-femoral kinematics

Once the 3D-to-2D registration technique was completed, the 3D implant orientations were imported into an in house developed software package called Kinetic Analysis of Rigid Body Systems (KARBS). This package developed in MATLAB (Mathworks, NC©) enables for further determination of kinematic parameters of interest at the tibio-femoral and cam-post interface of the TKA implant components. Using this package, the anterior/posterior (A/P) contact positions for both the medial and lateral condyles, axial rotation of the femoral component relative to the tibial component, axial rotation of the tibial component relative to the polyethylene bearing component and weight-bearing range-of-motion (ROM) is evaluated.

4.2.5.2 Cam-post analysis

Since the cam-post interaction is of particular focus to this study, the analysis to determine the flexion angle of cam-post contact and the contact area is carried out with higher precision than tibio-femoral calculations. This involves the following steps:

1. The mesh size of the femoral cam and the tibial post are imported into a CAD software and the mesh size pertaining to those areas are refined to contain ≈10000 tetrahedral elements (Figure 4-8).

2. The refined models are then re-introduced into KARBS and the contact between the cam and the post is determined. This is done by designating the femoral cam and the tibial post parts of the models as separate surfaces.
3. Next the contact algorithm of the KARBS package is executed to determine the distance between the corresponding polyethylene and femoral condyle.
4. This analysis is conducted for every degree of flexion from full extension to maximum knee flexion. A distance of less than 1mm is considered to signify contact between the femoral condyle and the polyethylene insert. The center of this area is assigned as the contact location (on both the surfaces) and the flexion angle at which contact is first determined is assigned as the cam-post contact angle (Figures 4-9 and 4-10).
5. All elements on the tibial post that have a distance of less than 1mm with any element in the femoral cam are assigned a red color and increasing distances between the two surfaces are designated other color codes. This provides an estimated contact area between the two surfaces.
6. Once this analysis is completed, six parameters are determined:
    a. Cam-post contact angle.
    b. Cam-post contact area (only the elements less than 1mm distance area considered).
    c. Distance between the femoral cam and the tibial post throughout the DKB activity (Figure 4-11).

d. Height of the contact point on the tibial post with respect to the medial tibio-femoral contact point.

e. Height of the contact point on the tibial post with respect to the lateral tibio-femoral contact point (Figure 4-12).

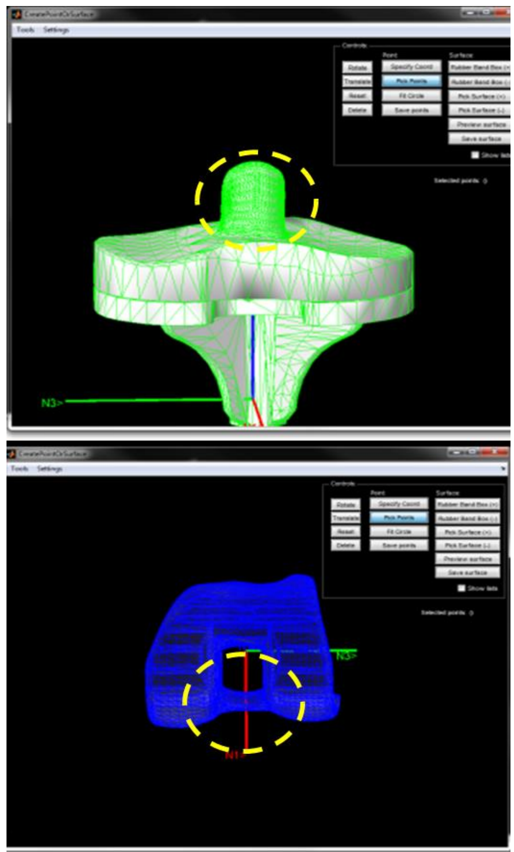

Figure 4-8: Refined meshing of the cam-post interaction.

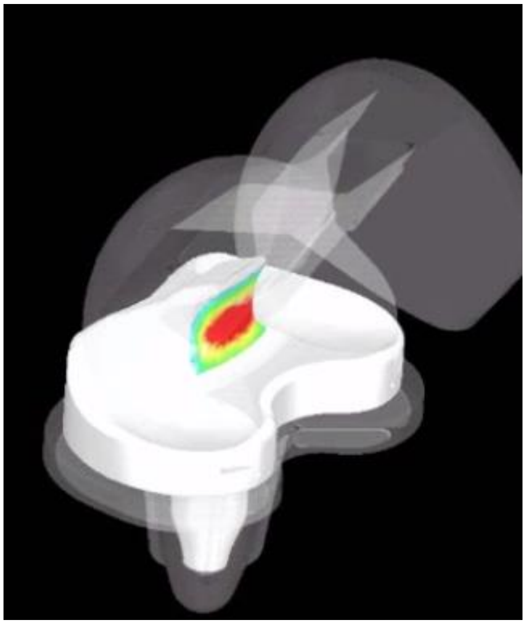

Figure 4-9: Cam-post contact determination in the Sigma PS-RP TKA.

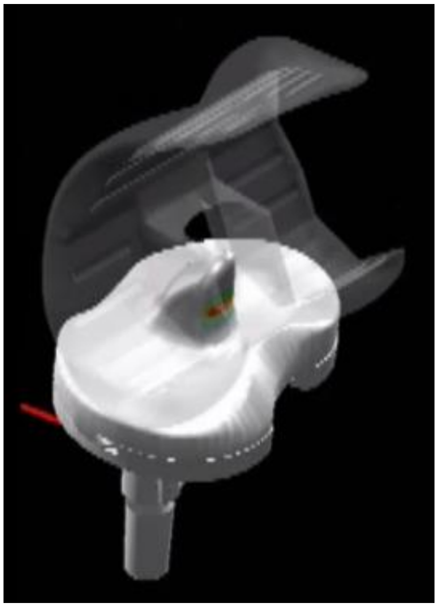

Figure 4-10: Cam-post contact determination in the Journey BCS TKA.

Figure 4-11: Cam-post contact distance determination in the Sigma PS-RP TKA.

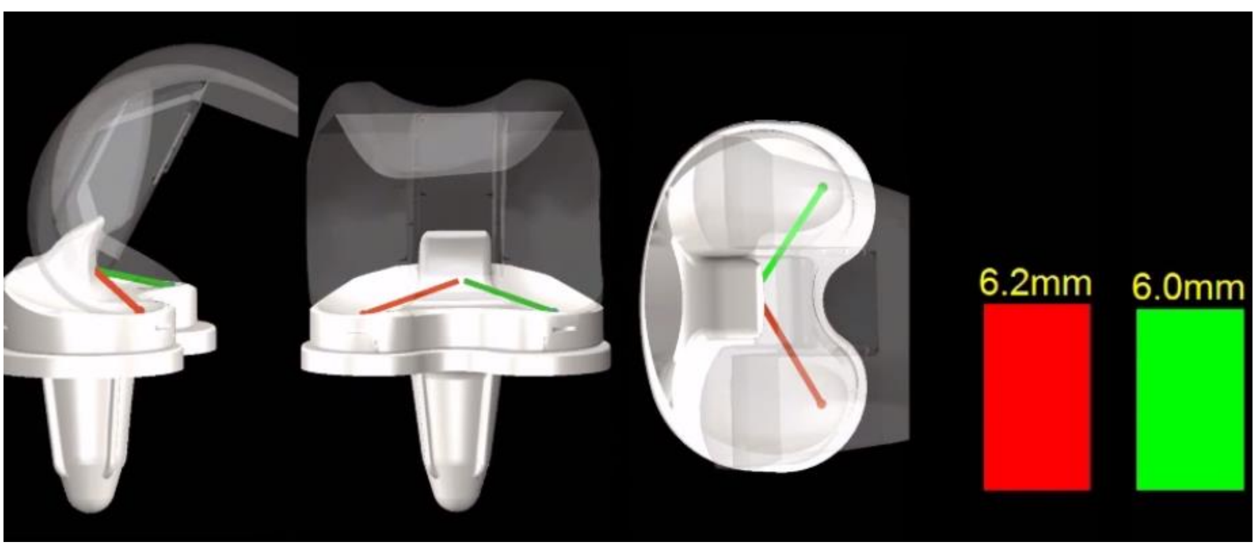

Figure 4-12: Cam-post height of contact determination in the Sigma PS-RP TKA.

4.3 Mathematical Modeling

In order to predict the in-vivo forces during the deep knee bend activity, a forward dynamics model was created. This model is based on the principle of rigid body dynamics and utilizes the reduction technique, where, the system is always kept determinate by keeping the number of unknowns equal to the number of equations. The underlying assumption in this technique is that certain muscles, which do not influence the system significantly, are neglected. Moreover, the modeled muscles are grouped together and it is assumed that the force within the grouped muscles represents a good estimate of the force acting within each separate muscle. The model was developed using Autolev^{TM} (Online Dynamics Inc, Sunnyvale, CA), a symbolic manipulator based on Kane's dynamics (Kane, 1985; Komistek, 1998). This method is extremely efficient and well suited for multibody systems having large degrees of freedom. This method allows for the solution of a maximum of six kinetic terms associated with each rigid body.

4.3.1 Model Description

The forward solution model (FSM) acts as an in vivo simulator of an implanted human knee joint performing a deep knee bend. This simulator functions by using either five or six rigid bodies depending on whether a fixed bearing (FB) or mobile bearing (MB) implant is being analyzed. For FB simulations, the foot, tibia, femur, patella, and pelvis/trunk are the bodies modeled. In the case of RP simulations, the polyethylene is also defined as a separate body. Furthermore, various soft tissues surrounding the knee as well as quadriceps and hamstrings muscles are included.

The FSM, written in the AUTOLEV language allows ridged body systems to be defined by inputting all known positions, forces, and torques. Then, the equations of motion were solved for using Kane's dynamics. A C++ file was automatically generated based on these equations of motion which calculated the motions and forces from the system at iterative time steps using a Runge-Kutta method. This system is capable of either a forces in/motions out, motions in/forces out, or any combination thereof. In the FSM, some motions are specified (tibia and pelvis rotations and translations) while other motions are solved for (femur and patella translations and rotations). Furthermore, tibiofemoral, patellofemoral, hip forces, and quadriceps forces are were calculated. The intersection of the foot and tibia was defined by sequential rotations about the subtalar axis and the ankle axis. The intersection of the femur and pelvis was defined as a ball of socket joint which keeps the center of the femoral head aligned with the center of the pelvis. The joints at the knee featured a much more complex definition which employs the actual geometry of the implants. The contact detection at the knee surfaces worked by defining a polynomial surface to the region of interest on one body and a point cloud to the region of interest on the other body. For example, at the patellofemoral joint, the trochlear groove was defined with a polynomial surface (Figure 4-13). A point cloud was defined on the patella (Figure 4-14).

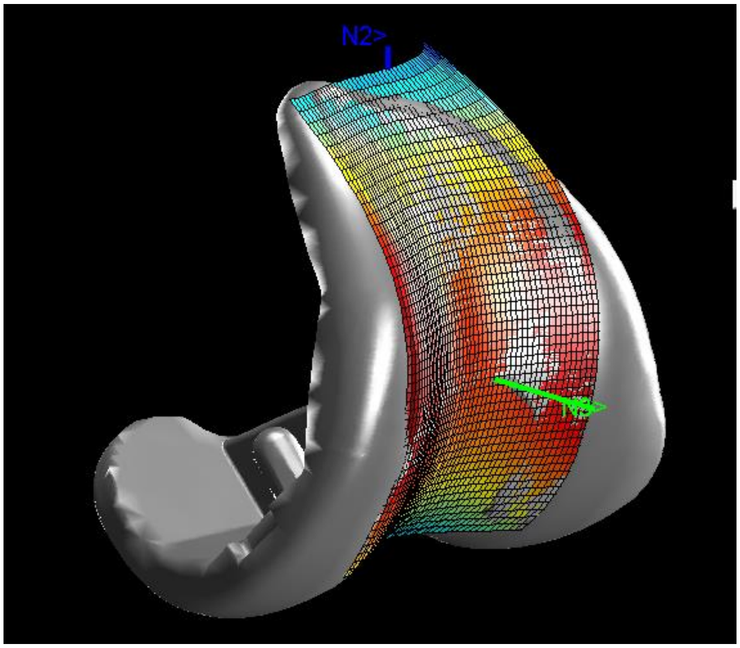

Figure 4-13: Definition of the trochlear groove surface of a Sigma PS-RP TKA.

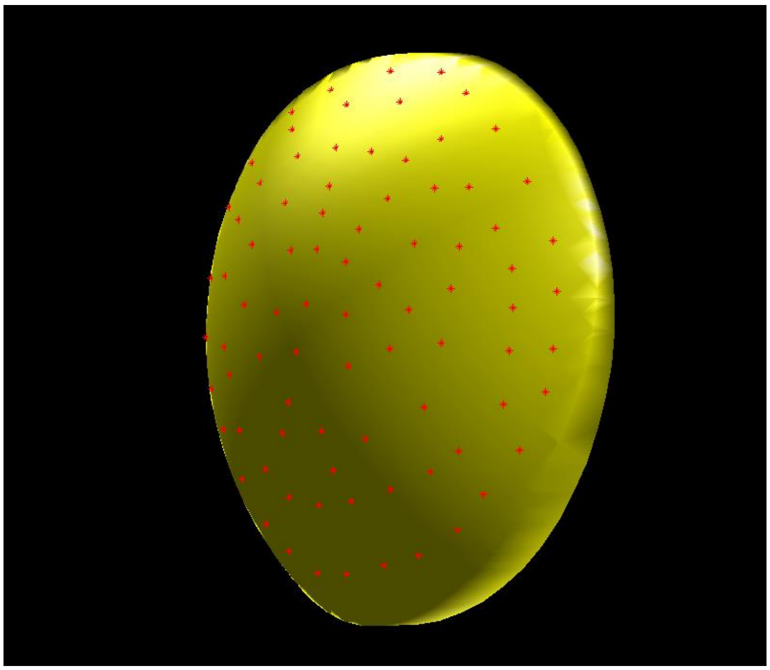

Figure 4-14: Definition of the patella button surface of a Sigma PS-RP TKA.

Then during the simulation, the model checked the height of each point in the trochlear reference frame versus the height of the polynomial at the corresponding location. If the point height was less than the polynomial height, contact was detected and a force proportional to the penetration depth was applied at the point along the normal vector of the polynomial. The same method was applied using a point cloud on the femur and a polynomial on the polyethylene (Figure 4-15 & 4-16). Finally, the post was defined using a polynomial and 12 contact points defined on the post (Figures 4-17 & 4-18). The number of contact points on the post was kept small to allow easier determination of which specific area of the cam the force was occurring on (Figure 4-19).

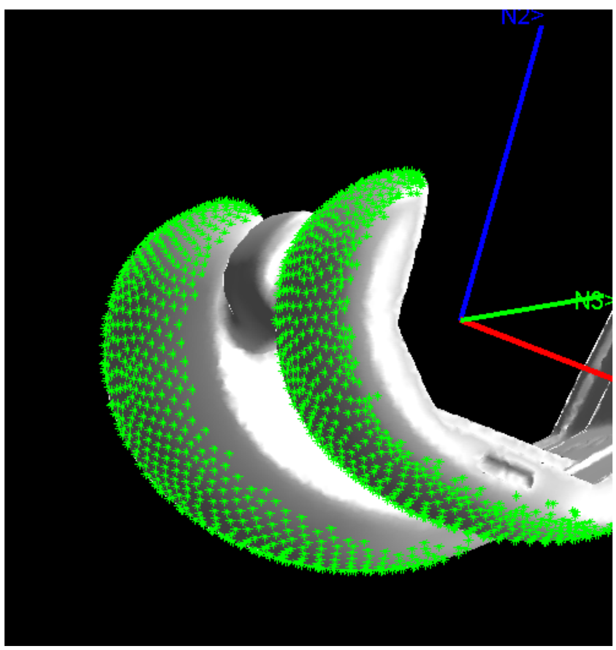

Figure 4-15: Definition of the tibio-femoral contact surface on the femur for a Sigma PS-RP TKA.

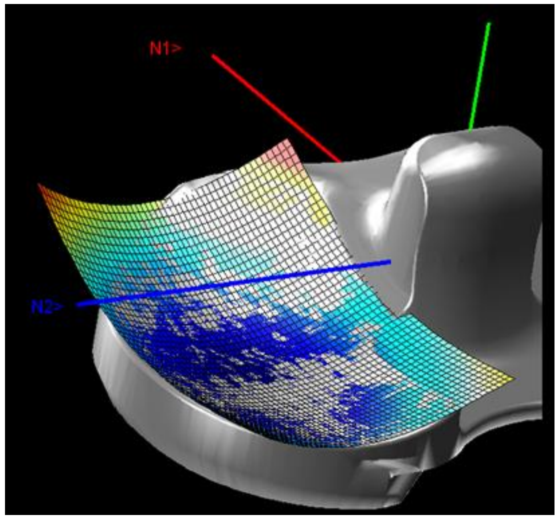

Figure 4-16: Definition of the tibio-femoral contact surface on the tibia for a Sigma PS-RP TKA.

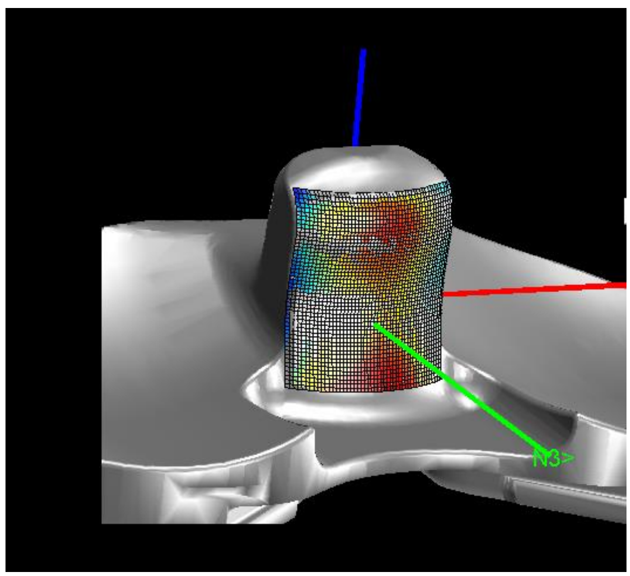

Figure 4-17: Definition of the cam-post contact surface on the tibia for a Sigma PS-RP TKA.

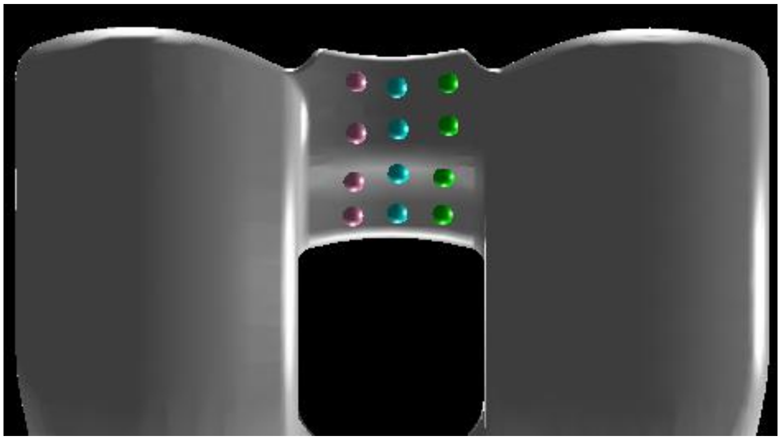

Figure 4-18: Definition of the cam-post contact surface on the femur for a Sigma PS-RP TKA.

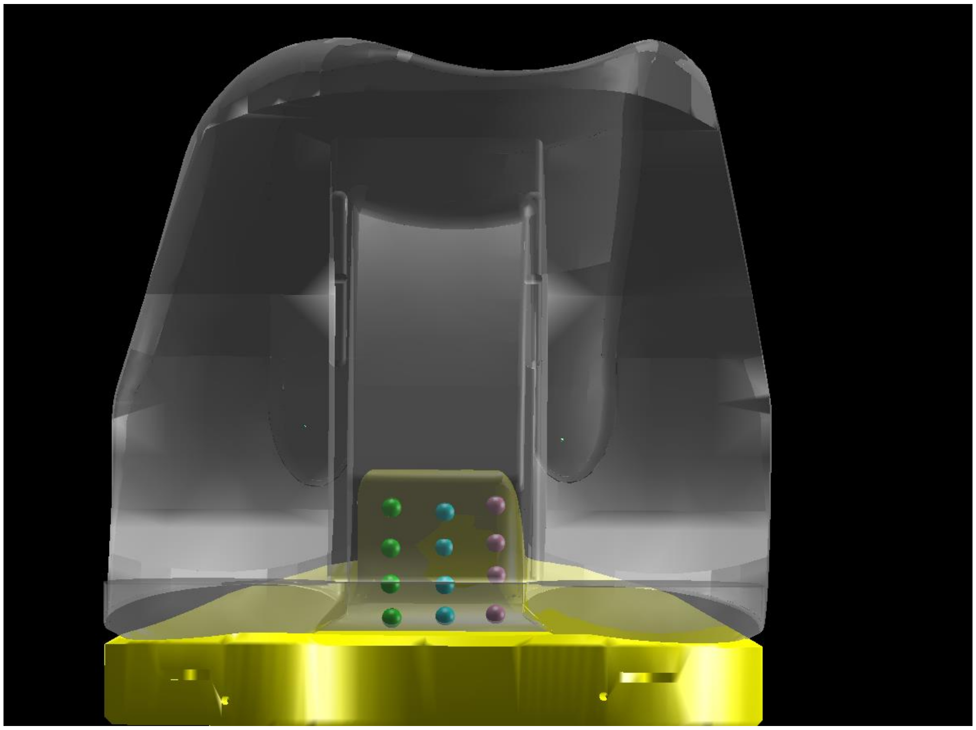

Figure 4-19: Determination of cam-post contact for the forward dynamic mathematical model.

In addition to the joint bearing surface forces, the model also incorporated the force of the medial collateral ligament, lateral collateral ligament, medial patellofemoral ligament, and the lateral patellofemoral ligament. The anterior and posterior cruciate ligaments can be included, but were not in these simulations as both of those ligaments were resected during the surgeries. Furthermore, the patella was connected to the tibia via four bundles of the patellar ligament. These soft tissues were modeled as nonlinear springs. The medial collateral ligament was modeled as three different bundles to incorporate both the deep and superficial bundles allowing the proper forces throughout flexion.

In additions to the ligaments, the four quadriceps muscles as well as the hamstring muscle were modeled. The hamstring muscle was input as a known function (typically a constant). However, the quadriceps force was computed using a proportional, integral, derivative (PID) controller (Figure 4-20). The controller attempts to match the flexion rate to a desired flexion rate, which is input (Figure 4-21). This controller functions by adjusting the quadriceps force based primarily on the velocity error of the flexion vs the desired flexion. If the knee is flexing faster than desired, the model increases the quadriceps forces to slow it down. To provide more stability, the derivative of velocity is also controlled (acceleration). Because the rate of flexion is a constant for most of the activity, the model also adjusts the muscle forces to keep accelerations low. The model also adjusts the muscle force based on the integration of the error between the desired flexion and the actual flexion to avoid a steady state error in the velocity.

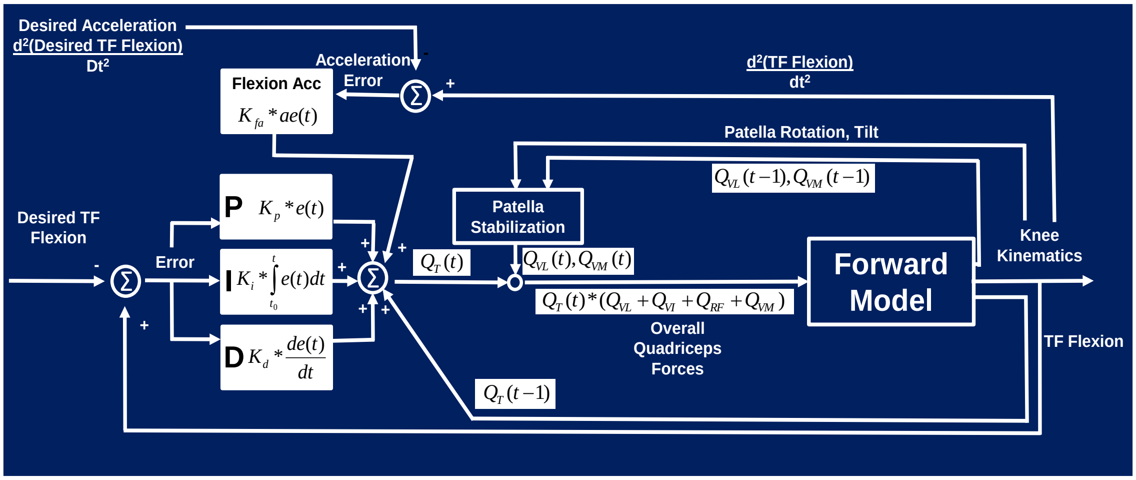

Figure 4-20: The PID controller used in the forward dynamic model to control quadriceps muscle forces (Mueller et al).

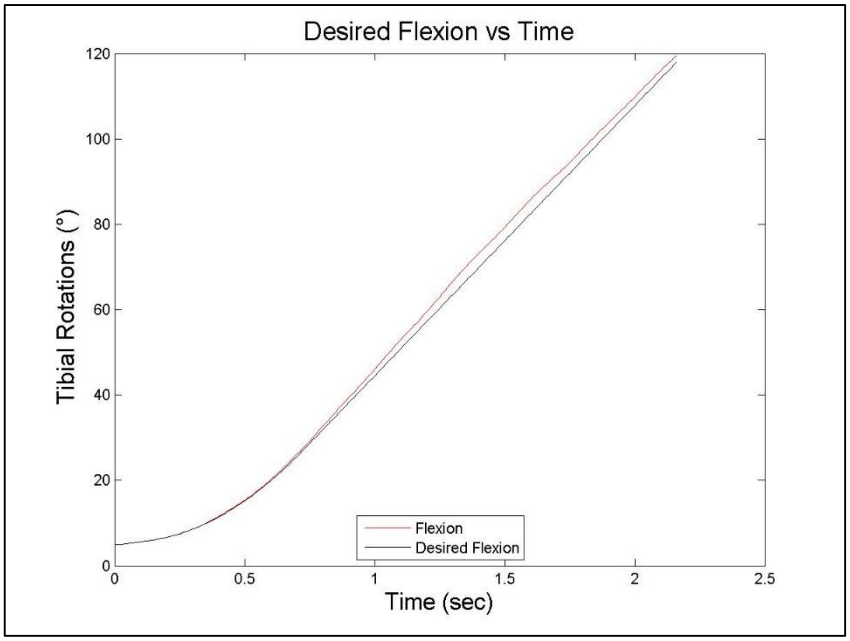

Figure 4-21: Example of the resulting output from the PID controller in matching flexion angle to desired rate in order to regulate quadriceps force.

After the overall quadriceps force is computed using the PID controller, a further PD controller is used to compute the distribution of this force throughout the four quadriceps muscles. Depending on the application, this controller either minimizes rotation or medial-lateral translation of the patella. When the patella internally rotates or translates laterally, it shifts more of the muscle for to the Vastus Lateralis which serves to pull the patella back to the center of the trochlear groove. If the patella translates medially or internally rotates, the muscles force is shifted to the Vastus Medius to pull the patella back to a neutral location.

Ground reaction force, obtained from a force plate, was also used as an input to the model. Though this resulted in a variation in the magnitudes of the round reaction force for each patient, however, the variable nature of each curve with respect to flexion angle was similar.

The dimensions of the bones, location of prominences and their inertial parameters are obtained from previously published anthropometric data (Zatsiorski, 1983; White, 1989; deLeva, 1996). The attachments of the muscles are considered as points and are also obtained from previous studies (Yamaguchi, 2001). Since these studies use different axes systems, therefore, the data is transformed to the axis system in this study before being used. The patella is assumed to be a disc whose dimensions are measured directly from the fluoroscopic images at full extension. Finally, the relevant femoral, polyethylene and tibial component dimensions of the TKA were directly measured form the CAD models of the components.

Using this methodology, it was possible to calculate the possible cam-post force during a DKB activity for all the three different TKA designs analyzed in this study.

4.4 Vibroarthrography of the Knee Joint

4.4.1 Data capture

The vibration data was collected for total 96 normal, degenerative and implanted knees. The goal of is to assess if it is possible to distinguish, just based on vibration data, the occurrence of uni-compartmental degeneration and the difference between normal and degenerative knee joint signals. Patients with normal and well functioning TKA were analyzed under in vivo, conditions using video fluoroscopy and vibration sensors while performing various normal day activities. For subjects who did not undergo fluoroscopic surveillance (degenerative and failed TKA), a detailed questionnaire was requested from the intra-surgery (primary or revision as the case might be) which schematically distinguished the area and level of damage to the tibio-femoral interface (Figure 4-22). During the TKA procedure, after opening the joint capsule, the surgeon examined the condition of the articular cartilage and filled out an intrasurgical evaluation sheet. This assessment provided an insight into the exact condition of the cartilage and the amount of damage at every compartment of the knee joint, as well as any other factors possibly altering the vibration pattern, such as any ligament deficiency or meniscal injuries. Having this information provided for the means to successfully correlate the condition of the joint with the vibration pattern for patients who did not undergo fluoroscopic studies.

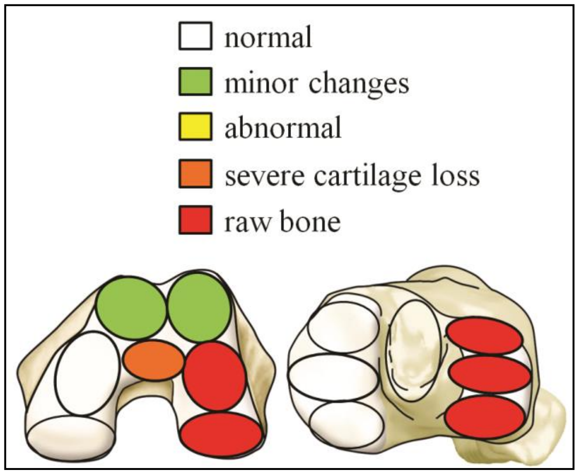

Figure 4-22: Intra-surgery evaluation sheet for example patient distinguishing the area and level of damage to the tibio-femoral interface.

The data collection setup consists of 3 miniature, 3-axial accelerometers (Model 356A12, 100 mV/g, 50 g, 0.5 to 5k Hz, PCB Piezotronics Inc., Depew, NY) attached to the surface of the skin at the lateral and medial femoral epicondyle and the tibial tuberocity respectively by means of elastic wrap and hypoallergenic adhesive tape (Figure 4-23).

A signal conditioner (Model 583A, PCB Piezotronics Inc., Depew, NY) is used to increase the magnitude of the vibration signal by the factor of ten and to low-pass filter the data at cut-off frequency of 4700Hz prior to analog-to-digital conversion (Model DI-720, DATAQ Instruments Inc., Akron, OH). Video cameras record the feed from the fluoroscopy device as well as the live scene in the examination room. Both, the vibration signals and the video inputs are then synchronized using a light trigger before being stored on a laptop computer (Figure 4-24).

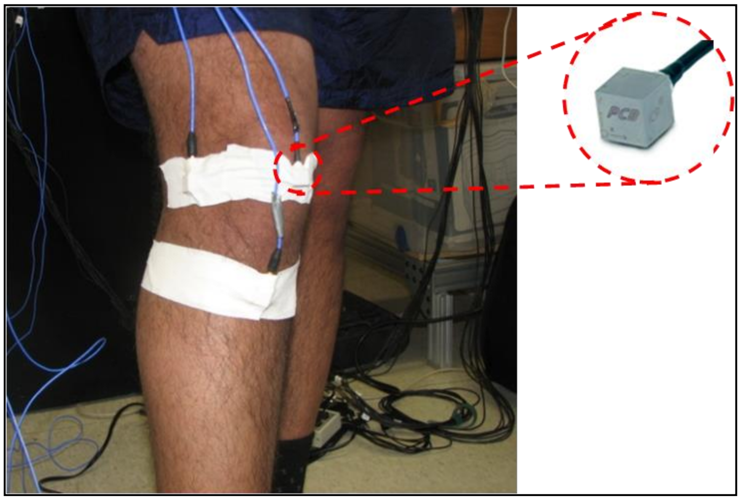

Figure 4-23: Location of attached of the tri-axial accelerometers at the knee joint.

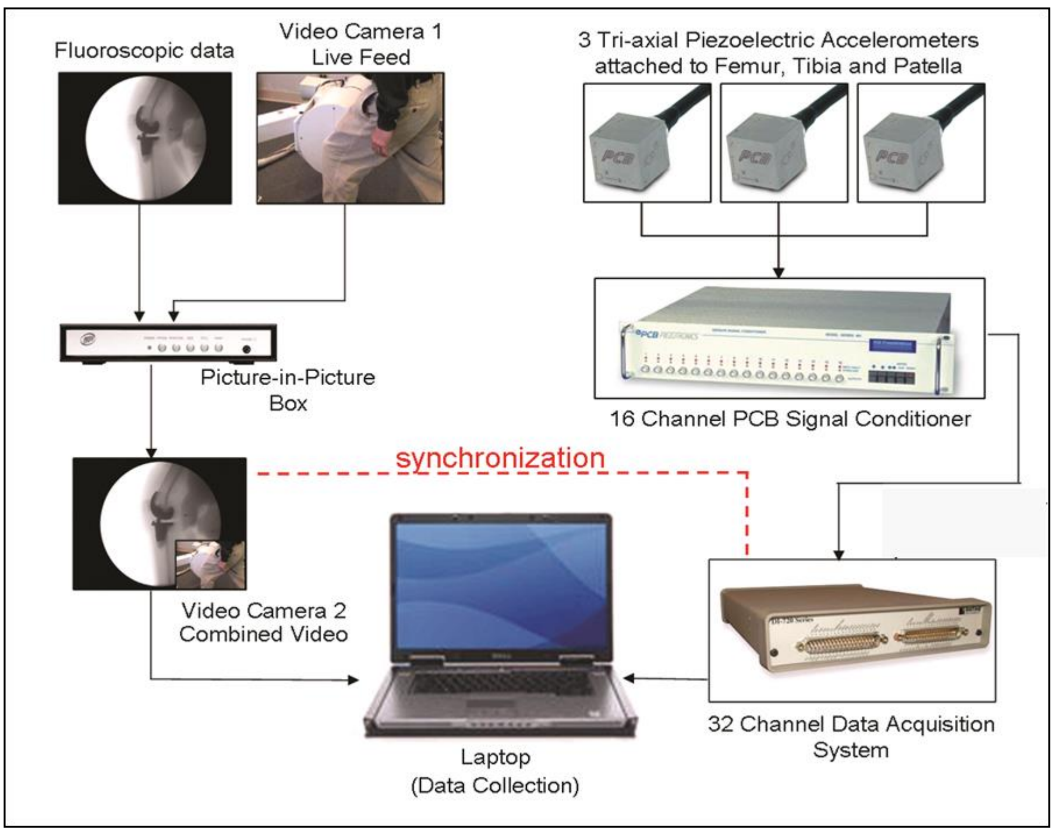

Figure 4-24: Data collection setup to collect vibroarthrography data.

4.4.2 Data analysis

The accelerometers record the change in acceleration resulting from both the movement of the joint as well as from the vibration of the bones. Therefore the raw accelerometer signals are decomposed into the motion and vibration components. This is achieved by high-pass filtering the acceleration signal using Butterworth Infinite Impulse Response (IIR) filter attenuating the signal by 80dB at the cut-off frequency of 20Hz. This eliminates the low frequency, motion components of the signals and yields a vibroarthrogram suitable for further analysis (Figure 4-25).

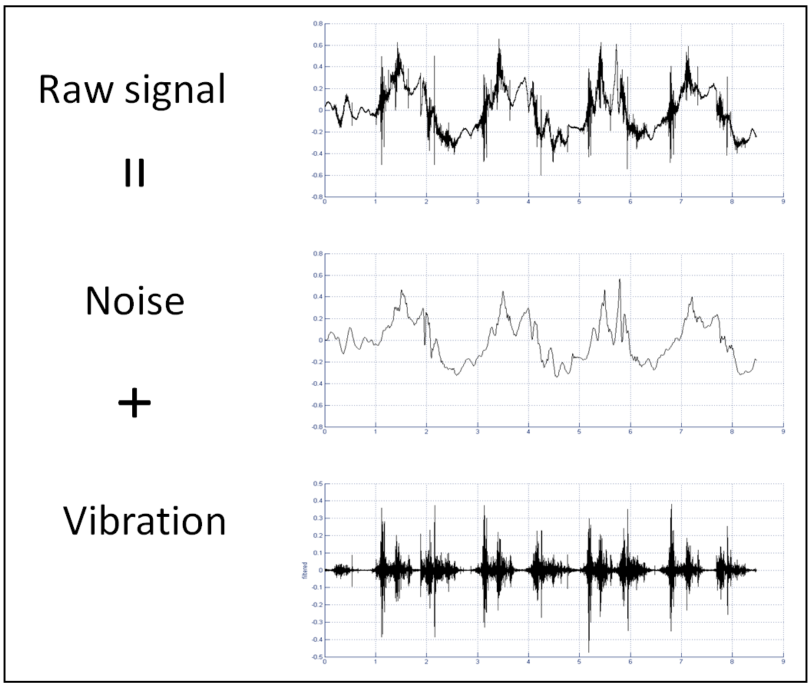

Figure 4-25: Removal of motion component (noise) from the accelerometer signal to obtain the vibroarthrogram.

The filtered vibroarthrogram can be also converted into audible form and correlated with the fluoroscopy or regular video footage (Figure 4-26).

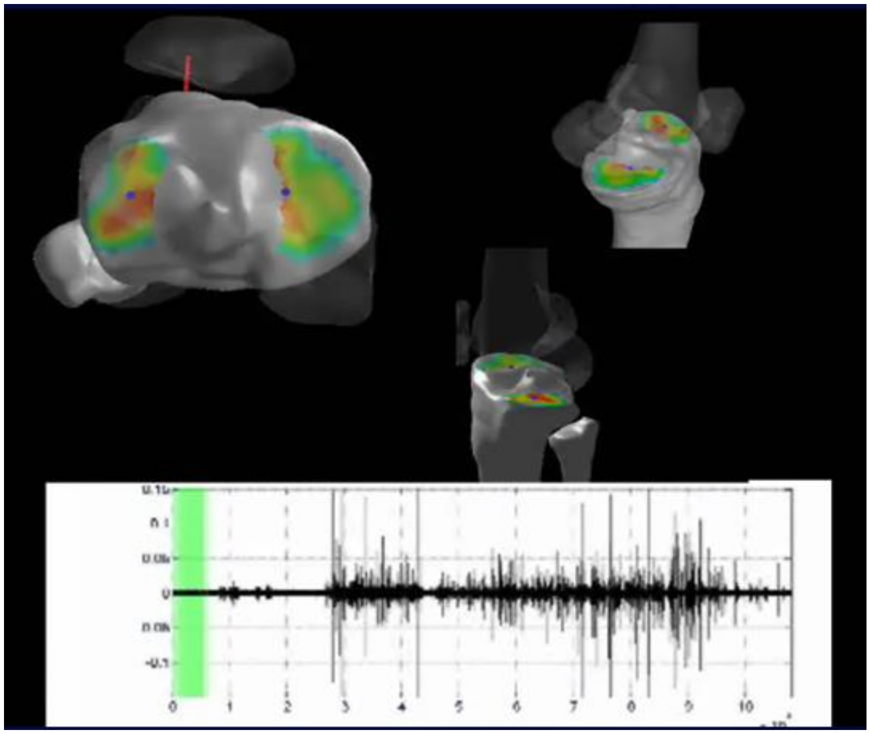

Figure 4-26: Correlated kinematics and vibroarthrography signals.

Several statistical parameters of the original and rectified vibroarthrograms are calculated to examine features that could be used to form the feature vector of the signals. They included, mean, standard deviation, skewness, kurtosis, 90th, 95, 97th and 99th quantiles.

After selecting the candidate features of the signals, a pattern classifier was designed. The objective of the classifier was to classify the given pattern of the VAG signal to one of the two groups: healthy or arthritic. The minimum-error-rate classification (Duda 2001) was chosen for the first attempt to design the classifier. This classification can be achieved by the use of the discriminant functions:

$$g_i(x)=\ln p(x|w_i)+\ln P(w_i) \qquad (20)$$

and assuming that the densities $p(x|w_i)$ are multivariate normal, the Eq. 20 becomes:

$$g_i(x)=-\frac{1}{2}(x-m_i)^t E_i^{-1}(x-m_i)-\frac{d}{2}\ln 2p-\frac{1}{2}\ln|E_i|+\ln P(w_i), \quad (21)$$

At the current stage of analysis there is no premise to classify the patient as either arthritic or healthy, therefore the prior probabilities for both categories are assumed to be equal $(P(w_1)=P(w_2)=\frac{1}{2})$

One feature, the mean of the signal was used to design the dichotomizer. Successful determination was possible between normal knees with and without articular cartilage damage up to an accuracy level of 86%. This is very similar to published literature by Rangayan et al. Also, it was seen that in cases where the surgeon had reported unicompartmental damage to the tibiofemoral interface, the signals obtained from the two accelerometers was very different from one another (Figure 4-27). Next, the second feature, standard deviation, was included in the discriminant function, and the success rate increased to 87%. Adding the third feature, 99^{th} quartile, did not improve the classification and the success rate actually dropped back to 70%.

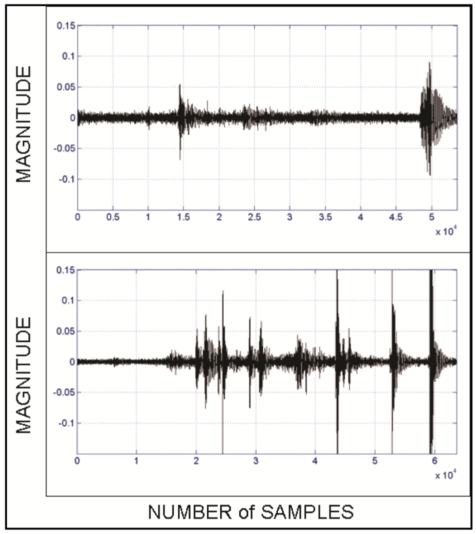

Figure 4-27: Filtered vibration signals from the medial (top) and lateral (bottom) femoral accelerometers, depicting the difference in vibration data.

Chapter 5: Results

5.1 Kinematics

5.1.1 Anteroposterior Translation

On average, from full extension to maximum knee flexion, subjects having the Sigma PS RP TKA experienced posterior femoral rollback (PFR) of the lateral condyle and anterior movement of the medial condyle relative to the tibia. At full extension, the average lateral and medial condyle contact position was -5.7 mm (-8.7 mm to -2.2 mm, SD=2.0) and -5.3 mm (-7.2 mm to -3.0 mm, SD =1.4), respectively. At 90 degrees, the average contact position of the lateral condyle moved posterior to -8.4 mm (-11.8 mm to -6.0 mm, SD =1.9), while the medial condyle moved in the anterior direction resulting in an average contact position of -3.4 mm (-7.8 mm to -1.0 mm, SD =2.1). Therefore, from full extension to 90 degrees, the average amount of PFR of the lateral condyle was -2.7 mm (-7.7 mm to 1.3 mm, SD =2.5), and the average amount of anterior slide of the medial condyle was 1.9 mm (-0.6 mm to 4.6 mm, SD =1.9). At maximum knee flexion, the lateral condyle continued to move posterior and with an average contact position of -10.0 mm (-17.2 mm to -6.0 mm, SD =3.9), with the medial condyle moving slightly posterior as well with an average overall anterior contact position of -4.4 mm (-9.2 mm to -1.0 mm, SD =2.4). Analysis of the data from full extension to maximum flexion, revealed the average amount of posterior femoral rollback of the lateral condyle and anterior slide of the medial condyle was -4.3 mm (-11.6 mm to 1.3 mm, SD =4.2) and 0.9 mm (-4.8 mm to 5.3 mm, SD =3.1), respectively (Figure 5-1 and Figure 5-2). All but one of the subjects (88.9%) experienced PFR of the lateral condyle, and 2 of 9 subjects (22.2%) experienced PFR of the medial condyle. Four of 9 subjects (44.4%) experienced a change in magnitude of 2 mm or less on the lateral side from full extension to full flexion. Four of 9 subjects (44.4%) also experienced a change in magnitude of 2 mm or less on the medial side from full extension to full flexion.

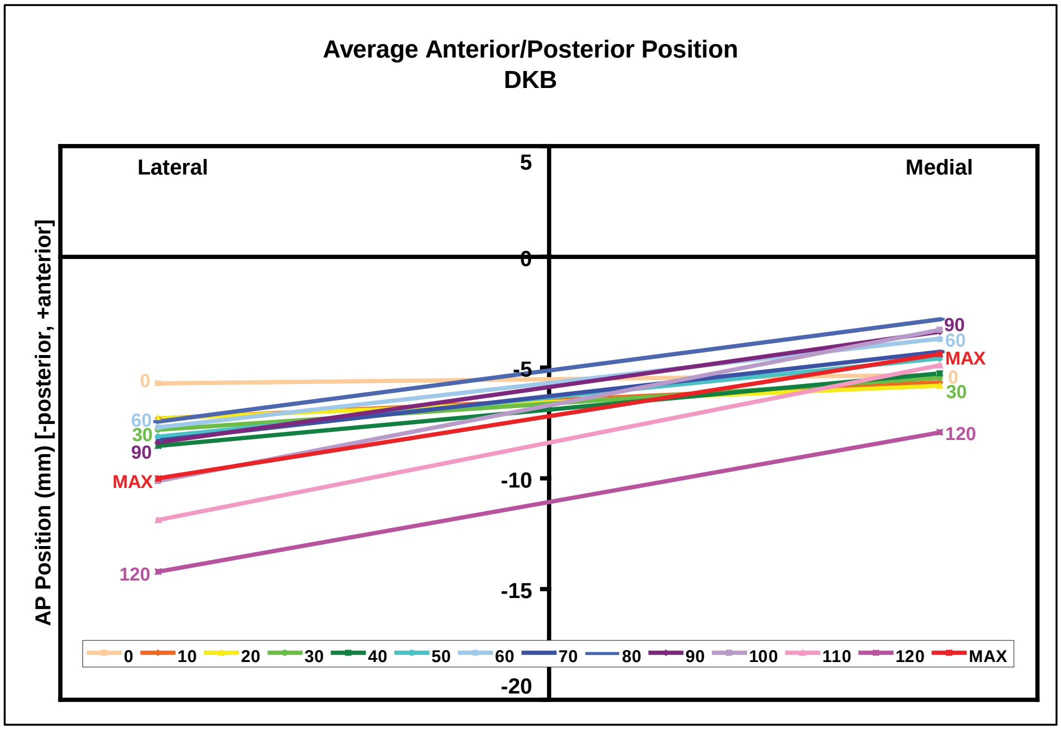

Figure 5-1: Average A/P position plot showing the femoral contact positions of the medial and lateral condyle for Sigma PS RP TKA.

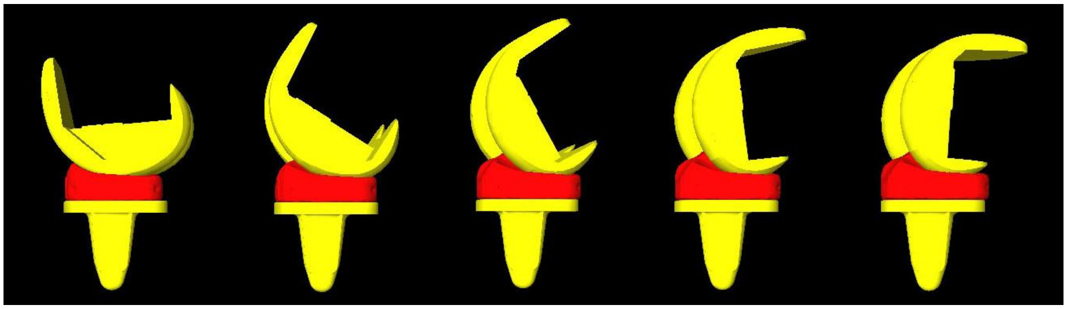

Figure 5-2: Lateral view of femoral contact positions relative to the tibia showing posterior femoral rollback for a random patient with a Sigma PS RP TKA

All (100%) Journey Bi-Cruciate TKA in this study experienced posterior femoral rollback (PFR) of their medial and lateral condyles from full extension to maximum knee flexion. At full extension, the average medial and lateral condyle contact position was 5.2 mm (-4.6 mm to 14.6 mm, SD=3.5 mm) and 7.2 mm (-4.1 mm to 18.5 mm, SD=6.3 mm), respectively. At maximum knee flexion, the average medial condyle contact position moved posterior to -8.8 mm (-14.4 mm to -1.4 mm, SD=2.8 mm), and the lateral contact position also moved in the posterior direction to -15.9 mm (-27.2 mm to -6.9 mm, SD=3.8 mm). Therefore, from full extension to maximum knee flexion, the average amount of posterior femoral rollback for the medial condyle was -14.0 mm (-25.2 mm to -7.0 mm, SD=3.9 mm) and the average amount of posterior femoral rollback for the lateral condyle was -23.0 mm (-36.7 mm to -5.8 mm, SD=7.2 mm), (Figure 5-3 and 5-4).

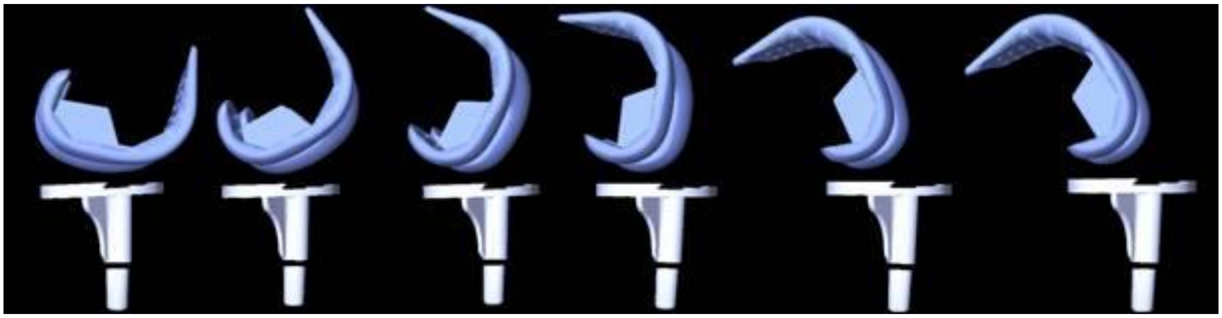

Figure 5-3: Lateral view of femoral positions relative to the tibia showing posterior femoral rollback for patient with a Journey Bi-Cruciate TKA.

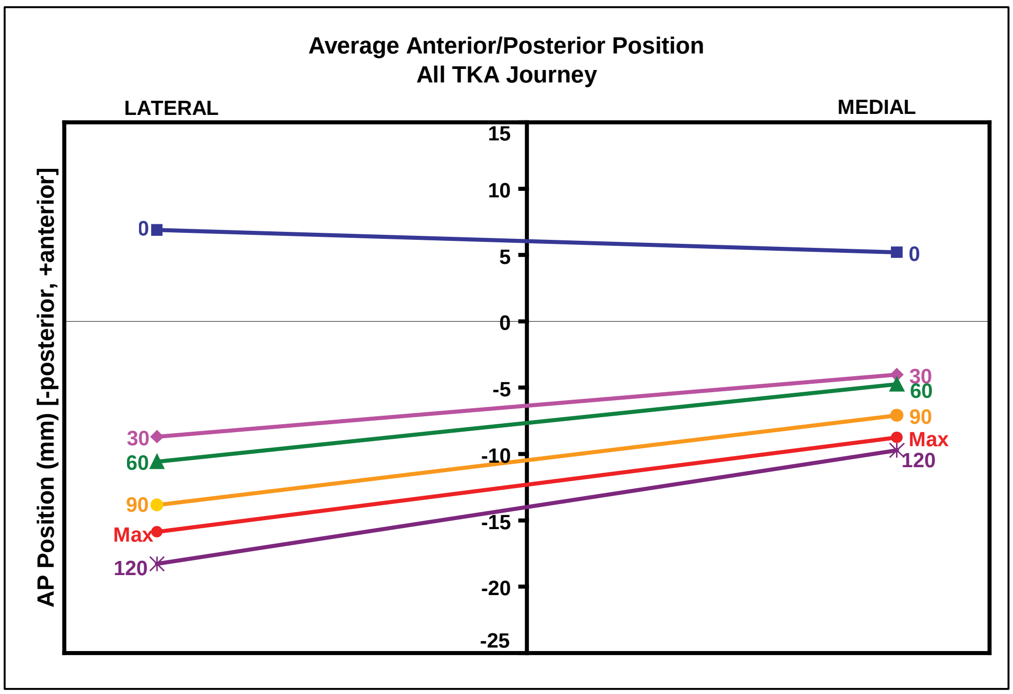

Figure 5-4 Average Anterior/Posterior Position plot for patients with a Journey Bi-Cruciate TKA.

All 5 Zimmer PS TKA in this study experienced posterior femoral rollback (PFR) of their medial and lateral condyles from full extension to maximum knee flexion. At full extension, the average medial and lateral condyle contact position was -5.4 mm (-10.4 mm to 1.2 mm, SD=2.6 mm) and -4.5 mm (-10.5 mm to 0.8 mm, SD=2.6 mm), respectively. At maximum knee flexion, the average medial condyle contact position moved posterior to -7.3 mm (-14.9 mm to -1.2 mm, SD=4.7 mm), and the lateral contact position also moved in the posterior direction to -8.5 mm (-15.3 mm to -1.3 mm, SD=4.9 mm). Therefore, from full extension to maximum knee flexion, the average amount of posterior femoral rollback for the medial condyle was -1.9 mm (-6.5 mm to -1.0 mm, SD=4.9 mm) and the average amount of posterior femoral rollback for the lateral condyle was -4.1 mm (-13.8 mm to –0.9 mm, SD=4.8 mm).

5.1.2 Axial Rotation for the Sigma RP-PS TKA

5.1.2.1 Tibio-Femoral Rotation

Axial rotations were derived for the femoral component relative to the tibial base plate. On average, subjects having the Sigma PS RP TKA experienced normal axial rotation (Figure 5-5). The average axial rotation at full extension, 90 degrees, and maximum flexion was 0.9° (-4.1° to 7.4°, SD=3.6), 6.5° (-0.5° to 12.2°, SD =4.7), and 6.7° (-1.3° to 12.8°, SD =5.1), respectively. From full extension to 90 degrees, the average amount of normal axial rotation was 5.6° (1.4° to 15.6°, SD =4.9) while from full extension to maximum knee flexion the average amount of normal axial rotation experienced by subjects was 5.8° (1.4° to 16.6°, SD =5.1). Analysis from one DKB increment to the next revealed that all nine subjects experienced instances of reverse axial rotation at some point through flexion a total of 34 times. However, the majority of these occurrences of opposite rotation, 22 of

34 (64.7%), had magnitudes less than 1°. In addition, all subjects were noted as having an overall normal axial rotation pattern moving from both full extension to 90 degrees and from full extension to maximum knee flexion.

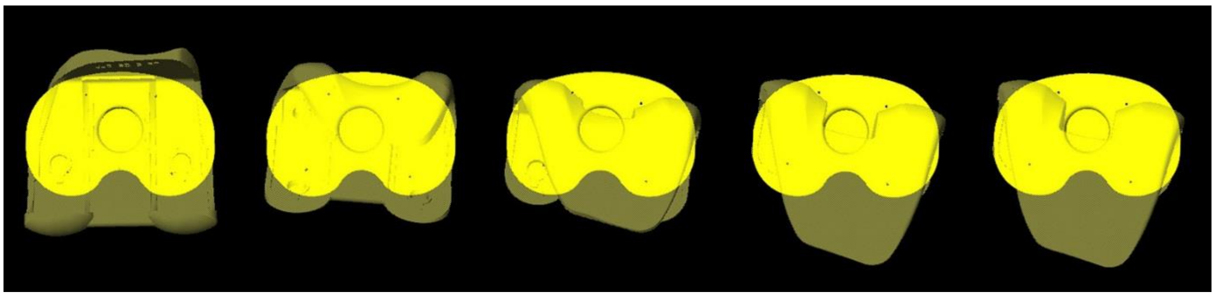

Figure 5-5: Top view of femoral positions relative to the tibia of a right Sigma PS RP TKA from full extension to full flexion (left to right) showing positive axial rotation.

5.1.2.2 Tibio-Polyethylene Rotation

Axial rotations were calculated for the polyethylene bearing relative to the tibial base plate. Subjects having the Sigma PS RP TKA experienced, on average, normal axial rotation of the polyethylene relative to the tibia (Figure 5-6). The average axial rotation at full extension, 90 degrees, and maximum flexion was 1.6° (-2.3° to 7.4°, SD =3.4), 6.1° (-1.0° to 11.6°, SD =5.0), and 5.9° (3.9° to 12.0°, SD =3.5), respectively. From full extension to 90 degrees, the average amount of normal axial rotation was 4.5° (-0.3° to 12.1°, SD =4.4), and from full extension to maximum knee flexion, subjects experienced 4.3° (-0.3° to 12.5°, SD =4.2) of normal axial rotation. Overall, 4 of the 9 (44.4%) subjects experienced greater than 3° of axial rotation of the polyethylene bearing relative to the tibia during

DKB. Additionally, four of the nine (44.4 %) subjects experienced between 1° and 3° of axial rotation, while one subject experienced less than 1° of rotation. Further analysis revealed that although subjects only experienced, on average, 4.3° of bearing rotation from full extension to maximum knee flexion, greater axial rotation values were achieved at various increments of DKB. Therefore, the minimum and maximum amount of axial rotation of the polyethylene bearing relative to the tibia for each TKA was determined regardless of knee flexion angle and allowed for the calculation of the maximum overall bearing range of motion. On average, subjects experienced 7.1° (2.1° to 14.0°, SD =3.8) of maximum normal polyethylene bearing rotation occurring between any increment of knee flexion.

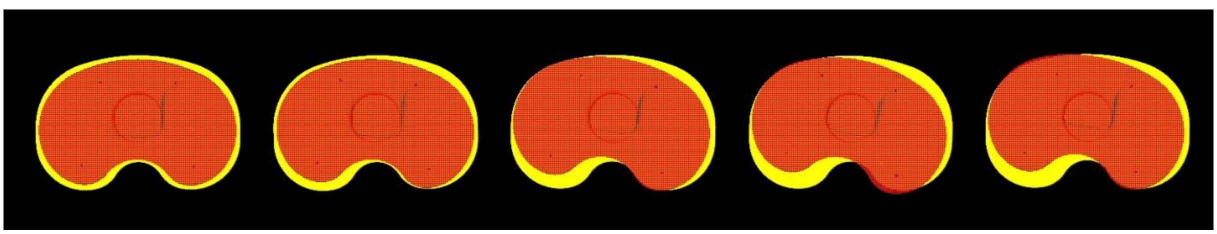

Figure 5-6: Top view of polyethylene positions relative to the tibia of a right Sigma PS RP TKA from full extension to full flexion (left to right) showing positive axial rotation.

5.1.2.3 Femoro-Polyethylene Rotation

The difference in the amount of axial rotation between the femoral component and the polyethylene bearing was found for all flexion angles (Figure 5-7). Subjects having the Sigma PS RP TKA experienced, on average, -0.7° (-2.6° to 0.9°, SD =1.3), 0.4° (-0.8° to

1.5°, SD =0.8), and 0.8° (-0.2° to 2.5°, SD =0.9) of rotation between the femur and the polyethylene at full extension, 90 degrees, and maximum flexion, respectively. From full extension to 90 degrees, the average axial rotation difference was 1.1° (-0.5° to 3.6°, SD =1.4), and from full extension to maximum knee flexion, the average amount of axial rotation between the femur and polyethylene was 1.5° (-0.5° to 4.1°, SD =1.5). In addition, subjects were observed to experience greater than average axial rotation between the polyethylene bearing and the femoral component when the maximum overall bearing rotation was evaluated. Values were calculated based on the minimum and maximum axial rotation differences between the polyethylene and femoral component. On average, subjects experienced an axial rotation difference of 3.7° (1.8° to 4.8°, SD =1.1) between the polyethylene bearing and the femoral component when the DKB was evaluated regardless of flexion angle.

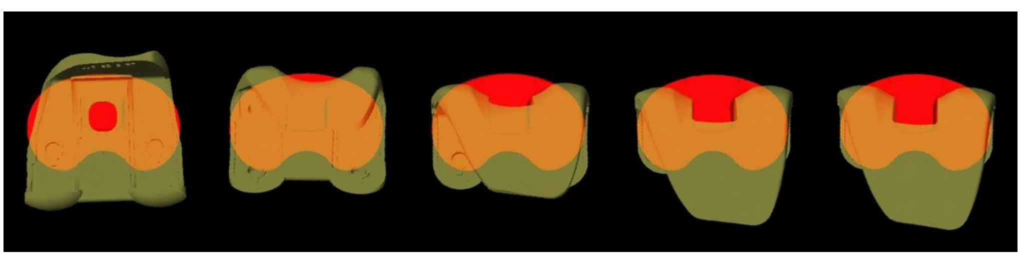

Figure 5-7: Top view of femoral positions relative to the polyethylene of a right Sigma PS RP TKA from full extension to full flexion (left to right) showing a minimal axial rotation difference.

The amount of axial rotation between the polyethylene and the femur was also evaluated based on absolute magnitude of rotation. This method ensured that the small negative and positive rotations between the PE bearing and the femoral component would not equate to a value near zero. Therefore, these calculations revealed that subjects having the Sigma PS RP TKA experienced, on average, 1.2° (0.3° to 2.6°, σ=1.2), 0.8° (0.1° to 1.5°, SD =0.5) and 0.9° (0.1° to 2.5°, SD =0.9) of absolute rotational magnitude between the femoral component and the polyethylene at full extension, 90 degrees, and maximum flexion, respectively. From full extension to 90 degrees, the average change in magnitude of absolute axial rotation was 0.4° (-2.5° to 0.7°, SD =1.0), and from full extension to maximum knee flexion, the average change in magnitude of absolute axial rotation between the femur and polyethylene was -0.3° (-2.5° to 2.3°, SD =1.3). Subjects were also observed to experience a greater than average change in the magnitude of absolute axial rotation between the polyethylene bearing and the femoral component when the overall maximum absolute change in rotational magnitude of the PE bearing was evaluated. On average, subjects experienced 2.3° (0.9° to 4.5°, SD =1.0) of absolute change in the magnitude of axial rotation between the polyethylene bearing and the femoral component when DKB was evaluated regardless of flexion angle and calculated with respect to absolute change in the magnitude of axial rotation values.

5.1.3 Axial Rotation for the Journey BCS and Zimmer FB PS TKA

On average, the Journey Bi-Cruciate TKA analyzed in this study experienced normal axial rotation from full extension to maximum flexion (Figure 5-8). The average amount of axial rotation from full extension to maximum flexion was 10.8° (-4.2° to 24.7°, SD=6.2°).

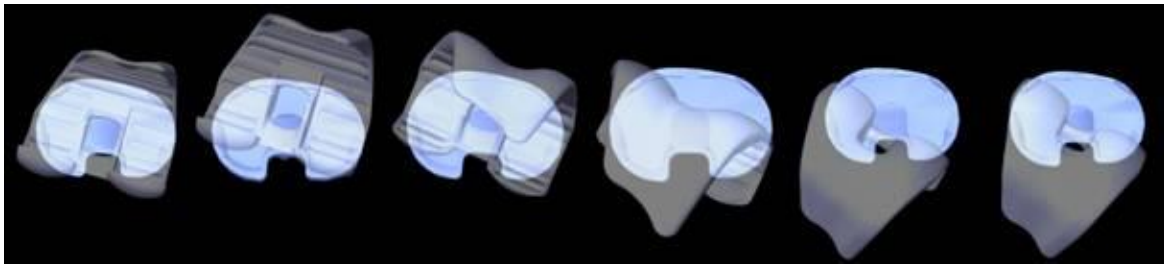

Figure 5-8: Top view of femoral positions relative to the tibia for Journey Bi-Cruciate TKA from full extension to full flexion (left to right) showing positive axial rotation.

On average, the Zimmer FB PS TKA analyzed in this study experienced normal axial rotation from full extension to maximum flexion. The average amount of axial rotation from full extension to maximum flexion was 5.0° (2.0° to 16.5°, SD=5.4°).

5.2 Analysis of the Cam-post Interaction

5.2.1 Angle of Contact

For the subjects in the BCS group, 7/10 knees analyzed had the femoral component engaged with the anterior aspect of the tibial post at full extension (Figure 5-9). However, the contact between them was lost in very early flexion (average: 4.9°; range: 0.0 to 9.9°). When the posterior cam-post mechanism was analyzed for the three groups, it was seen that the engagement occurred at 34° for the BCS (range: 17° to 68°) (Figure 5-10), 93° for the FB-PS (range: 88° to 100°) (Figure 5-11) and at 97° (range: 90° to 104°) for RP-PS TKA (Figure 5-12). Cam-post contact occurred at a significantly lower flexion angle for the BCS group when compared to the FB-PS group ($p<0.0001$) as well as the RP-PS group ($p<0.001$). There was not statistical difference between patients in the FB-PS and RP-PS groups ($p>0.05$). There were two knees in the BCS group and one knee in the RP-PS group that did not exhibit cam-post engagement through their range of motion.

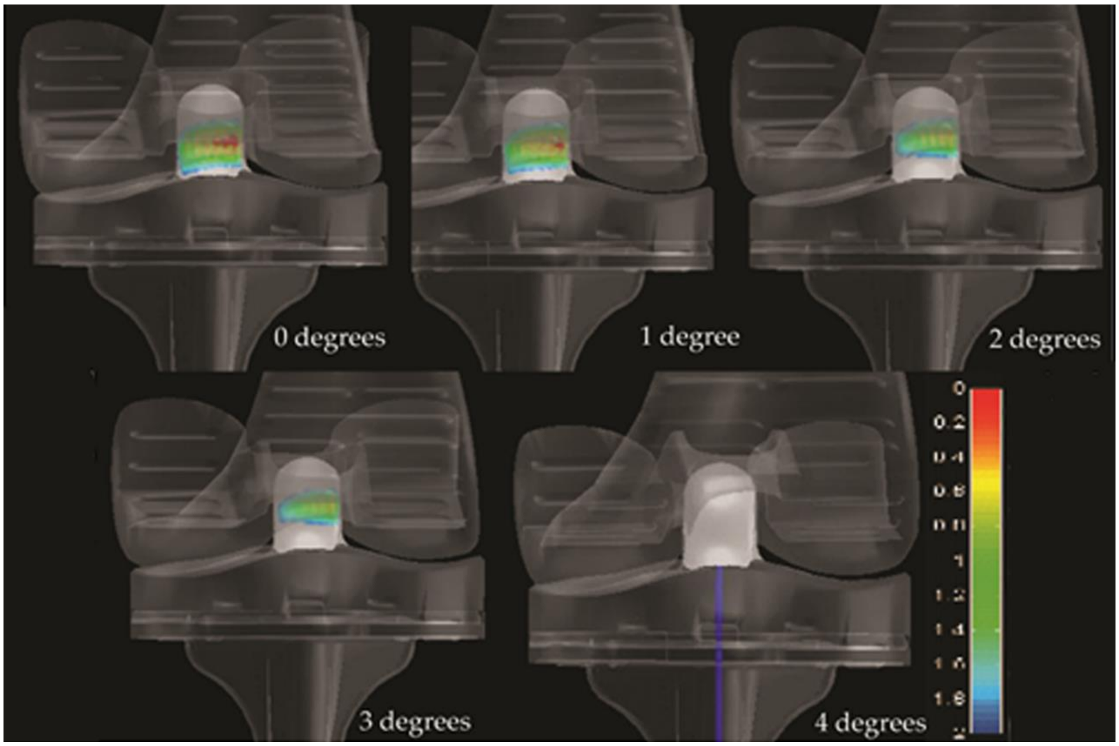

Figure 5-9: Example of anterior cam-post contact for a patient in the BCS group

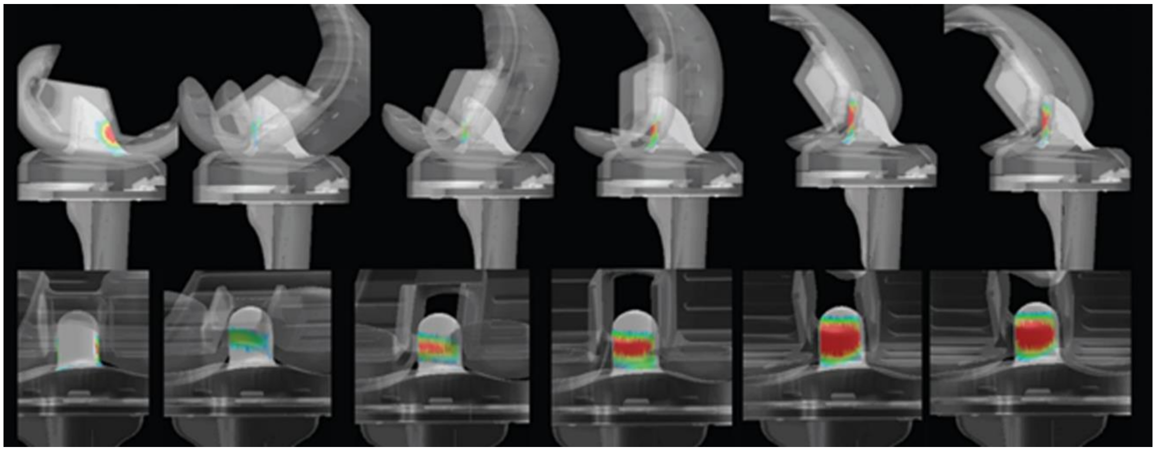

Figure 5-10: Example of posterior cam-post contact for a patient in the BCS group

Figure 5-11: Example of cam-post contact for a patient in the Zimmer PS FB TKA group

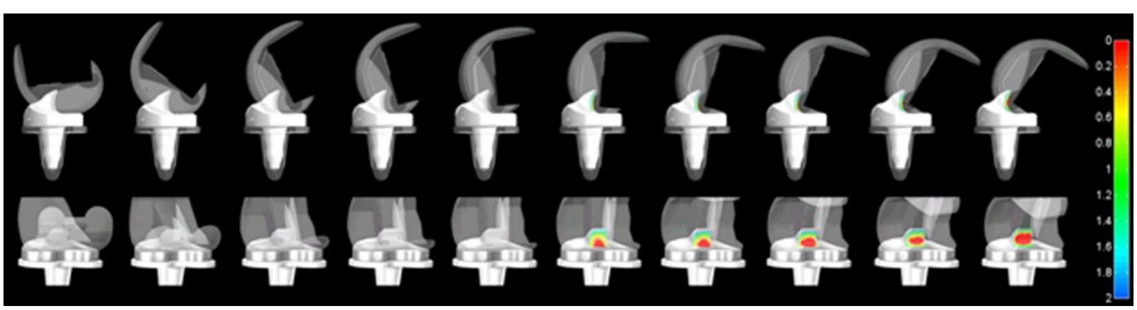

Figure 5-12: Example of cam-post contact for a patient in the Sigma RP-PS TKA group

5.2.2 Effect of Dwell Point

The effect of the initial dwell point of the femur on the polyethylene insert played a major role in determining when cam-post contact occurred. The average distance between the cam and the posterior aspect of the post at full extension was 9.3mm (range: 5.5mm to 11mm) for the BCS group (Figure 5-13), 19.1mm (range: 13mm to 23mm) for the FB-PS group (Figure 5-14) and 17.3 (range: 14mm to 21mm) for the RP-PS group (Figure 5-14). The subjects in the BCS group experienced a significantly lower cam-post distance than their FB-PS ($p<0.0001$) and RP-PS ($p=0.003$) counterparts. There was no significant difference between the FB-PS and RP-PS TKA groups.

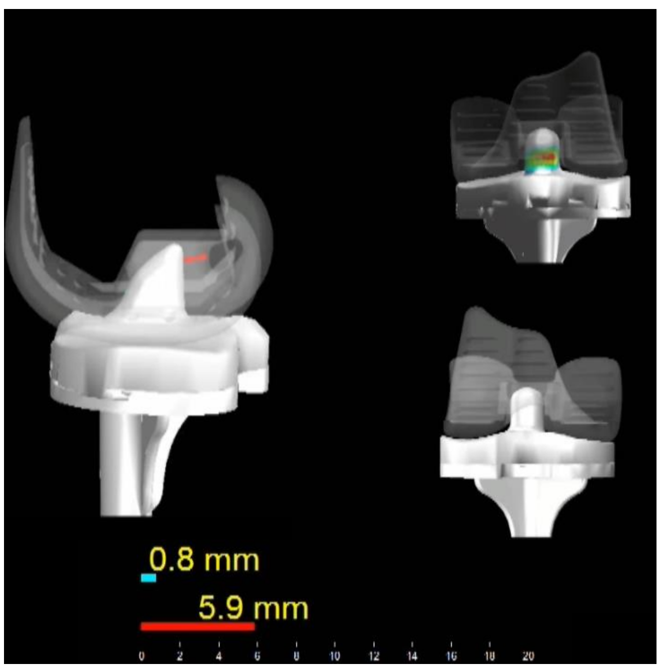

Figure 5-13: Example of cam-post distance for a patient in the Journey BCS TKA group

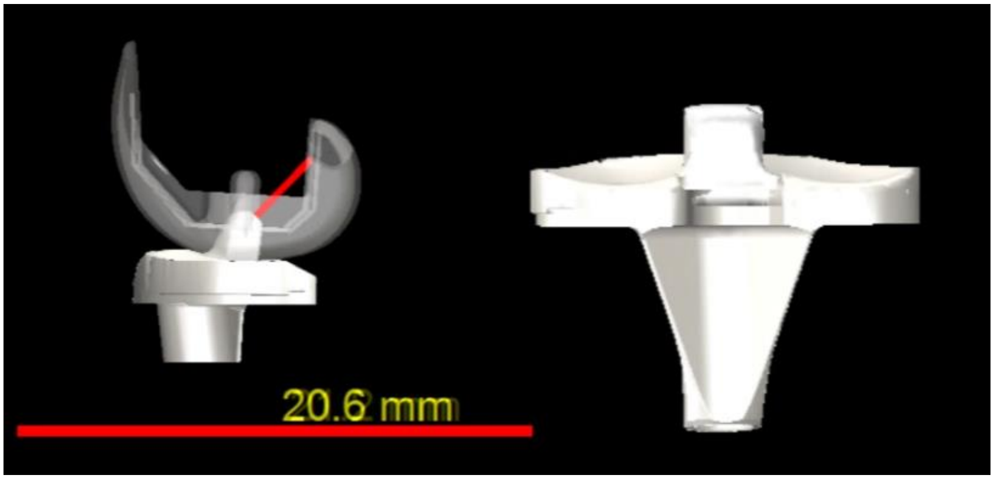

Figure 5-14: Example of cam-post distance for a patient in the Zimmer PS FB TKA group

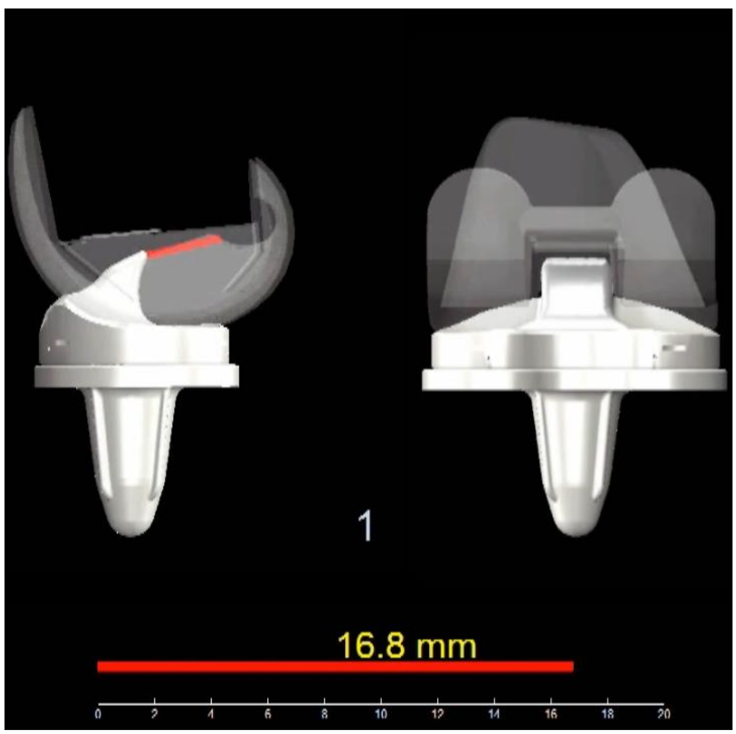

Figure 5-15: Example of cam-post distance for a patient in the Sigma RP-PS TKA group

5.2.3 Nature of Contact

The anterior contact in the BCS group was always located centrally on the anterior aspect of the tibial post. As far as the posterior contact was concerned, in the BCS and FB-PS knees, the contact initially occurred on the medial aspect of the tibial post and then gradually moved centrally and superiorly with increasing flexion (Figures 5-16 and 5-17), while for the RP-PS TKA it was located centrally on the post at all times (Figure 15-18). The amount of medialization of the contact in the BCS and FB-PS groups was found to correlate with the amount of tibio-femoral axial rotation experienced by the subject, with subjects experiencing higher axial rotation, having a higher tendency to demonstrate medial contact at the tibial post interface.

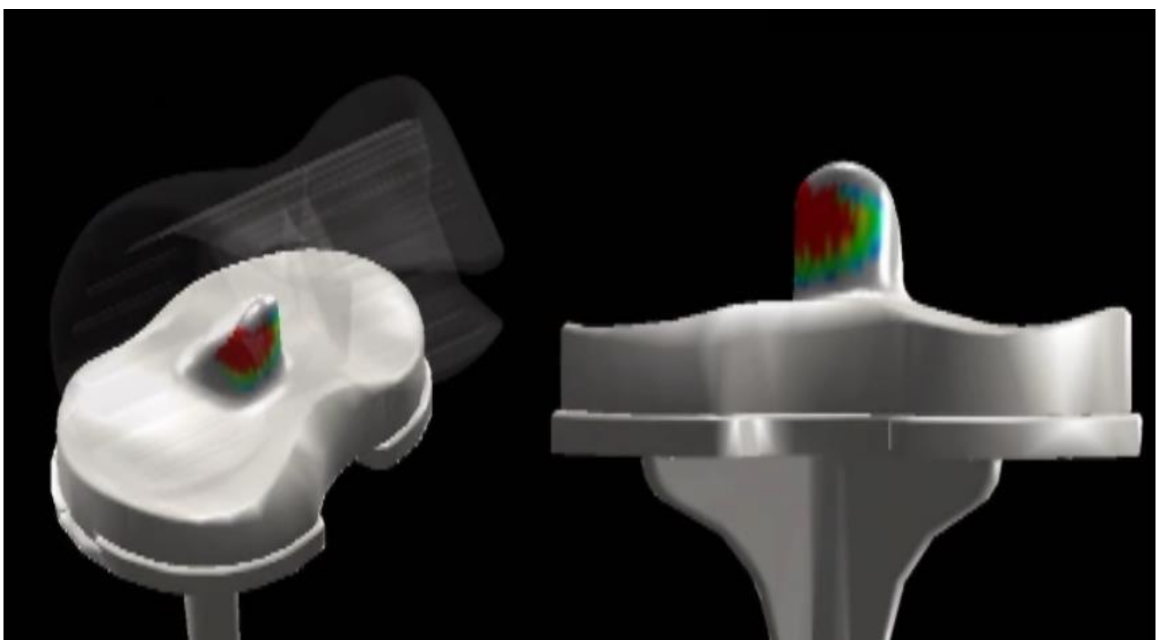

Figure 5-16: Occurrence of cam-post contact with of the femur on the medial aspect of the tibial post in the Journey BCS TKA due to the prevalence of high amounts of tibio-femoral axial rotation.

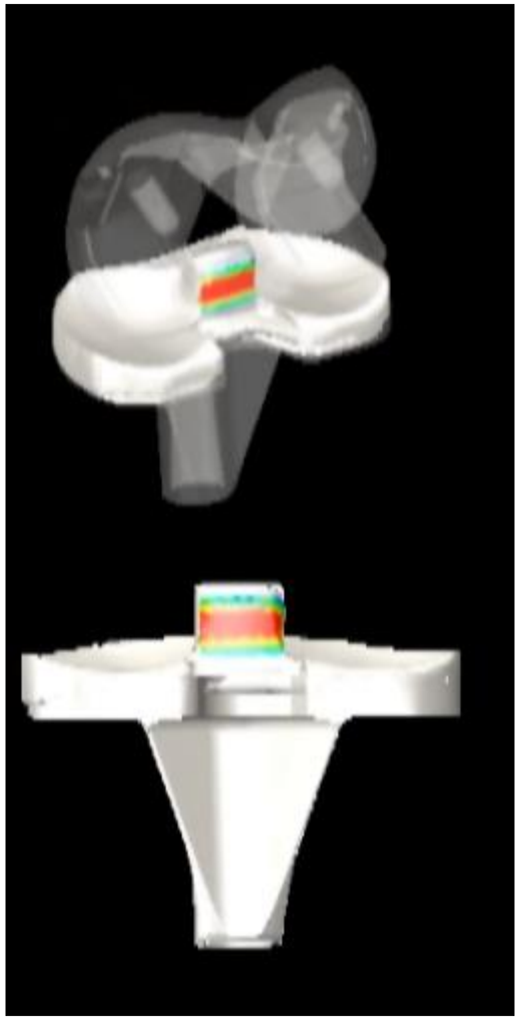

Figure 5-17: Central cam-post contact exhibited by a patient implanted with the Zimmer FB PS TKA.

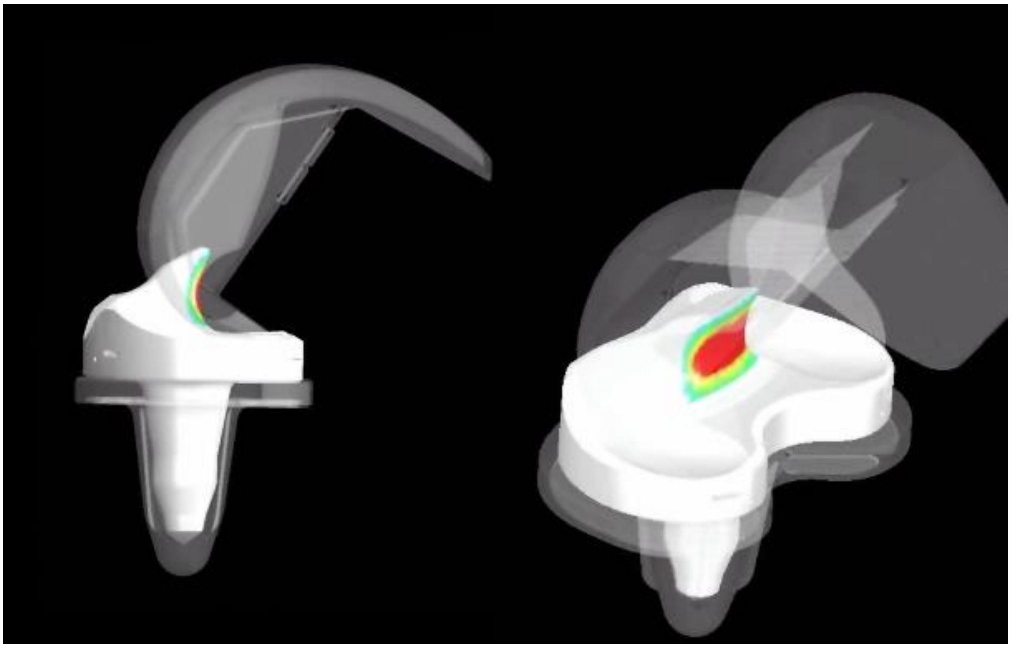

Figure 5-18: Central cam-post contact exhibited by a patient implanted with the Sigma RP-PS TKA.

5.2.4 Height of Contact

The height at which the contact occurred on the posterior aspect of the post was variable among the three groups. The BCS group experienced a significantly higher height on the tibial post from either the medial tibio-femoral contact point or the lateral tibio-femoral contact point (Figure 5-19) (average: 12.5mm, range: 7.0mm to 18.5mm) than their FB-PS (average: 7.2mm, range: 6.1mm to 10.0mm) (p=0.02) (Figure 5-20) and RP-PS (average: 6.2, range: 3.0mm to 11mm) (p=0.0092) (Figure 5-21) counterparts. There was no statistical difference on the cam-post contact height between the FB-PS and RP-PS groups.

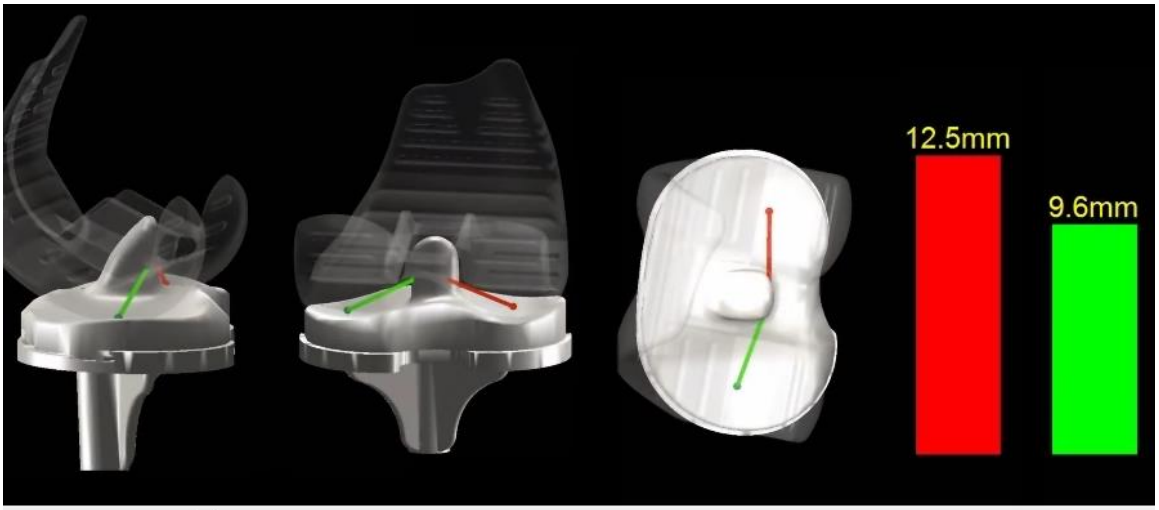

Figure 5-19: Contact height for patients in the Journey BCS TKA group were found to be the highest among the three groups analyzed.

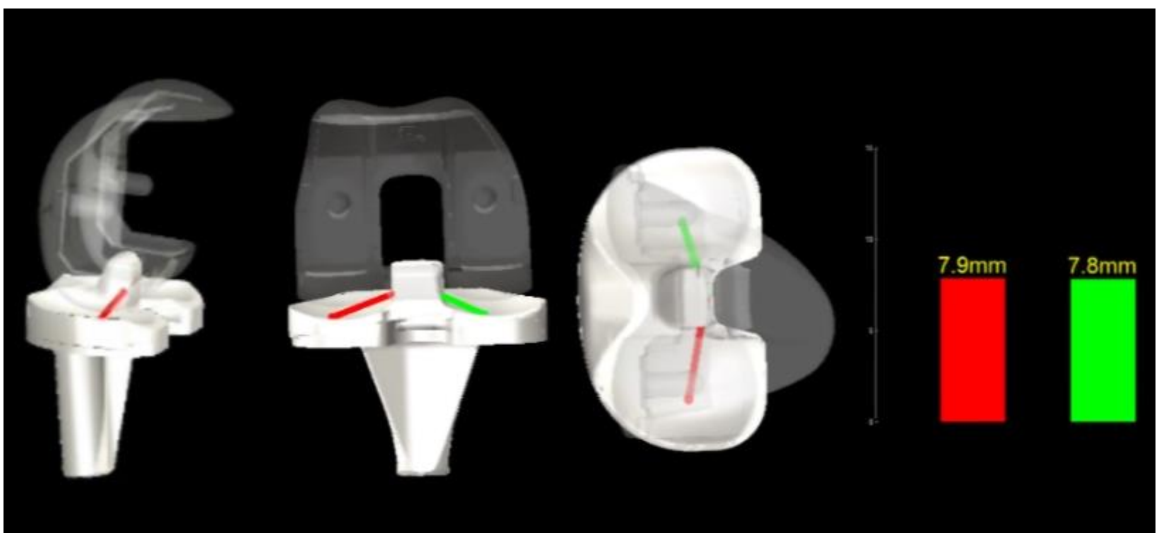

Figure 5-20: Contact height for patients in the Zimmer FB PS TKA group were found to be similar to those in the Sigma RP PS TKA group.

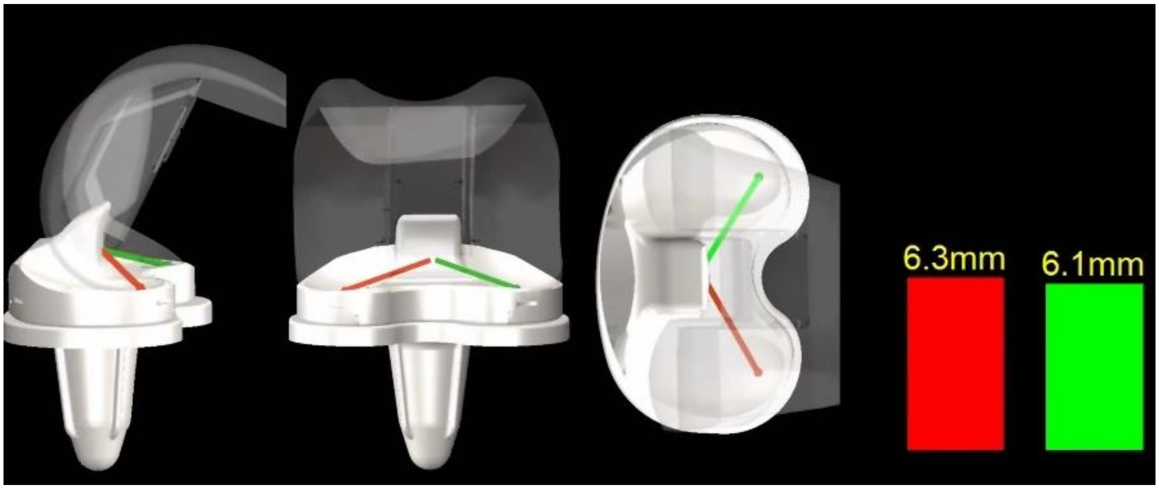

Figure 5-21: Example of the contact height for patients in the Sigma RP PS TKA group.

5.3 Kinetics

5.3.1 Cam-Post Forces

The forces in the cam-post mechanism were different for all the implant simulations owing to the fact that patients in the BCS TKA group experienced an early cam-post contact when compared to the other two groups. The simulation for the BCS TKA approximated cam-post contact to occur at 55 degrees of flexion. The resultant force increased after contact through the rest of the flexion cycle to 2.0BW. The simulation for the FB-PS TKA approximated cam-post contact to occur at 87 degrees of flexion. From initial contact the force steadily increased to 1.29BW at 120 degrees of flexion. A similar nature and magnitude of total cam-post force was observed for the simulation involving the RP-PS TKA. The simulation approximated contact to occur at 88 degrees after which it steadily increased to 1.6BW at 120 degrees of flexion (Figure 5-22). Throughout the range of motion when the cam and post were in contact, the simulation for the BCS TKA experienced a significantly higher force when compared to the FB-PS and RP-PS TKA.

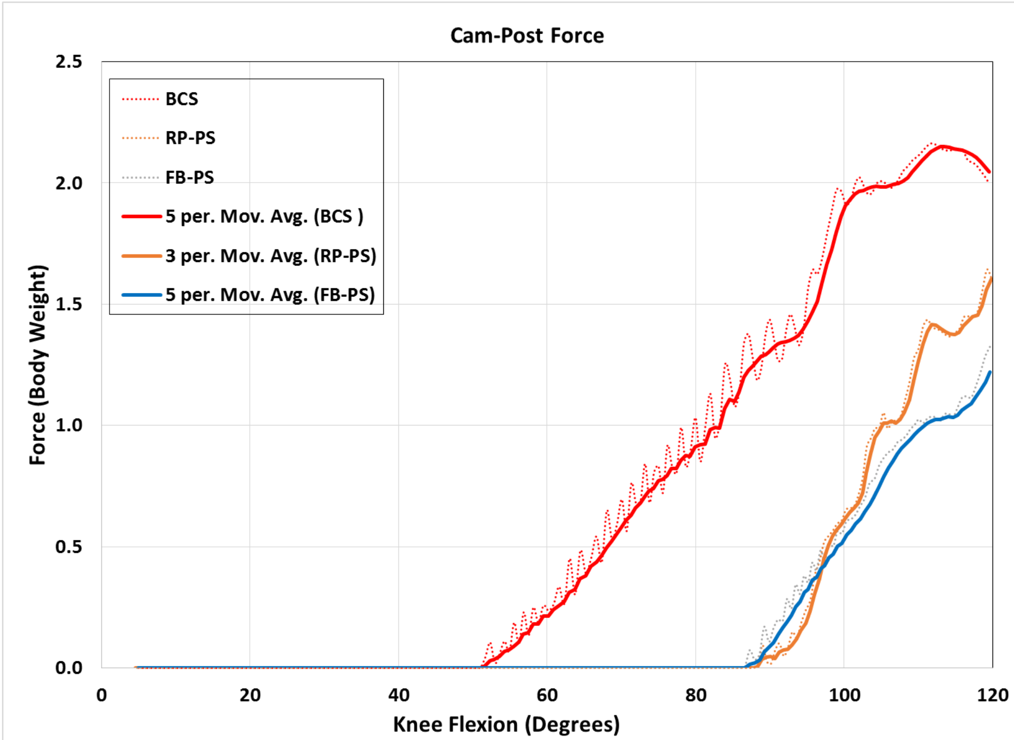

Figure 5-22: Cam-post contact forces produced by the simulations for the BCS, FB-PS and RP-PS TKAs.

Though the magnitudes of the forces between the FB-PS and RP-PS TKA were similar in magnitude, the nature of the contact played an important role in determining where the contact occurred. For the BCS TKS simulation at initial contact the force was located in a central position, but rapidly decreased and in deeper flexion the force was located on the outer surface of the tibial post. Initial cam-post contact was achieved at 52 degrees, but by 60 degrees the percentage of force on the central part of the post reduced to 39%. This futhre reduced to 20% at 95 degrees of flexion, before slightly increasing in deeper flexion to 41%.

The FB-PS TKA exhibited a different pattern of force distribution. At initial contact close to 0% of the force was located on the central post. This increased from initial contact into deeper flexion with 18% of the cam-post force located on the central post at 120 degrees. On the contrary, RP-PS TKA forces were initially located on the central post at first contact and continued to stay on the central post through the range of motion. Hence the percentage of force exerted on the central portion of the post was very high in the simulation for the RP-PS TKA, starting at 100% at initial contact before slightly reducing to 81% at 120 degrees of flexion (Figure 5-23).

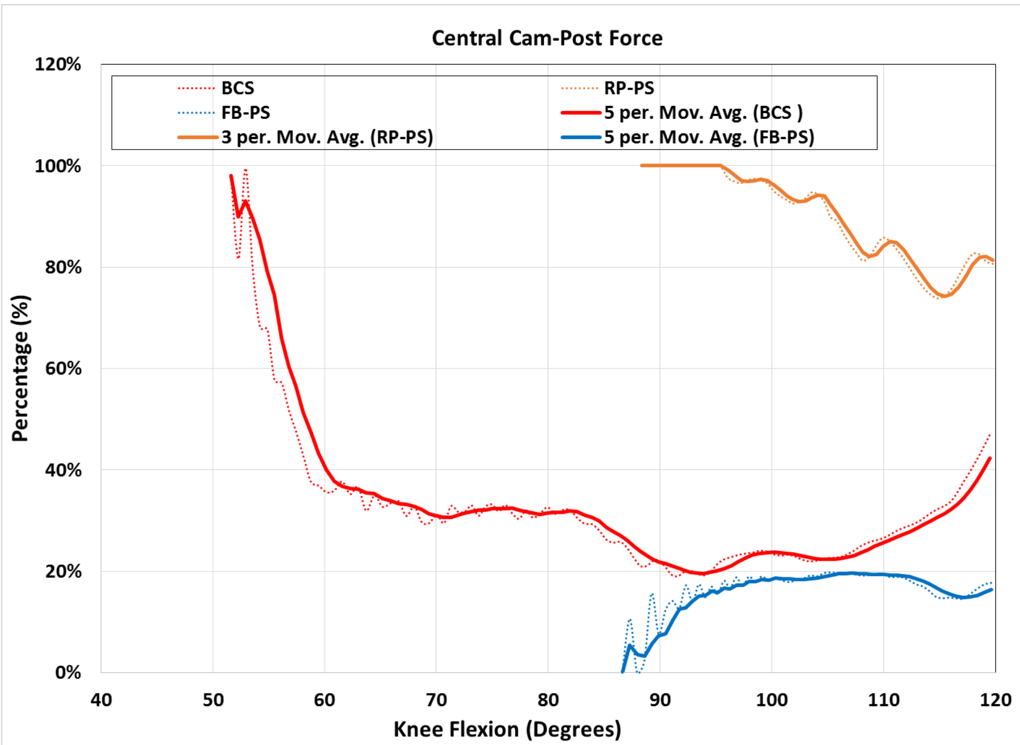

Figure 5-23: Cam-post force distribution produced by the simulations for the BCS, FB-PS and RP-PS TKAs.

5.3.2 Tibio-Femoral Forces

The tibio-femoral contact forces for the BCS TKA simulation increased with increasing knee flexion. The simulation with a BCS TKA experienced, on average, a force at full extension of 0.5BW to a force of 3.7BW at maximum knee flexion. The maximum contact force was observed at 115 degrees of flexion (4.0 times BW). The simulation for the FB-PS TKA revealed a slightly different pattern, with the contact forces increasing from full extension to 93 degrees of flexion before reducing in deeper flexion. At full extension, the simulation for the FB-PS TKA showed a total contact force of 0.5BW which increased in nature to 3.6BW at 93 degrees of flexion before reducing in deeper flexion to 2.95BW. The RP-PS TKA exhibited a similar nature with the simulation starting with 0.5BW at full extension and reaching a maximum value of 3.5BW at 87 degrees before reducing in deeper flexion to 3.2BW at 120 degrees of flexion (Figure 5-24). Until 80-85 degrees of flexion the three simulation exhibited similar forces, after which the BCS TKA forces increased in nature and magnitude, while those for the FB-PS and RP-PS TKA reduced in deeper flexion.

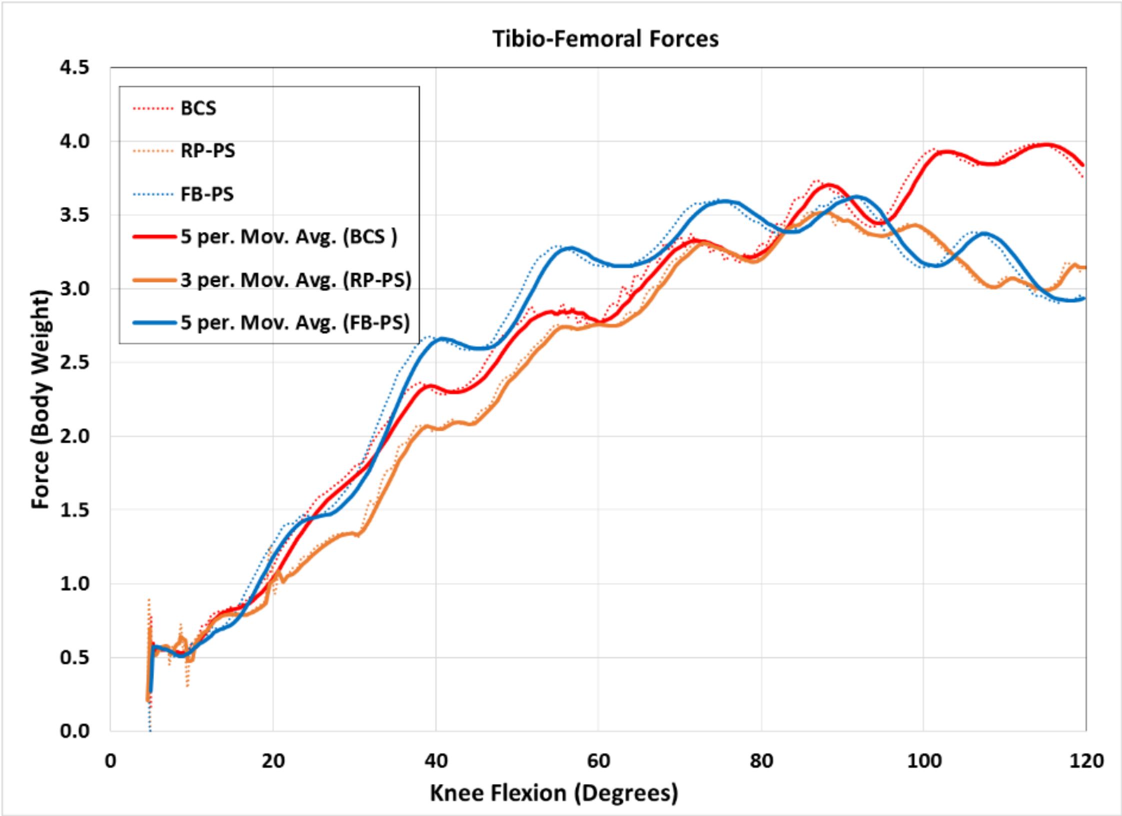

Figure 5-24: Tibio-femoral forces produced by the simulations for the BCS, FB-PS and RP-PS TKAs.

5.3.3 Quadriceps Forces

The force in the quadriceps muscle varied from 0BW at full extension to 4.0BW at full knee flexion for the simulation of the BCS TKA subject. The nature of this variance in force was different than that seen for the tibio-femoral force for this implant. The force was increasing in nature from full extension to 85 degrees of flexion (5.8BW), after which it reduced in deeper flexion.

The simulation for the FB-PS TKA revealed a similar pattern, with the quadcriceps forces increasing from full extension to 79 degrees of flexion before reducing in deeper flexion. At full extension, the simulation for the FB-PS TKA showed a total quadriceps force of 0.1BW which increased in nature to 4.6BW at 79 degrees of flexion before reducing in deeper flexion to 3.05BW. The RP-PS TKA also exhibited a similar nature with the simulation starting with 0.1BW at full extension and reaching a maximum value of 4.5BW at 70 degrees before reducing in deeper flexion to 3.0BW at 120 degrees of flexion (Figure 5-25). Except for early flexion (0-40 degrees) when the three simulation exhibited similar magnitudes of force, the simulation for the BCS TKA always exhibited a higher force when compared to the FB-PS and RP-PS TKA.

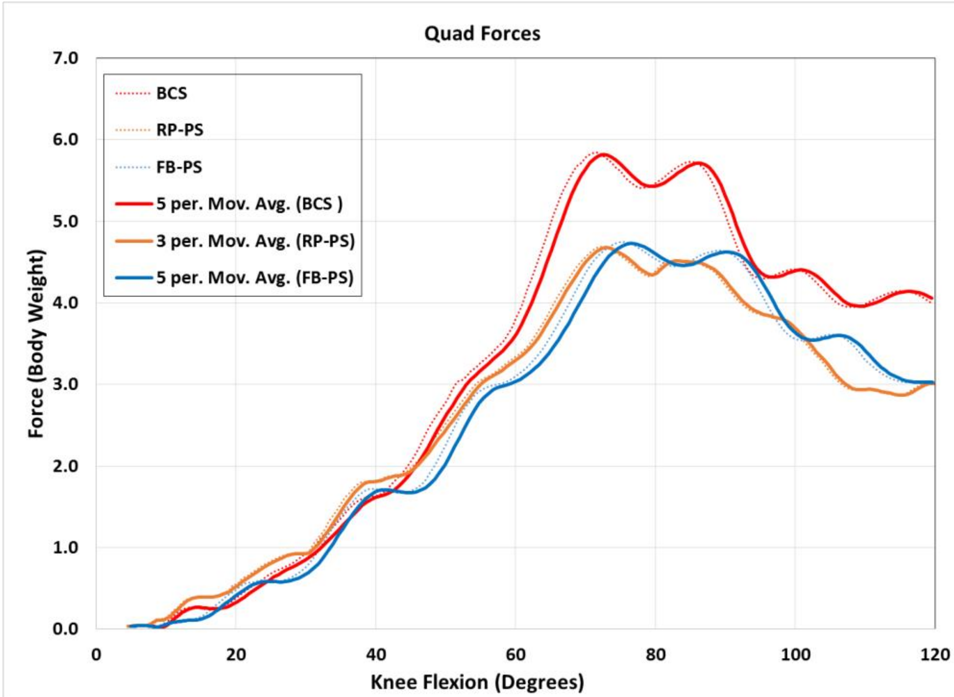

Figure 5-25: Quadriceps forces produced by the simulations for the BCS, FB-PS and RP-PS TKAs.

5.3.4 Patello-Femoral Forces

The patella-femoral contact force varied from 0BW at full extension to 1.9BW at full knee flexion for the simulation of the BCS TKA subject. The nature of this variance in force was different than that seen for the tibio-femoral force for this implant. The force was increasing in nature from full extension to 72 degrees of flexion (5.2BW), after which it reduced in deeper flexion.

The simulation for the FB-PS TKA revealed a similar pattern, with the patella forces increasing from full extension to 80 degrees of flexion before reducing in deeper flexion. At full extension, the simulation for the FB-PS TKA showed a total contact force of 0.1BW which increased in nature to 4.5BW at 80 degrees of flexion before reducing in deeper flexion to 1.9BW. The RP-PS

TKA also exhibited a similar nature with the simulation starting with 0.1BW at full extension and reaching a maximum value of 4.3BW at 70 degrees before reducing in deeper flexion to 1.7BW at 120 degrees of flexion (Figure 5-26). Except for early flexion (0-40 degrees) when the three simulation exhibited similar magnitudes of force, the simulation for the BCS TKA always exhibited a higher force when compared to the FB-PS and RP-PS TKA.

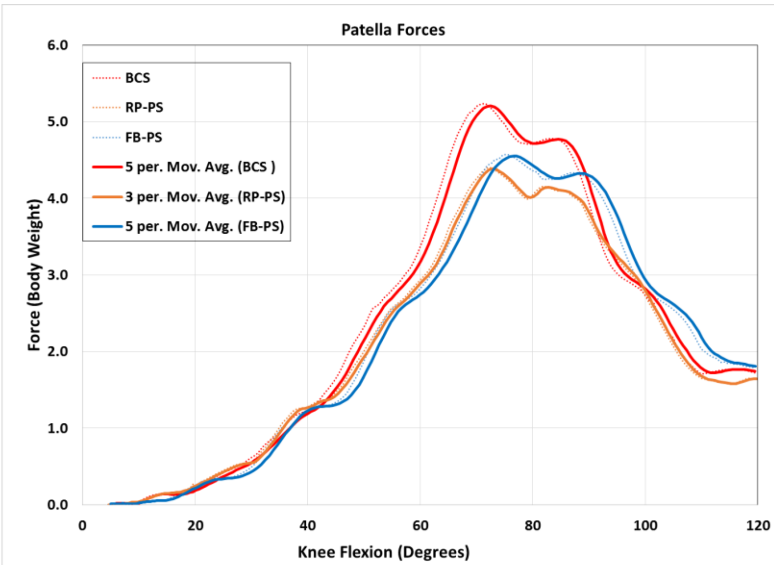

Figure 5-26: Patello-femoral forces produced by the simulations for the BCS, FB-PS and RP-PS TKAs.

5.4 Vibroarthrography

5.4.1 Building of the sound Analyzer

The first key to analyzing vibration data in conjunction with the motion of the knee in to effectively synchronize the two data streams to seamlessly visualize the vibration emitted by the knee joint at specific degrees of flexion. In order to achieve this task we created a graphical user interface that can import, analyze and synthesize the video fluoroscopy/live video, 3D in vivo kinematics and sound data simultaneously in one interface.

The sound analyzer uses existing platform of the Kinematic Analysis of Rigid Body Systems (KARBS) software currently in use at the center for musculoskeletal research. The KARS software, written in Matlab, is capable of importing raw fluoroscopy images and conducting a 3D-to-2D registration of the CAD components to the fluoroscopy images to determine 3D kinematics throughout the range of motion. This if possible for both, TKA images as well as native knee images. The sound analyzer uses these two functional capabilities of the KARBS system and adds the capability to import and analyze vibration data which is synched to the in-vivo motion.

The sound analyzer has 4 main components. The first component is the time synched fluoroscopy/live video collected from the patient. The second component is the 3D kinematics of the knee joint determined from 3D-to-2D registration. The third component is the ability to import and analyze vibration data that is time synched to the video feed and finally the forth component can export the analyzed data as one seamless output (Figure 5-27).

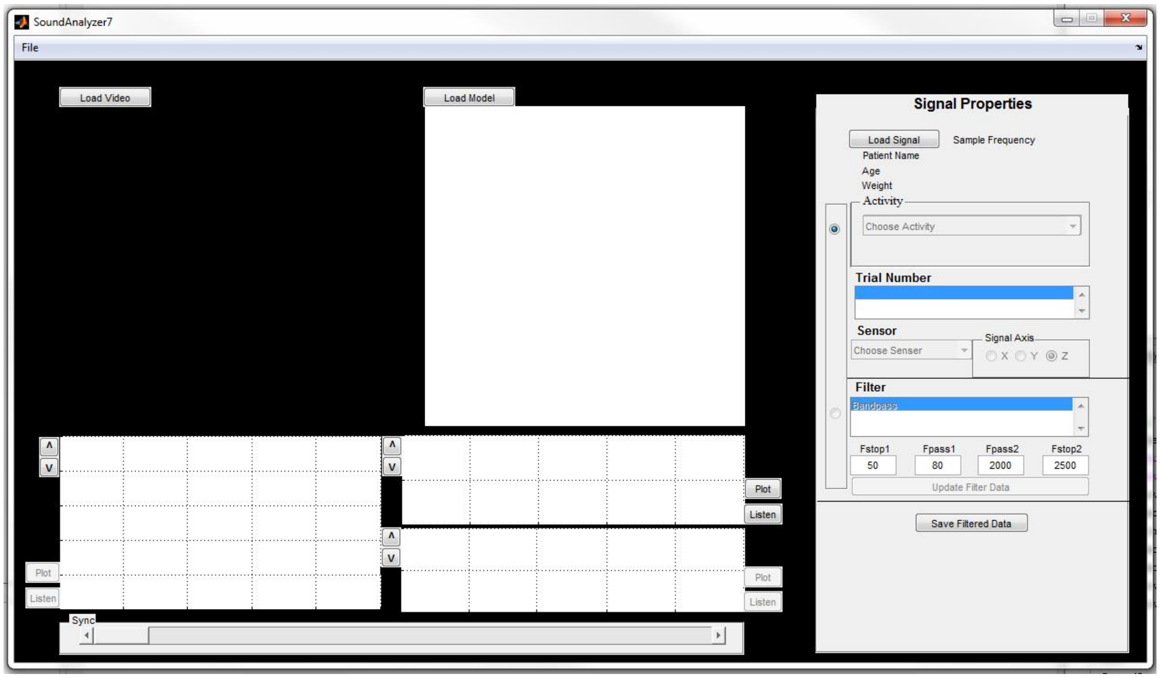

Figure 5-27: The basic GUI interface for the sound analyzer.

The operator can import the fluoroscopy video in the top left corner. The corresponding 3D kinematics are imported simultaneously, in the top right. The panel on the right enables the operator to control the visualization of time synched vibration signals for the particular patient (Figure 5-28). The raw vibration signals are populated on the bottom left of the GUI. The right hand panel also includes various filters that can be utilized to analyze the vibration data. Each iteration of the vibration analysis populates on the bottom right with the ability to save a particular analysis for further comparison.

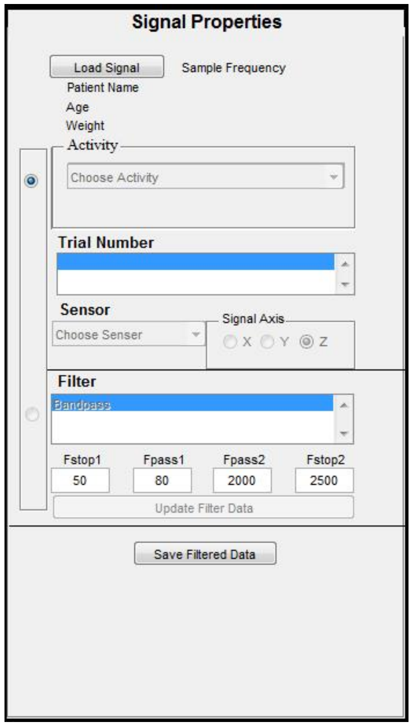

Figure 5-28: The analysis panel that enables the analysis of the vibration data.

Using this GUI it becomes possible to analyze vibration and in-vivo data simultaneously in a time synched environment (Figure 5-29). This analysis is possible through the whole range of knee flexion (Figure 5-30). In the case of native knees it is possible to demarcate the areas of knee degeneration (if existing) and the analysis can provide a visual feedback on the contacting surfaces that are responsible for producing particular vibration patterns Figure 5-31).

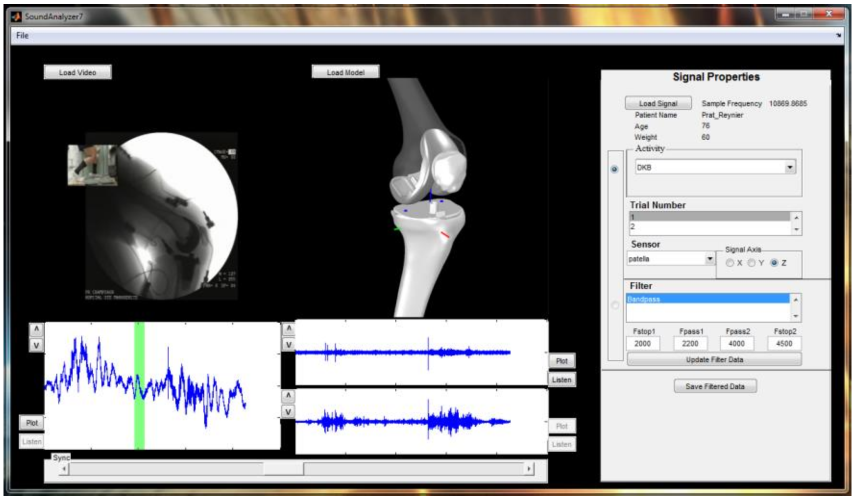

Figure 5-29: Example of analysis of the vibration data along with in-vivo fluoroscopy.

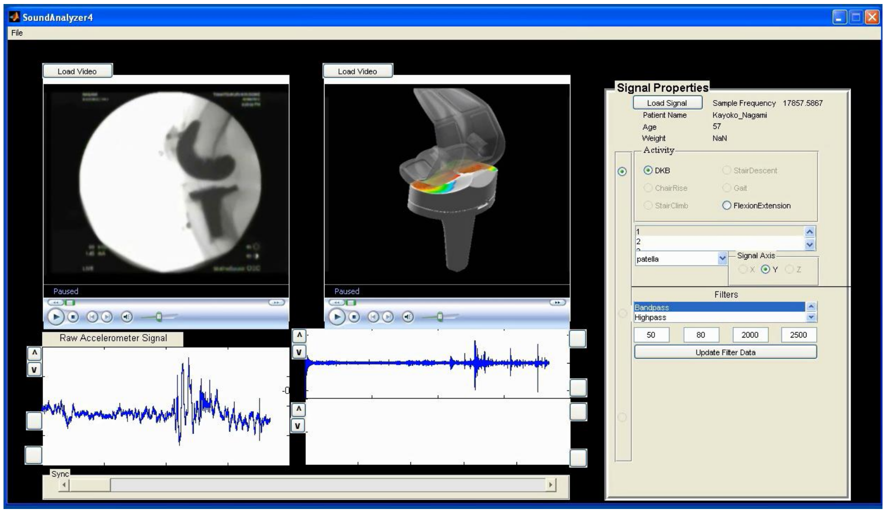

Figure 5-30: Example of analysis of the vibration data along with in-vivo fluoroscopy for deep knee bend.

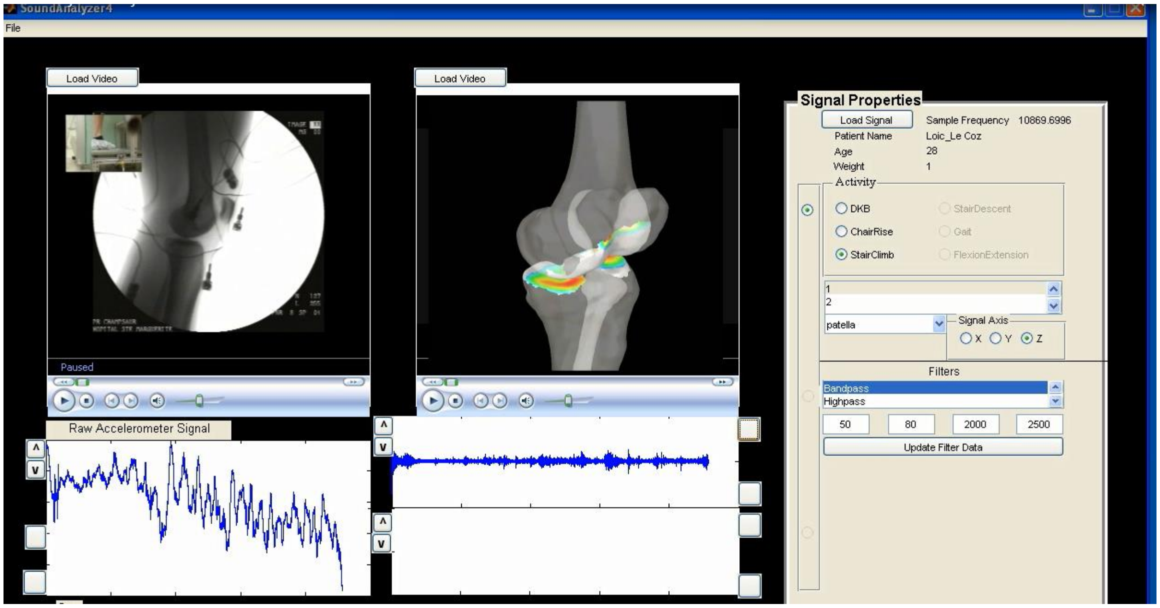

Figure 5-31: Example of analysis of the vibration data along with in-vivo fluoroscopy for the native knee.

Once the analysis is complete, the sound analyzer enable the export of a single file that contains the time synched in-vivo fluoroscopy and the resulting vibration associated with the tested motion patter (Figure 5-32). This can then be utilized to analyze differences between various knee joint conditions.

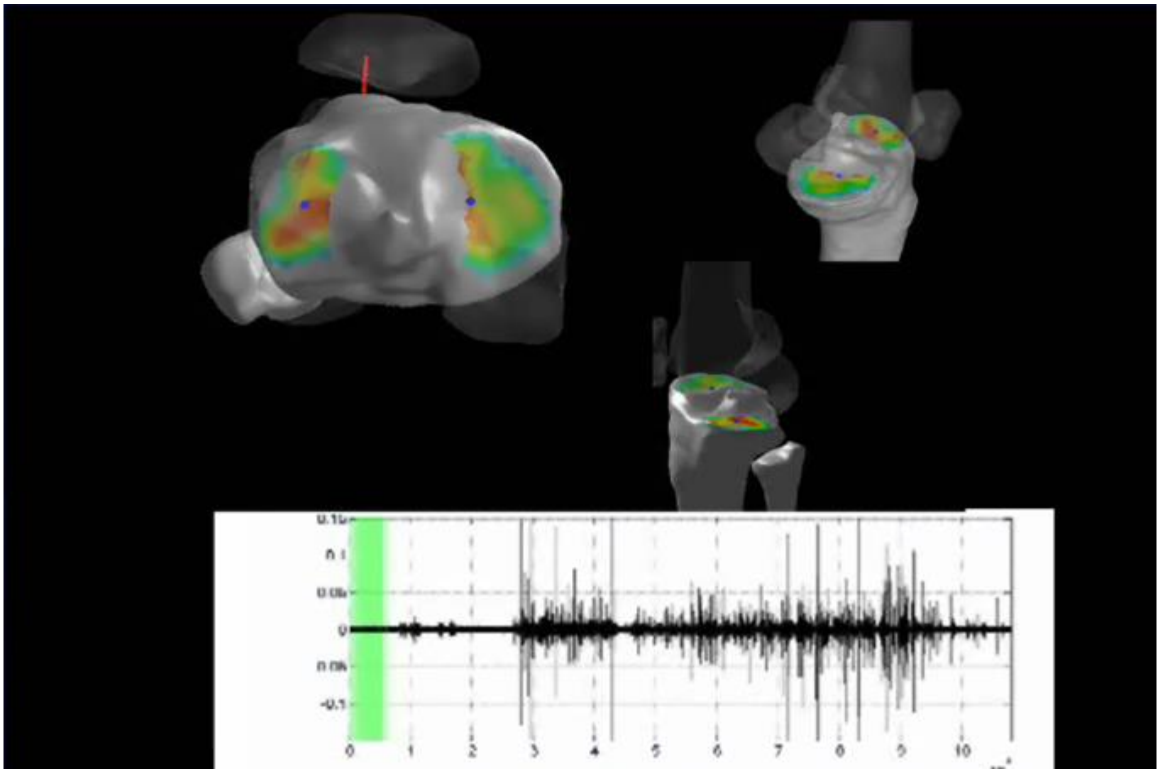

Figure 5-32: Example of output of the analysis for the native knee.

5.4.2 Qualitative Analysis

Using the sound analyzer GUI described in the previous section, data was analyzed for patients who exhibited various knee condition in an attempt to validate the ability of the system to synchronize and analyze in-vivo and vibration data. This analysis was also able to differentiate the various conditions based on the vibration data. The condition that were analyzed included:

1) Native knees for young subjects with no degeneration vs Native knee for older patients vs patients with osteoarthritic degeneration. This analysis clearly showed the differences in the vibration content between the three conditions. Subjects with a native knee with no

degeneration exhibited with little to no vibration content throughout the range of motion during a DKB activity (Figure 5-33). Compared to this analysis, patients who had no reported degeneration, but were older in age also exhibited little vibration content, albeit more than the younger subjects (Figure 5-34). Lastly patients who were diagnosed with end stage OA and who were candidate for TKA surgery exhibited an increased vibration content when compared to subjects with no degeneration (Figure 5-35).

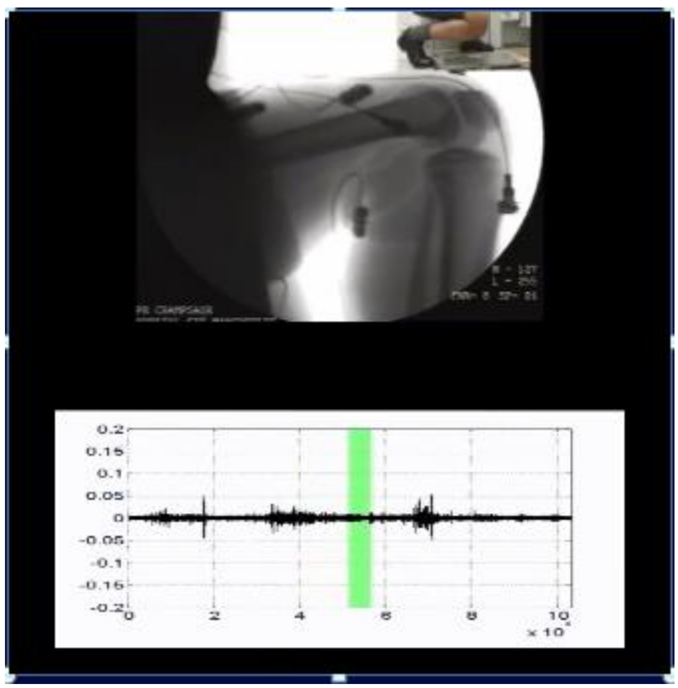

Figure 5-33: Vibration analysis for a young patient exhibiting little vibration content due to smooth articulating surfaces.

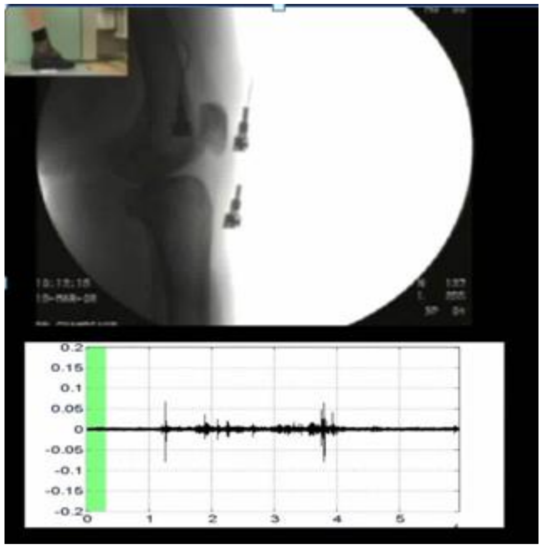

Figure 5-34: Vibration analysis for an old patient exhibiting little vibration content due to smooth articulating surfaces.

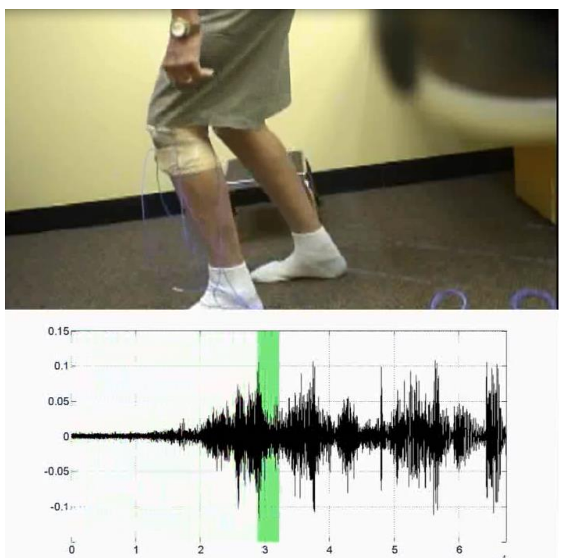

Figure 5-35: Vibration analysis for a patient with end stage OA exhibiting increased vibration content through range of motion.

2) Analysis of patients with failed TKAs and well-functioning TKAs revealed a similar trend. Patients with a failed TKA and who were candidates for replacement TKA surgery exhibited a significantly large vibration content than patients with well-functioning TKA (Figures 5-36 and 5-37).

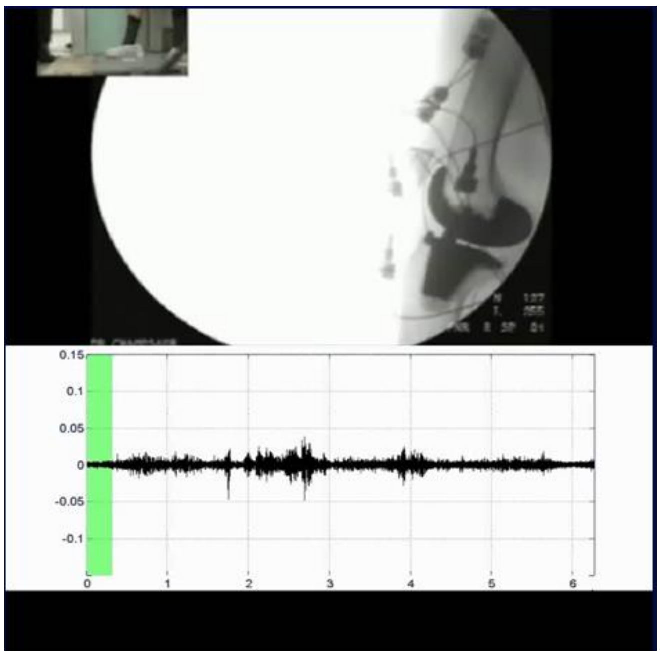

Figure 5-36: Vibration analysis for patient with well-functioning TKA exhibiting little vibration content due to smooth articulating surfaces.

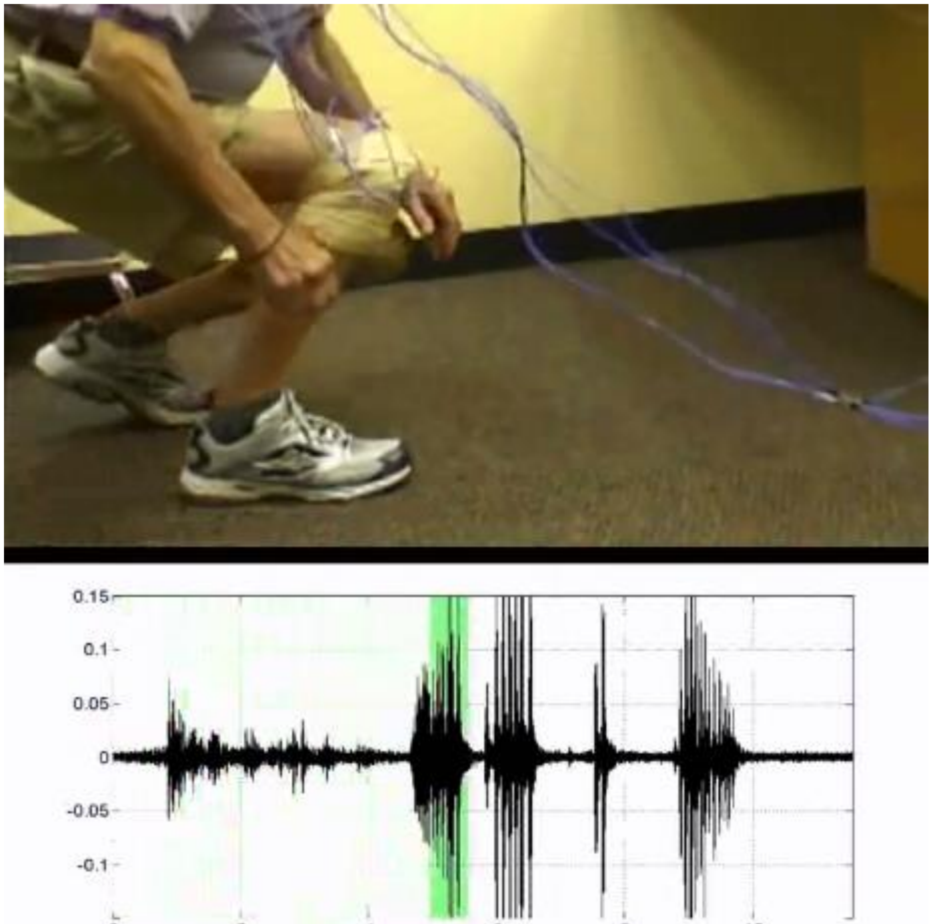

Figure 5-37: Vibration analysis for a patient with a failed TKA exhibiting increased vibration content through range of motion.

3) Analysis to determine the location of OA wear in patients with uni-comparmental degeneration revealed that having OA in a single compartment can be effectively identified using vibration sensors. The compartment with higher amount of wear exhibited significantly higher vibration content that compartment with little wear (Figure 5-38). This experiment demonstrated the ability of the vibration sensors to capture data closest to the point of application, thus making it possible to isolate the location of degeneration.

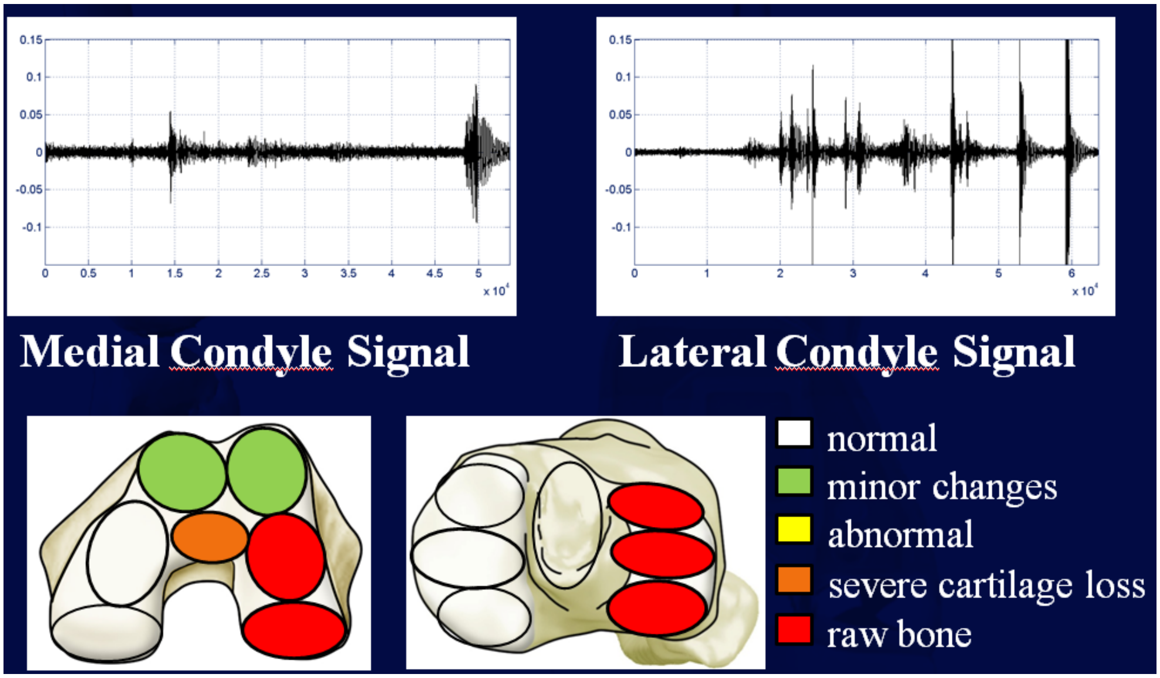

Figure 5-38: Vibration analysis for a patient with uni-compartmental OA. The results clearly indicate that vibration analysis can determine the location of degeneration.

4) Analysis of patients that exhibit lift-off during range of motion. This analysis was conducted during a leg swing activity for a patient with joint laxity. The hypothesis was that the laxity of the joint will result in lift-off on the femoral condyle during a high velocity activity. The analysis of the 3D kinematics in conjunction with the vibration data revealed that it was possible to correlate specific spikes in the vibration signal that correspond to lift-off of the femoral condyle as determined my the 3D-to-2D kinematic evaluation. The vibration content in the signal was seen to be very little, except when the femoral cam contacted the tibial post and when the distance between the femoral and tibial surface contacted after a period of "no contact" or lift-off. The spike related to the cam-post

interaction was larger and in the flexion phase of the leg swing, while the spike corresponding to the lift-off was smaller and on the extension phase of the leg swing activity (Figure 5-39).

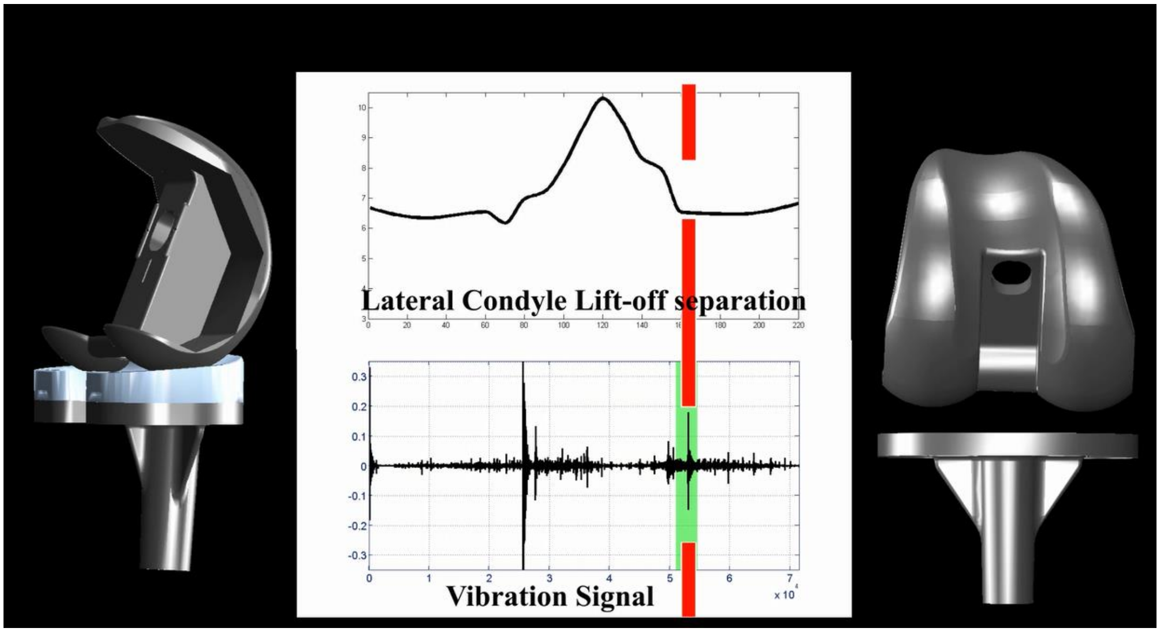

Figure 5-39: Analysis and correlation of vibration data with lift-off during a leg swing activity.

5) Analysis of a patient receiving visco-supplementation. This analysis clearly showed the differences in the vibration content between the two conditions. The patient was tested prior to receiving a visco-supplementation injection and exhibited high amounts of vibration content similar to a patient with OA. After visco-supplementation was completed the patient was retested and exhibited significantly lower vibration. This test demonstrated

the ability of the visco-supplementation to lubricate the joint, there-by reducing the vibrations in the knee joint space (Figures 5-40 and 5-41).

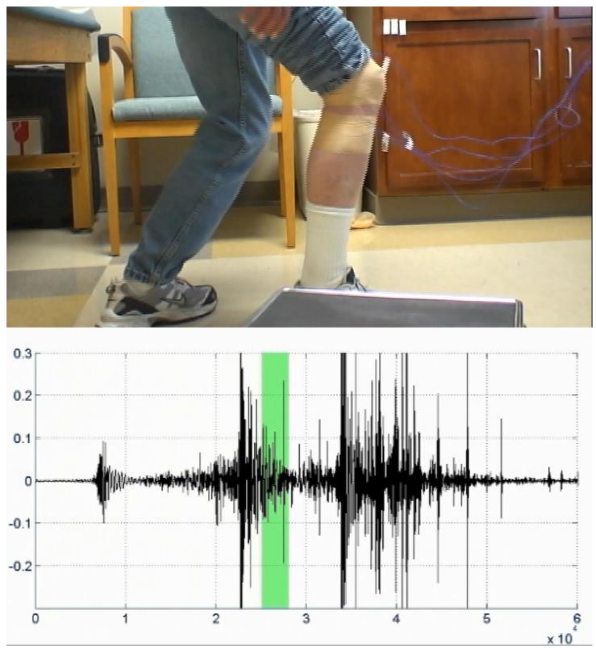

Figure 5-40: Analysis of a patient prior to visco-supplementation exhibiting high vibration content.

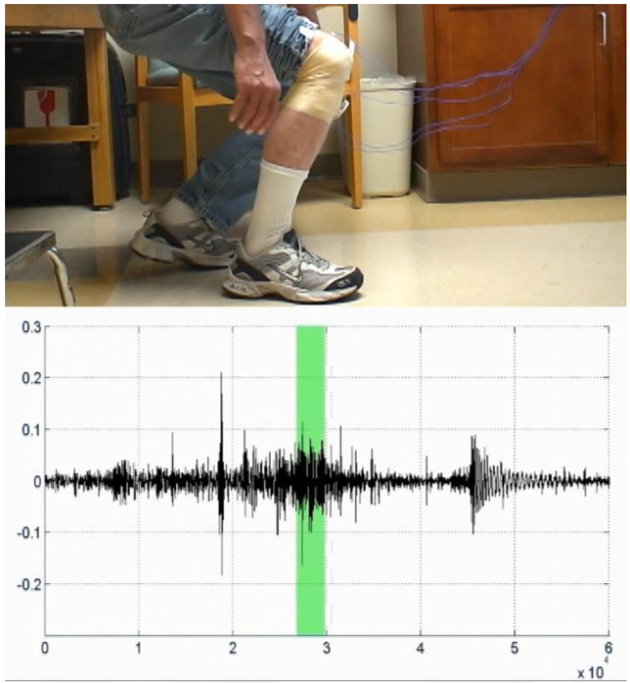

Figure 5-41: Analysis of a patient after to visco-supplementation exhibiting lower vibration content.

6) Analysis of cam-post engagement. This analysis was conducted on patients with well-functioning knees in order to test the feasibility of the detecting the nature of contact. The test revealed that vibration data can effectively pick up cam-post interaction. Additionally, it seems to demonstrate that contact occurring with a smooth transition on the central aspect of the cam produces less impact, while contact occurring on the outer edges of the post with an abrupt contact produces a larger impact spike (Figures 5-42 and 5-43).

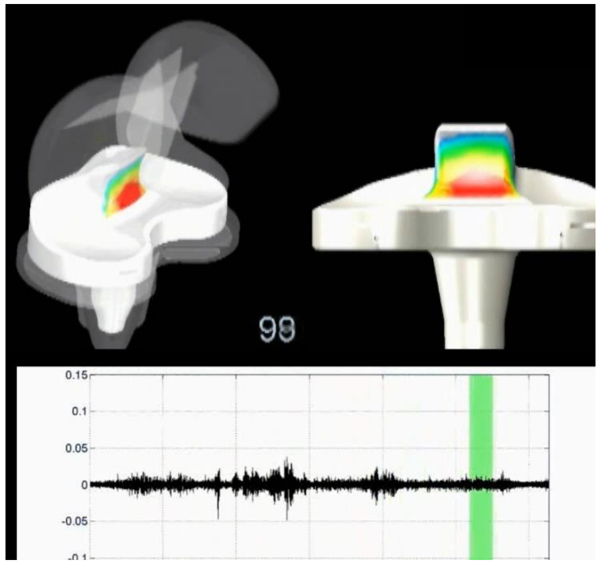

Figure 5-42: Analysis of cam-post contact for a RP-PS TKA exhibiting lower vibration content associated with a smooth transition during initial contact.

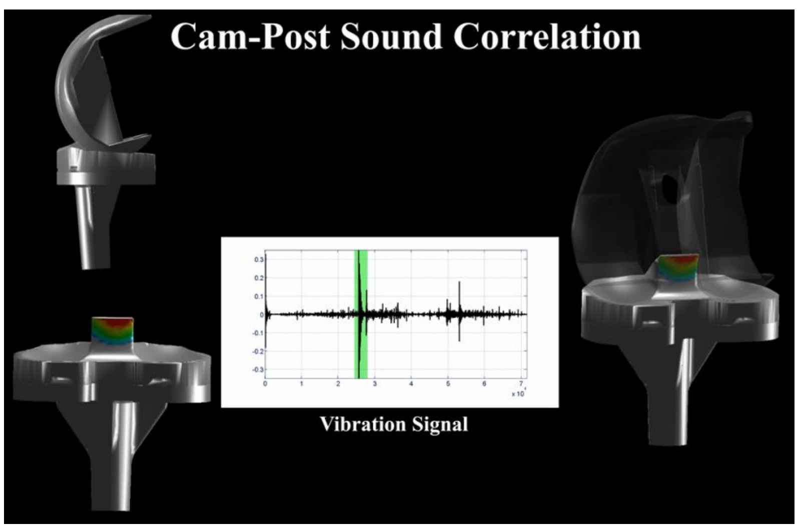

Figure 5-43: Analysis of cam-post contact for a FB-PS TKA exhibiting an impact spike associated with an irregular transition during initial contact.

5.4.3 Pattern Recognition

VAG signals were collected for 23 healthy and 53 arthritic subjects. After selecting the candidate features of the signals, a pattern classifier was designed. The objective of the classifier was to classify the given pattern of the patellofemoral VAG signal to one of the two groups: healhty or arthritic. The minimum-error-rate classification was chosen for the first attempt to design the classifier. This classification can be achieved by the use of the discriminant functions:

$$g_i(x) = \ln p(x|\omega_i) + \ln P(\omega_i) \qquad (1)$$

and assuming that the densities $p(x|\omega_i)$ are multivariate normal, the Eq. 20 becomes:

$$g_i(x) = -\frac{1}{2}(x-\mu_i)^t E_i^{-1}(x-\mu_i) - \frac{d}{2}\ln 2\pi - \frac{1}{2}\ln|E_i| + \ln P(\omega_i), \quad (2)$$

Since at the current stage of analysis there is no premise to classify the patient as either arthritic or healthy, the prior probabilities for both categories were assumed to be equal

$$(P(\omega_1) = P(\omega_2) = \frac{1}{2}).$$

The analysis showed that the signal range, 25 and 75th quantiles do not provide any significant discrimination improvement compared to the other parameters, and were excluded. Instead, the integral of the signal’s envelope was calculated for evaluation. Also, the VAG signal’s envelope seemed to be higher for those subjects who performed the activity faster, therefore the product of the integral of the envelope and activity duration was selected as the last (11th) signal feature.

The DKB activity were selected for investigation using all the 76 datasets. However, it was noticed that the vibration patterns may differ between the trials even for the same subject. Therefore, it was decided to analyze all the trials of DKB performed by each subject rather than a single one. Once the statistical parameters (i.e. mean, SD, skewness, kurtosis, quantiles, etc.) were calculated for VAG signals from each trial, the mean, the absolute minimum, and the absolute maximum from all trials were calculated. That provided the total of 33 signal features selected for the assessment of their classification effectiveness.

The results obtained for the 23 healthy and 53 arthritic subjects, confirmed that the mean of rectified signal is higher for the arthritic than for the healthy subjects. However, surprisingly the variance was lower for the damaged than for the intact knees. The skewness and kurtosis were also lower for the affected knees, but in general all the other parameters were higher for this group.

In order to better study the discrimination effectiveness of these statistical parameters, the two-sample *t*-test without assuming variances are equal was used. The null hypothesis (H_0) was that the data in both groups are independent random samples from normal distributions with equal means, against the alternative that the means are not equal. The H=1 indicated the rejection of the null hypothesis at the 5% significance level. The signal features, which means are not equal (p<0.05) could be considered good candidates for the pattern classification.

This approach identified 6 signal features, for which means were significantly different for both groups:

- minimum of the signal means from all trials,
- minimum of the signal median from all trials,
- mean of the signal 90^{th} quantiles from all trials,
- minimum of the signal 90^{th} quantiles from all trials,
- minimum of the signal 95^{th} quantiles from all trials,
- minimum of the integrals of signal envelope from all trials.

If the hypothesis, that the signals are different between the two knee conditions, is true, it should be valid for all activities, and including more activities could potentially enhance the classification rate. Therefore, it was decided to expand the analysis on all the activities collected for each subject; Deep Knee Bend, Chair Rise, Stair Climb, Stair Descent, Gait and Flexion-Extension. Then the feature means, absolute minimum and maximum were calculated for all trials of all activities (Figure 5-44).

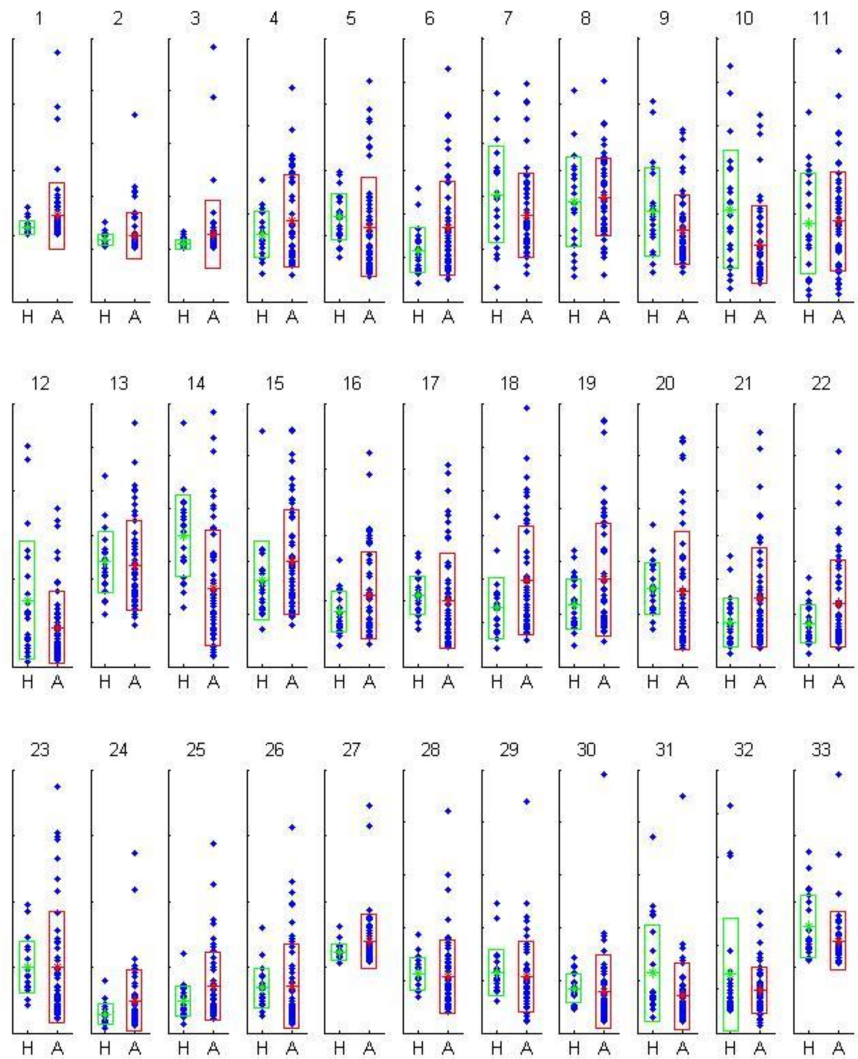

Figure 5-44: Distribution of selected 33 signal features for all 23 healthy (H), and 53 arthritic (A) subjects determined for all trials of the deep knee bend activity.

Taking into account all activities, has more strongly confirmed the initial hypothesis that the signal mean and variance are higher for arthritic than healthy knees. As a matter of fact, all signal features except kurtosis were higher for the affected knee joints. Also it was found that including all activities has yielded significantly better separation of the data than analyzing the DKB only. The means of 15 out of 33 signal features were significantly different for the two groups. Many of the parameters indicated extremely significant differences between the groups

In order to find the set of features providing the best classification, all 528 possible combinations of 2, 5456 combinations of 3 and 40920 possible combinations of 4 signal features taken from all 33 parameters have been evaluated. The highest success rate obtained using two signal features was 93.67%.

Using a set of three features increased the classification rate up to 96.2% using a combinations of features nr 4, 14, 28 (Figures 5-45, 5-46, 5-47).

Adding the 4^{th} parameter to pattern classification increased the success rate up to 97.4%, as summarized in following table:

The best classification utilizing a set of three features was achieved using the following set:

- feature 14: minimum of the signals' median from all trials,
- feature 29: mean of the signal's mean from all trials,
- feature 28: mean of the signal envelope integral times activity duration from all trials.

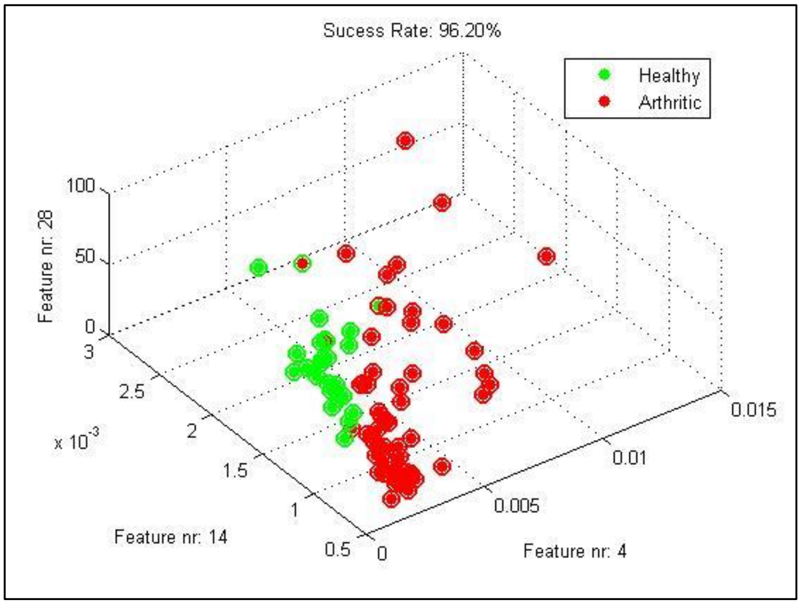

Figure 5-45: Classification using 3 features 4, 14 and 28 resulting in a 96.2% classification strength.

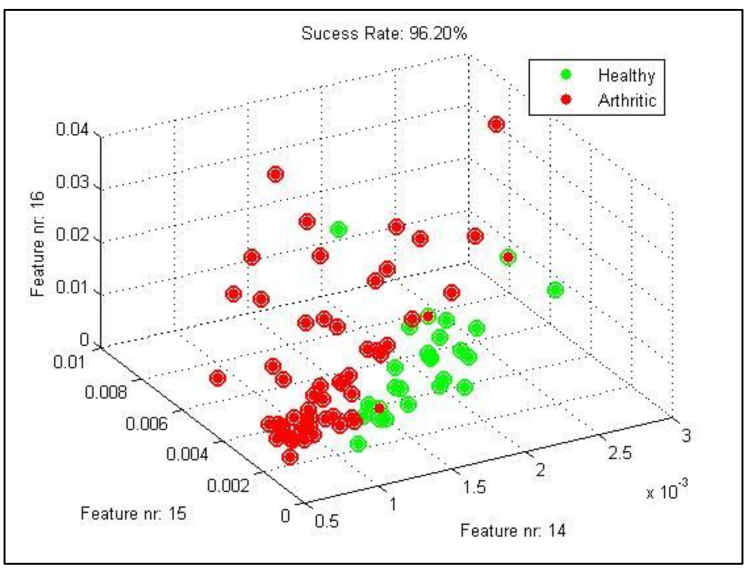

Figure 5-46: Classification using 3 features 14, 15 and 16 resulting in a 96.2% classification strength.

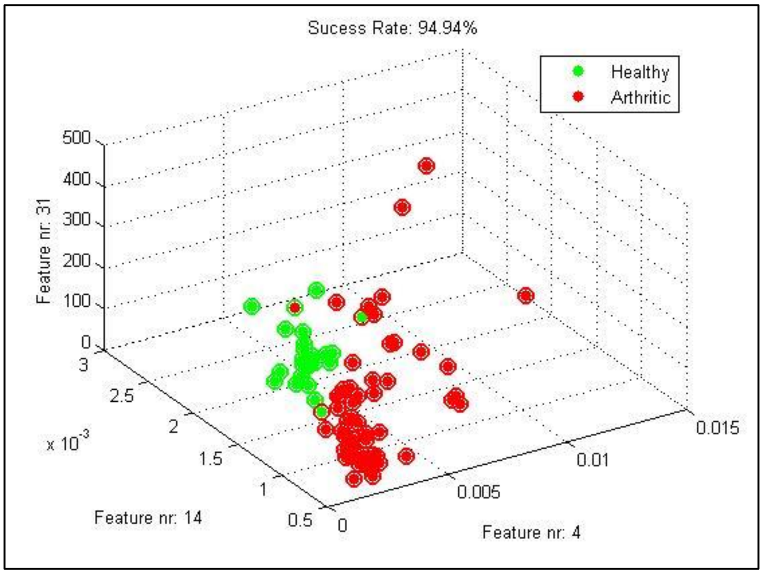

Figure 5-47: Classification using 3 features 4, 14 and 31 resulting in a 94.9% classification strength.

Chapter 6: Discussion

Multiple studies have demonstrated the kinematic performance of CR and PS type TKA designs. Also, other studies have investigated the kinematic efficacy of a mobile polyethylene when compared to a fixed bearing device. However, limited data exists investigating the various aspects pertaining to the cam-post interaction, and the role bearing mobility plays in terms of cam-post mechanics. The present study investigates the cam-post mechanism in three different types of PS TKA and demonstrates the differences in terms of contact angle, nature of contact and height of cam-post contact between the devices.

Numerous kinematic evaluations have found larger magnitudes of PFR in native knees when compared to TKAs. In order to replicate normal knee kinematics in TKAs, and to felicitate higher range-of-motion post-surgery, implant manufacturers have used various philosophies. One of the commonly used configurations of TKA in the market today utilizes a cam-post mechanism to engage in mid-flexion and felicitate PRF to achieve higher flexion. Early cam-post engagement is not ideal, as it would mean that engagement would occur during every cycle of common day activities (eg walking) not requiring high flexion and increase the possibility of early tibial post wear.

Studies conducted to evaluate the cam-post interaction in FB-PS TKA designs during common daily activities have exhibited cam-post engagement angles ranging from 40^{o} during a step-up maneuver, to 91^{o} during lunge activities. A study conducted by Catani et al, on five BCS TKA revealed anterior cam post engagement to occur only in early flexion, while posterior cam-post engagement to occur at ≈63°, ≈58°, and ≈50° during the chair-rise, step-up and step-down activities respectively. The current study suggests similar results for the two PS type designs, with cam-post engagement occurring at 93° and 97° for the FB-PS and RP-PS groups respectively. However, the BCS group experienced an average of 34° during the DKB activity which is contrary to that reported by Catani et al.

Polyethylene design also plays an important role in determining the cam-post engagement. Designs which incorporate an anteriorized dwell point at full extension reduce the initial cam-post distance, thereby increasing the possibility of early cam-post engagement. This seems to explain the early engagement angle experienced by the subjects in the BCS group. Among all the three groups analyzed, the BCS group experienced the most anterior tibio-femoral contact points at full extension (Table 6-1). The FB-PS and RP-PS groups experienced a contact point which was posterior to the midline of the tibial component. This ensured a larger distance between the femoral cam and tibial post, thereby ensuring a late cam-post interaction. One subject in the RP-PS group did not experience cam-post engagement. However, this patient exhibited a lower maximum knee flexion (86°) than the average cam-post contact angle (97°) for this group.

On the posterior cam-post interaction site, for the BCS and FB-PS groups, the initial contact with the tibial post was achieved on the medial aspect, before the contact area tended to move centrally and superiorly with increasing flexion. Interestingly, in the RP-PS group, the contact between the cam and post was located centrally on the post at all times when engaged. This is probably due to the mobility of the polyethylene, characteristic for the analyzed TKA design. The polyethylene insert rotated axially in accord with the rotating femur (Figure 6-1). Therefore the posterior surface of the mobile bearing post was able to remain parallel to the surface of the femoral cam. This phenomenon was not observed in the FB TKAs and may increase the chances of edge loading on the polyethylene, resulting in wear patterns on the post.

Another consideration in designing the cam-post interaction is the ability of the cam-post contact point to remain low on the tibial spine with increasing flexion. This provides greater stability by increasing the jump height and also reduces stress in the tibial post by introducing the cam-post force at a location of maximum material. The cam-post contact height for the BCS TKA was significantly higher than the other two groups. For the FB-PS and RP-PS groups the contact occurred mid-spine and remained in the lower part of the tibial post. This finding suggests that cam-post design for FB-PS and RP-PS TKAs could result in lower cam-post stresses, thus reducing the chances for failure of the tibial post.

Table 6-1: Tibio-femoral contact location at full extension for subjects in the three groups.

Group	Full Extension (mm)					
	Lateral A/P Contact			Medial A/P Contact		
	Average	Range	Std	Average	Range	Std
RP-PS Group	-5.7	-8.7 to -2.2	2.0	-5.3	-7.2 to -3.0	1.4
FB-PS Group	-2.1	-5.4 to 0.8	2.1	-3.9	-8.7 to -0.2	2.3
BCS Group	4.6	-3.0 to 18.4	8.0	6.6	3.9 to 9.4	1.6

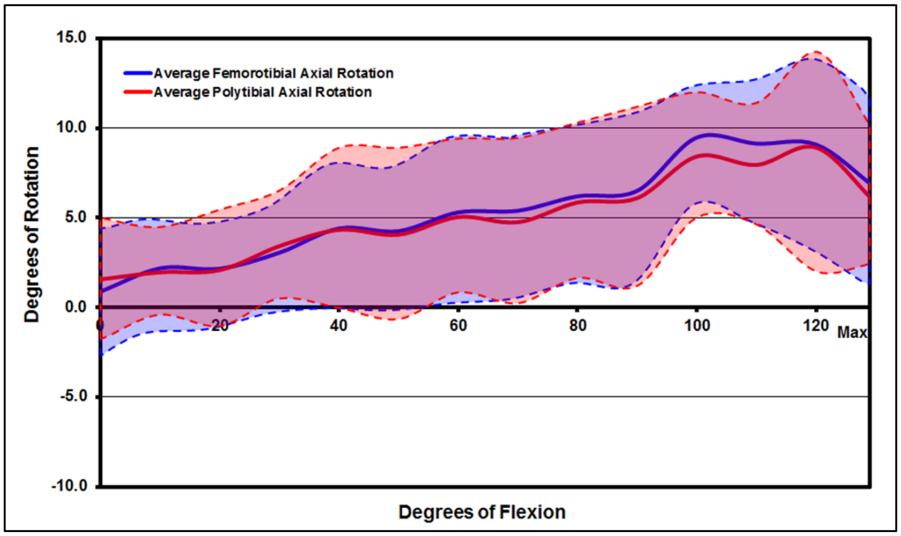

Figure 6-1: Similar rotation of the femur and poly ensured full contact of the cam-post mechanism.

The use of a forward dynamic model to simulate the function of a TKA has previously been successfully demonstrated by Mueller et al. building on the results from that study, the current model incorporates the cam-post interaction as an added output from the same model. Results indicate that cam-post forces vary between designs. Previous research (Suggs et al and Nakayama et al) by suggested that the cam-post force is in the range of 500-800N. However, these studies were conducted on a knee simulator and the results need not be transferable to in-vivo conditions. Greenwald et al. used mathematical modeling to determine knee forces in the native knee and suggested that the AP force on the tibio-femoral interface are between 1-1.2 times body weight. A recently study by Piangiani et al conducted a robust cadaveric experiment on cam-post forces during various activities on TKAs and found the cam-post force to be around 1000N (1.2 time body weight based on this study) during a squat activity.

Results from this study indicate similar results for the FB-PS and RP-PS TKA, with the maximum cam-post force being 1.3 and 1.6 times BW. The cam-post forces in the BCS TKA were found to be higher and can be attributed to the fact that the contact in these knees occurs at an early engagement angle when compared to the other knees.

Interestingly, the location of the cam-post force followed a similar pattern to the in-vivo kinematics. The simulation for the RP-PS TKA exhibited the force being located on the central part of the post at all times. For the BCS and FB-PS TKA the force was mainly located on the edge of the post. These results seem to indicate that due to the rotating poly in the RP-PS TKA which ensures central contact, the force distribution is likely to be within the “meat” of the post. Also, rotation of the femur over the tibia does not influence the location of the force. These two findings could play a crucial role in increasing the longevity of the post in RP-PS TKA. On the other hand, both FB TKA exhibited forces on the edges of the post. This could be due to the fact that the femur in these knees do not rotate in conjunction with the polyethylene, thus leading to situations where the cam encounters the edge of the post during interaction. This could potentially lead to edge loading conditions undesirable from a wear stand point.

The vibration signals have been collected to evaluate their potential application to diagnose the articular cartilage condition. According to the hypothesis vibrations should increase as the cartilage degenerates. To prove this concept, the signals were collected from a group of subjects with osteoarthritis and a control group of healthy individuals. This initial analysis confirmed the hypothesis, because in general the vibrations had higher variation in the arthritic group. Recently

Rangayyan et al. also reported that larger variability was observed in abnormal knee joints. The differences were also heard when the signals are converted to audible forms. These distinct sound differences were utilized to test six conditions:

1. Native knees for young subjects with no degeneration vs Native knee for older patients vs patients with osteoarthritic degeneration
2. Analysis of patients with failed TKAs and well-functioning TKAs
3. Analysis to determine the location of OA wear in patients with uni-comparmental degeneration
4. Analysis of patients that exhibit lift-off during range of motion
5. Analysis of a patient receiving visco-supplementation
6. Analysis of cam-post engagement

These analysis were successful in finding distinct differences that can be used in future to distinguish between patients with these condition by only the use of vibroarthrography. These also build on the early observations made by Blodgett and Walters who could hear more grating and cracking knee joint sounds being emitted by older subjects, who's articular cartilage most probably deteriorated with age.

Analysis of all the 76 samples confirmed that the variance is indeed significantly higher in the arthritic group, but other signal features yielded even better discrimination. A number of signal parameter combinations were evaluated and eventually sets of features yielding accuracy up to

96.2% were identified. Such high success rate is very promising and confirms that the vibration data could be potentially used for diagnostic purposes.

Krishnan and Rangayyan also studied knee vibroarthrographic signals for screening purposes. They used one accelerometer attached at the middle of the patella and collected signals for 19 healthy and 18 pathologic knee joints during extension exercise. They decomposed the signals using wavelet packets and matching pursuit methods and computed the signal features based on energy and frequency parameters. The analysis allowed them to classify the signals with 83.8% accuracy.

Recently Rangayyan and Wu presented more extensive work evaluating vibroarthrography (VAG) samples collected for 51 healthy and 38 abnormal knee joints. The abnormal conditions included various pathologies; patella chondromalacia of different grades, meniscal tears, tibial chondromalacia and ACL injuries. They normalized the VAG signals so that the amplitude ranged between 0 and 1, and then calculated a number of statistical parameters; mean, SD, skewness, kurtosis, entropy, as well as the "`form factor"' representing the variability of the signal. In the current study, the skewness and kurtosis were found to be the parameters providing the lowest discrimination. Using the Fisher's linear discriminant analysis, they were able to classify normal vs abnormal cases with 75.6% accuracy. They achieved better classification of 85.9% when the conditions were narrowed down to discriminate only between normal and the 20 patella chondromalacia cases.

Kim et al. studied knee joint sounds by means of an electro-stetoscope. They gathered data for 20 non-symptomatic subjects and 11 patients with diagnosed degenerative arthritis performing exion-extension activity. The authors obtained features from the time-frequency distribution of VAG signals using segmentation by dynamic time warping. Next, they used back-propagation neural network for classification and reported 91.4% accuracy.

Gajre et al. proposed using electrical impedance signals for non-invasive diagnosis of osteoarthritic knees. They collected the data around the knee by tetra-polar impedance plethysmography for 8 normal and 10 osteoarthritic subjects. They used variance and root mean square values as temporal features and energy band of 0- 5KHz as frequency domain feature. A trained artificial multilayer feed forward neural network provided accuracy of 85.19% based on the knee-swing data.

Though methods using transducers other than accelerometers have been proposed and reported encouraging results. The results in the current work have been obtained using accelerometers and have yielded higher success rate than any other study reported in the literature to date. Current study also evaluated more arthritic subjects than the previous studies.

This is the first study to compare the cam-post interaction mechanics in three different types of PS type TKAs. It suggests that the mobility of polyethylene insert as well as the polyethylene design with respect to dwell point play an important role in determining the amount and nature of cam-post interaction as well as distribution of the cam-post force. Additionally, this study investigated the use of vibroarthrography as a tool to determine various conditions in the knee joint and demonstrated the ability to determine differences in the joint purely based on the vibration content in the knee.

Chapter 7: Limitations and Future Work

This dissertation investigates the cam-post mechanism in three different types of PS TKA and demonstrates the differences in mechanics of the cam-post contact between the devices. Though this study is the first to compare cam-post interaction between fixed and mobile bearing TKAs, it does have some limitations.

Firstly, with regards to kinematics, the sample size of the study is small. This was due to the limitation in procuring subjects with beaded polyethylene RP inserts for recruitment to the study. However, the findings of this study clearly demonstrate the differences in the three groups of TKAs and are a good first indicator of trends between the groups. The subjects chosen were operated by different surgeons, and does not account for surgeon variability. However, each surgeon chosen was highly experienced in the implantation procedure for their chosen device, and each subject was deemed clinically successful with a HSS score>90, which would reduce the amount of variability that may arise between patients in each group. The cam-post engagement mechanism was estimated by utilizing a 3D-to-2D registration technique and 3D CAD models provided by the device manufacturers. The implant components (especially the polyethylene insert) do not take into account wear, subjects may have experienced post-surgery. However, this limitation would be inherent in any in-vivo analysis conducted on successful and well-functioning TKAs that are not scheduled for revision surgery (hence limiting the ability to retrieve the polyethylene component). This trade off, however, provides a detailed investigation of the cam-post mechanism in subjects with PS TKA assuming they still have intact polyethylene components. Future studies should look at the cam-post interaction in a larger patient population, ideally implanted by the same surgeon.

Secondly, the investigation of forces was conducted using a single sample for each of the groups and not on all patients. This is however, a limitation of the forward dynamic model, which does not provide for exact replication of the in-vivo kinematics of each subject. Nonetheless, the three simulations provide valuable insight into the variation in cam-post forces between the three TKAs analyzed. Future studies should investigate the use of an inverse dynamic model that will enable the determination of cam-post forces for varying kinematic patterns seen for the same implant type, as well as, between different implant designs.

Lastly, the vibroarthrography study was conducted on a set of native and arthritic knees. Though this did provide a good starting point for the validation of such methods, future studies should look into determination of various soft tissue injuries with the use of vibroarthrography. This will provide the valuable information that can be used to develop a tool to determine soft tissue injuries without the use of radiation methods.

References

1 Carr BC, Goswami T: Knee implants – Review of models and biomechanics; Materials and Design; 30:398–413 (2009).

2 Sharma A, Komistek RD, Ranawat CS, et al: In vivo contact pressures in total knee arthroplasties; J Arthroplasty; 22:3:404-415 (2007).

3 Freeman, MAR; How the Knee Moves; Current Orthopaedics; (2001) 15,444-450.

4 Dennis DA et al, In vivo Determination of Normal and Anterior Cruciate Ligament Deficient Knee Kinematics; Journal of Biomechanics; (2005) 38; 241-253.

5 Dennis DA et al, Multicenter determination of in vivo kinematics after total knee arthroplasty; Clin Orthop; (2003); 416:37-57.

6 Dennis DA, Komistek RD, Mahfouz MR, et al:. A multicenter analysis of axial femorotibial rotation after total knee arthroplasty. Clin Orthop Relat Res;428:180–189 (2004).

7 Scuderi GR et al, The impact of femoral component rotational alignment on condylar lift-off; Clin Orthop ;(2003) 410:148-154.

8 Haas BD et al, Kinematic comparison of posterior cruciate sacrifice versus substitution in a mobile bearing total knee arthroplasty; Journal of Arthroplasty;(2002) 17:685-692.

9 Bartel DL et al, The effect of conformity, thickness and material on stresses in ultra- high molecular weight components for total joint replacement; J Bone Joint Surg (Am); (1986);68:1041-1051.

10 Steihl JB et al, In vivo determination of condylar lift-off and screw-home in a mobile-bearing total knee arthroplasty, J. Arthroplasty; (1999); 14:293-299.

11 Komistek RD, Kane TR, Mahfouz MR, et al: Knee mechanics- a review of past and present techniques to determine in vivo loads; J Biomech; 38:215-228 (2005).

12 Howling GI, Barnett PI, Tipper JL, Stone MH, Fisher J, Ingham E, 2001. "Quantitative Characterization of Polyethylene Debris Isolated from Periprosthetic Tissue in Early Failure Knee Implants and Early and Late Failure of Charnley Hip Implants". Journal of Biomedical Materials Research 58, 415-420.

13 Currier JH, Bill MA, Mayor MB, 2005: "Analysis of Wear Asymmetry in a Series of 94 Retrieved Polyethylene Tibial Bearing". Journal of Biomechanics 38, 367-375.

14 Wimmer MA, Andriacchi TP, 1997: "Tractive Forces during Rolling Motion of the Knee Implications for Wear in Total Knee Replacement". Journal of Biomechanics 30, 131-137.

15 Sathasivam S, Walker PS, Campbell PA, Rayner K, 2001: "The Effect of Contact Area on Wear Relation to Fixed Bearing and Mobile Bearing Replacements". Journal of Biomedical Materials Research 58, 282-290.

16 Fregly BJ, Sawyer WG, Harman MK, Banks SA, 2005: "Computational Wear Prediction of a Total Knee Replacement from In Vivo Kinematics". Journal of Biomechanics 38, 305-314.

17 Walker PS, Sathasiviam S, 1999. "The Design of Guide Surfaces for Fixed Bearing and Mobile Bearing Knee Replacements". Journal of Biomechanics 32(1), 27-34.

18 Harman M, DesJardins J, Banks S, Benson L, LaBerge M, Hodge W, 2001: "Damage Patterns on Polyethylene Inserts After Retrieval and After Wear Simulation". Proceedings 47th Orthopaedic Research Society, 1003.

19 Komistek RD, Dennis DA, Mabe JA, Walker SA, 2000: “An In Vivo Determination of Patellofemoral Contact Positions”. Clinical Biomechanics 15, 29-36.

20 Komistek RD, Dennis DA, Mahfouz MR, Walker SA, Outten J, 2004: “In Vivo Polyethylene Bearing Mobility is Maintained in Posterior Stabilized Total Knee Arthroplasty”. Clinical Orthopaedics and Related Research 428, 207-213.

21 Dennis DA, Komistek RD, Mahfouz MR, 2003: “In Vivo Fluoroscopic Analysis of Fixed Bearing Total Knee Replacements”. Clinical Orthopaedics 410, 114-130.

22 Kellis E, Baltzopoulos V, In vivo determination of the patella tendon and hamstrings moment arms in adult males using videofluoroscopy during submaximal knee extension and flexion, in: Clinical Biomechanics, 1999;14:118–124.

23 Fellows R, Hill N, Gill H, MacIntyre N, Harrison M, Ellis R, Wilson D, Magnetic resonance imaging for in vivo assessment of three-dimensional patellar tracking, in: Journal of biomechanics, 2005;38:1643–1652.

24 Baker R, ISB recommendation on definition of joint coordinate systems for the reporting of human joint motion—part I: ankle, hip and spine, in: Journal of Biomechanics, 2003;36:300–302

25 Sylvester A, Mahfouz M, Quantifying relative shape variation in modern human femora and humeri, in: The FASEB Journal, 2009;23:648–4.

26 Kostuik JP et al, A study of weight transmission through the knee joint with applied varus and valgus loads, Clin Orthop; (1975); 108:95–98.

27 Scuderi GR et al, The impact of femoral component rotational alignment on condylar lift-off, Clin Orthop; (2003) 410:148-154.

28 Insall J et al, Correlation Between Condylar Lift-Off and Femoral Component Alignment, Clin Ortho and Rel Res; (2004) 403:143–152.

29 Wasielewski RC et al, Correlation of compartment pressure data from an intraoperative sensing device with postoperative fluoroscopic kinematic results in TKA patients, Journal of Biomechanics; (2005) 38:333–339.

30 Antonsson EK, Mann RW, 1989: "Automated 6-DOF Kinematic Trajectory Acquisitions and Analysis". ASME Journal of Dynamic Systems Measurement and Control 111, 31-39.

31 Cappozzo A, Catani F, Della CU, Leardini A, 1993 : "Calibrated Anatomical Systems Technique in 3-D Motion Analysis Assessment of Artifacts". Proceedings of the International Symposium on 3D Analysis of Human Movement. Poiters, France, Jul 1, 45-52.

32 Chao EYS, 1980: "Justification of Triaxial Goniometry for the Measurement of Joint Rotation". Journal of Biomechanics 13, 989-1006.

33 Banks SA, Hodge WA, 1996: "Accurate Measurement of Three-Dimensional Knee Replacement Kinematics using Single Plane Fluoroscopy". IEEE Transactions on Biomedical Engineering 43(6), 638-649.

34 Hoff WA, Komistek RD, Dennis DA, Gabriel SM, Walker SA, 1998: "Three- Dimensional Determination of Femoral-Tibial Contact Positions under In Vivo Conditions using Fluoroscopy". Clinical Biomechanics 13, 455-472.

35 Karrholm J, 1989: “Roentgen Stereophotogrammetry, Review of Orthopaedic applications”. Acta Orhtopaedics Scandinavica 60(4), 491-503.

36 LaFortune MA, Cavanagh PR, Sommer HJ, Kalenak A, 1992: “Three-Dimensional Kinematics of the Human Leg During Walking”. Journal of Biomechanics 25, 347-357.

37 Holden JP, Orsini JA, Holden SJ, 1994: “Estimates of Skeletal Motion – Movement of Surface Mounted Targets Relative to Bone during Gait”. Proceedings of the Thirteenth Southern Biomedical Engineering Conference, Washington DC, April 16.

38 Murphy MA, 1990: “Geometry and the Kinematics of the Normal Human Knee”. PhD Dissertation, MIT, Cambridge. MA.

39 Sati M, deGuise JA, Larouche S, Drouin G., 1996: "Quantitative Assessment of Skin-Bone Movement at the Knee". The Knee 3, 121-138.

40 Alexander EJ, Andriacchi TP, 2001: “Correcting for Deformation in Skin-Based Marker Systems”. Journal of Biomechanics 34, 355-361.

41 Andriacchi TP, Alexander EJ, Toney MK, Dyrby CO, Sum JA, 1998: “A Point Cluster Technique Method for In Vivo Motion Analysis: Applied to a Study of Knee Kinematics”. Journal of Biomechanical Engineering 120, 743-749.

42 Lucchetti L, Cappozzo A, capello A, Della CU, 1998: “Skin Movement Artifact Assessment and Compensation in the Estimation of Knee Joint Kinematics”. Journal of Biomechanics 31, 977-984.

43 Lu TW, O'Connor JJ, Taylor SJG, Walker PS, 1998: "Validation of a Lower Limb Model with In Vivo Femoral Forces Telemetered from Two Subjects". Journal of Bomechanics 31, 63-69.

44 Spoor CW, Veldpas FE, 1988: "Rigid Body Motion Calculated from Spatial Coordinates of Markers". Journal of Biomechanics 13, 391-393.

45 D'Lima D.D, Patil S, Steklov N, et al: Tibial forces measured in vivo after total knee arthroplasty. J Arthroplasty; 28:255-262 (2006).

46 Fisher J, McEwen HM, Tipper JL, et al. Wear, debris, and biologic activity of cross-linked polyethylene in the knee:benefits and potential concerns. Clin Orthop Relat Res; 428:114 (2004).

47 Fisher J, McEwen H, Tipper J, et al. Wear-simulation analysis of rotating-platform mobile-bearing knees. Orthopedics;29(9 Suppl):S36 (2006).

48 Post ZD, Matar WY, Van de leur T, et al: Mobile-bearing total knee arthroplasty- better than a fixed bearing?; J Arthroplasty; Article in Press (2009).

49 Ranawat AS, Rossi R, Loreti I, et al. Comparison of the PFC Sigma fixed-bearing and rotating-platform total knee arthroplasty in the same patient: short-term results. J Arthroplasty;19:35 (2004).

50 Kim YH, Yoon SH, Kim JS. The long-term results of simultaneous fixed-bearing and mobile-bearing total knee replacements performed in the same patient. J Bone Joint Surg Br;89:1317(2007).

51 Pagnano MW, Trousdale RT, Stuart MJ, et al. Rotating platform knees did not improve patellar tracking: a prospective, randomized study of 240 primary total knee arthroplasties. Clin Orthop Relat Res;428:221(2004)

52 Wasielewski RC, Komistek RD, Zingde SM, et al: Lack of axial rotation in mobile-bearing knee designs; Clin Orthop Relat Res;466(11): 2662–2668 (2008).

53 Cates HE, Komistek RD, Mahfouz MR, et al: In vivo comparison of knee kinematics for subjects having either a posterior stabilized or cruciate retaining high-flexion total knee arthroplasty; J Arthroplasty; 23(7):1057-1067 (2008)

54 Bourne RR, Baré JV: Failure in cam-post in Total Knee Arthroplasty. In Bellemans J, Ries MD, Victor JKM (ed): Total Knee Arthroplasty: a guide to get better performance; Springer Berlin Heidelberg, 2005, pp90-95.

55 Delp SL, Kocmond JH, Stern SH (1995) Tradeoffs between motion and stability in posterior substituting knee arthroplasty design. J Biomech 28:1155–1166

56 Piazza SJ, Delp SL, Stulberg SD, Stern SH (1998) Posterior tilting of the tibial component decreases femoral rollback in posterior-substituting knee replacement: a computer simulation study. J Orthop Res 16:264–270

57 Banks SA, Markovich GD, Hodge WA (1997) In vivo kinematics of cruciate-retaining and -substituting knee arthroplasties. J Arthroplasty 12:297–304

58 K. Nakayama, S. Matsuda, H. Miura, H. Higaki, K. Otsuka, Y. Iwamoto (2005); Contact stress at the post-cam mechanism in posterior-stabilised total knee arthroplasty; Journal of Bone and Joint Surgery 87, 326-331-B, 483-88

59 D'Lima D.D, Patil S, Steklov N, et al: Tibial forces measured in vivo after total knee arthroplasty. J Arthroplasty; 28:255-262 (2006).

60 D'Lima D.D, Patil S, Steklov N, et al: In vivo knee moments and shear after total knee arthroplasty. J Biomech; 40:S11-17 (2007).

61 Varadarajana KM, Moynihana AL, D'Lima DD, et al:In vivo contact kinematics and contact forces of the knee after total knee arthroplasty during dynamic weight-bearing activities. J Biomech, 41:2159–2168 (2008).

62 D'Lima DD, Steklov N, Patil S, et al: In vivo knee forces during recreation and exercise after knee arthroplasty. Clin Orthop Relat Res; 466:2605–2611(2008).

63 Taylor WR, Heller MO, Bergmann G, et al: Tibiofemoral loading during human gait and stair climbing. J Orthop Res; 22:625–632 (2004).

64 Sharma A, Komistek RD, Scuderi GR, et al: High-flexion TKA designs- what are their in vivo contact mechanics? Clin Orthop Relat Res; 464:117-126 (2007).

65 Lundberg HJ, Foucher KC, Wimmer MA: A parametric approach to numerical modeling of TKR contact forces. J Biomech; 42:541-545 (2009).

66 Andriacchi TP, Hurwitz DE:Gait biomechanics and total knee arthroplasty. Am J Knee Surg; 10:255–260 (1997).

67 Hsu RWW, Himeno S, Coventry MB, et al:Normal axial alignment of the lower extremity and load-bearing distribution at the knee. Clin Orthop Relat Res; 215–227 (1990).

68 Johnson F,Leitl S,WaughW:The distribution of load across the knee. A comparison of static and dynamic measurements. J Bone Joint Surg Br; 3:346–349(1980).

69 Shelburne KB,Torry MR,Pandy MG: Contributions of muscles, ligaments, and the ground- reaction force to tibiofemoral joint loading during normal gait. J Orthop Res; 10:1983–1990 (2006).

70 Brand RA, Crowninshield RD, Wittock CE, Pedersen DR, Clark CR, Vankrieken FM, 1982: “A Model of Lower Extremity Muscular Anatomy”. Journal of Biomechanics 104(4), 304-310.

71 Anderson FC, Pandy MG, 2001: “Dynamic Optimization of Human Walking”. Journal of Biomechanical Engineering 123, 381-190.

72 Piazza SJ, Delp SL, 2001: “Three-Dimensional Dynamic Simulation of Total Knee Replacement Motion during a Step-Up Task”. Journal of Biomechanical Engineering 123, 599-606.

73 Scuderi GR, Insall JN, Windsor RE, Moran MC, 1989: “Survivorship of Cemented Knee Replacements“. Journal of Bone and Joint Surgery (Br) 71, 798-803.

74 Ateshian GA, Kwak SD, Soslowsky LJ, Mow VC, 1994: “A Stereophotogrammetric Method for Determining In Situ Contact Areas in Diarthrodial Joints, a Comparison with Other Methods”. Journal of Biomechanics 27, 111-124.

75 Black JD, Matejczyk MB, Greenwald AS, 1981: “Reversible Cartilage Staining Technique for Defining Articular Weight Bearing Surfaces”. Clin Orthop 159, 265-267.

76 Kurosawa H, Fukubayashi T, Nakajima H, 1980: “Load Bearing Mode of the Knee Joint: Physical Behavior of the Knee Joint with or without the Menisci”. Clinical Orthopaedics 149, 283-290.

77 Yao JQ, Seedhom BB, 1991: "A New Technique for Measuring Contact Areas in Human Joint – the '3S technique'". Proceedings of the Institution of Mech. Engg. [H] 205: 69-72.

78 Stewart T, Jin ZM, Shaw D, Auger DD, Stone M, Fisher J, 1995: "Experimental and Theoretical Study of the Contact Mechanics of Five Total Knee Joint Replacements". Proceedings of the Institution of Mech Eng [H] 209, 255-231.

79 Ochoa JA, Sommerich RE, Zalenski EB, 1993: "Application of an Innovative Experimental Method to Characterize Contact Mechanics of Total Joint Replacements". Proceedings 39th Annual Orthopaedic Research Society, San Francisco, California.

80 Zdero R, Fenton PV, Rudan J, Bryant JT, 2001: "Fuji film and Ultrasound Measurement of Total Knee Arthroplasties Contact Areas". Journal of Arthroplasty 16(3), 369-375.

81 Mikosz RP, Andriacchi TP, Andersson GB, 1988: "Model Analysis of Factors Influencing the Prediction of Muscle Forces at the Knee". Journal of Orthopaedic Research 6, 205-214.

82 Buechel FF, Pappas MJ, Makris G, 1991: "Evaluation of Contact Stress in Metal Backed Patellar Replacements". Clinical Orthopaedics and Related Research 273: 190-197.

83 Ahmed AM, Burke DL, 1983: "In Vitro Measurement of Static Pressure Distribution in Synovial Joints – Part I: Tibial Surface of the Knee". Journal of Biomechanical Engineering 105: 216-225.

84 Godest AC, deCloke S, et.al., 2000: "A Computational Model for the Prediction of Total Knee Replacement Kinematics in the Sagittal Plane". Journal of Biomechanics 33, 435-442.

85 Bartel DL, Burstein AH, Toda MD, Edwards Dl, 1985: “The Effect of Conformity and Plastic Thickness on Contact Stresses in Metal Backed Plastic Implants”. Journal of Biomechanical Engineering 107, 193-199.

86 Lewis G, 1998: “Contact Stress at Articular Surfaces in Total Joint Replacements: Analytical and Numerical Methods”. Journal of Biomedical Materials.

87 Bartel DL, Bicknell VL, Ithaca, Wright TM, 1986: “The Effect of Conformity, Thickness and Material on Stresses in Ultra-High Molecular Weight Components for Total Joint Replacement”. Journal of Bone and Joint Surgery (Am) 68-A (7), 1041-1051.

88 D’Lima DD, Chen PC, Colwell CW, 2001: “Polyethylene Contact Stresses, Articular Congruity and Knee Alignment”. Clinical Orthopaedics and Related Research 393, 232-238.

89 Machan S, 2004: “Finite Element Analysis of Polyethylene Stresses in Total Knee Replacements”. PhD Dissertation, University of Sydney, Sydney, Australia.

90 Halloran JP, Petrella AJ, Rullkoetter PJ, 2005: “Explicit Finite Element Modeling of Total Knee Replacement Mechanics”. Journal of Biomechanics 38, 323-331.

91 Godest AC, Beaugonin M, Haug E, Taylor M, Gregson PJ, 2002: “Simulation of a Knee Joint Replacement during Gait Cycle using Explicit Finite Element Analysis”. Journal of Biomechanics 35, 267-275.

92 Heuter C, Grundriss der chirurgie, FCW Vogel, 3rd ed., 1885, ISBN 9783540202424.

93 Blodgett W, Auscultation of the knee joint, in: Boston Med Surg J, 1902;146:63–66

94 Walters C, The value of joint auscultation, in: Lancet, 1929;1:920–921.

95 Steindler A, Auscultation of Joints, in: The Journal of Bone and Joint Surgery, 1937;19:121.

96 Peylan A, Direct auscultation of the joints; preliminary clinical observations., in: Rheumatism, 1953;9:77–81.

97 Erb K, Über die Möglichkeit der Registrierung von Gelenkgeräuschen, in: Langenbeck's Archives of Surgery, 1933;241:237–245.

98 Fischer H, Johnson E, Analysis of sounds from normal and pathologic knee joints., in: Arch Phys Med Rehabil, 1961;42:233–40.

99 Chu M, Gradisar I, Mostardi R, A noninvasive electroacoustical evaluation technique of cartilage damage in pathological knee joints, in: Medical and Biological Engineering and Computing, 1978;16:437–442.

100 Chu M, Gradisar I, Railey M, Bowling G, Detection of knee joint diseases using acoustical pattern recognition technique., in: J Biomech, 1976;9:111–4.

101 Mollan R, McCullagh G, Wilson R, A critical appraisal of auscultation of human joints., in: Clin Orthop Relat Res, 1982;170:231–7.

102 Kernohan W, Mollan R, Microcomputer analysis of joint vibration, in: Journal of Microcomputer Applications, 1982;5:287–296.

103 Mollan R, Kernohan G, Watters P, Artefact encountered by the vibration detection system., in: J Biomech, 1983;16:193–9.

104Kernohan W, Beverland D, McCoy G, Shaw S, Wallace R, McCullagh G, Mollan R, The diagnostic potential of vibration arthrography., in: Clin Orthop Relat Res, 1986;210:106–12.

105McCoy G, McCrea J, Beverland D, Kernohan W, Mollan R, Vibration arthrography as a diagnostic aid in diseases of the knee. A preliminary report, in: Journal of Bone & Joint Surgery, British Volume, 1987;69:288–293.

106Gay T, The acoustical characteristics of the normal temporomandibular joint, in: Journal of Dental Research, 1988;67:56–60.

107Gay T, Bertolami C, Bruce Donoff R, Keuth D, Kelly J, The acoustical characteristics of the normal and abnormal temporomandibular joint, in: Journal of oral and maxillofacial surgery, 1987;45:397–407.

108Christensen L, Physics and the sounds produced by the temporomandibular joints. Part I., in: J Oral Rehabil, 1992;19:471–83.

109Christensen L, Physics and the sounds produced by the temporomandibular joints. Part II., in: J Oral Rehabil, 1992;19:615–617.

110Christensen L, Donegan S, McKay D, Temporomandibular joint vibration analysis in a sample of non-patients., in: Cranio, 1992;10:35–41.

111Ishigaki S, Bessette R, Maruyama T, Vibration of the temporomandibular joints with normal radiographic imagings: comparison between asymptomatic volunteers and symptomatic patients., in: Cranio, 1993;11:88–94.

112Gay T, Bertolami CN, Solonche DJ, Method and apparatus for the acoustic detection and analysis of joint disorders, 1989, united States Patent number: 4836218.

113Radke JC, Ryan GJ, Hershberger TW, Method and apparatus for diagnosing joints, 1995, united States Patent number: 5413116.

114Radke JC, Ryan GJ, Hershberger TW, Method and apparatus for diagnosing joints, 1996, united States Patent number: 5533519.

115Rangayyan RM, Krishnan S, Bell DB, Frank CB, Auscultation of Joints, 2003, united States Patent number: 6537233.

116Russell J, Carlson TC, Vipraio GA, Device for non-invasive diagnosis and monitoring of articular and periarticular pathology, 1989, united States Patent number: 4823807

117Krishnan S, Rangayyan R, Automatic de-noising of knee-joint vibration signals using adaptive time-frequency representations, in: Medical and Biological Engineering and Computing, 2000;38:2–8.

118Krishnan S, Rangayyan R, Bell G, Frank C, Adaptive time-frequency analysis of knee joint vibroarthrographic signals for noninvasive screening of articular cartilage pathology, in: IEEE Transactions on Biomedical Engineering, 2000;47:773–783.

119Umapathy K, Krishnan S, Modified local discriminant bases algorithm and its application in analysis of human knee joint vibration signals, in: IEEE Transactions on Biomedical Engineering, 2006;53:517–523.

120Rangayyan R, Wu Y, Screening of knee-joint vibroarthrographic signals using statistical parameters and radial basis functions, in: Medical and Biological Engineering and Computing, 2008;46:223–232.

121Jiang C, Lee J, Yuan T, Vibration arthrometry in the patients with failed total kneereplacement, in: Biomedical Engineering, IEEE Transactions on, 2000;47:219–227.

122Kane, T.R. and Levinson D.A, 1985: "Dynamics: Theory and applications". McGraw-Hill, New York, USA.

123Komistek RD, Stiehl JB, Dennis DA, 1998: "Mathematical Model of the Lower Extremity Joint Reaction Forces using Kane's Method of Dynamics". Journal of Biomechanics 31, 185-189.

124Mueller, John Kyle Patrick, "Development of a Rigid Body Forward Solution Physiological Model of the Lower Leg to Predict Non Implanted and Implanted Knee Kinematics and Kinetics." PhD diss., University of Tennessee, 2011.

125White SC, Yack HJ, Winter DA, 1989: "A Three-Dimensional Musculoskeletal Model for Gait Analysis. Anatomical Variability Estimates". Journal of Biomechanics 22, 885-893.

126deLeva P, 1996: "Adjustments to Zatsiorski-Sleluyanov's Segment Inertial Parameters". Journal of Biomechanics 29, 1223-1230.

127Yamaguchi GT, 2001: "Dynamic Modeling of the Musculoskeletal Motion: "A Vectorized Approach for Biomechanical Analysis in Three Dimensions". Kluwer Academic Publishers, Norwell, MA, USA.

128 Duda R, Hart P, Stork D, Pattern classification 2nd, in: 2nd Edition New York, 2001;.

Vita

Sumesh M Zingde was born in Bombay (now Mumbai), India on the 30th of March 1981. After completing his undergraduate education in Mechanical Engineering from the Manipal Institute of Technology in Manipal, India, he moved to the United States to pursue his higher education. He joined the University of Tennessee in 2004 and received his Master of Science degree in Mechanical Engineering in 2007. The outstanding work being conducted at the university persuaded him to continue at Tennessee and pursue a Doctor of Philosophy degree in Mechanical Engineering. In 2013, he moved to Massachusetts to work in the orthopedic industry as Clinical Manager at ConforMIS Inc., which is the first company in the world to provide customized knee replacements for patients with arthritis. He continues to live in Massachusetts with his wonderful wife (Reshma) of 8 years and their 10 month old son (Rayaan). After completing his education, he plans on continuing his career in the orthopedic medical device industry.